Validation of satellite obtained soil moisture with in-situ soil moisture sensor data and volumetric soil moisture samples in Bago, Myanmar.

Master Thesis Internship Utrecht University, VanderSat, VP Delta and TU Delft

Master Thesis
Wouter Zonneveld
Student number: 3238822
E-mail: wzonneveld@vandersat.com / w.zonneveld@students.uu.nl

Supervisor: Prof. dr. Steven de Jong
External supervisor: Ir. Teije van der Horst
Utrecht University
Faculty of Geosciences
Department of Physical Geography

October 2018

Abstract

Soil moisture is a small component, but essential variable in the hydrological cycle. Over the past years remote sensing techniques developed substantially. VanderSat developed a downscaling technique to deliver satellite soil moisture sampled at 100 m resolution, daily and worldwide. The aim of this study is to do a quality control on this product by comparing with in-situ soil moisture sensor data and volumetric soil moisture measurements collected in the field.

In June 2017, 5 locations were selected in Bago, Myanmar to monitor in-situ soil moisture content in the unsaturated zone. In-situ soil moisture is measured with Decagon GS1 ruggedized soil moisture sensors. At each location 5 sensors are present: one at surface level, two at 10cm and two at 20cm depth. The sensors are connected to an EM50 analogue data logger. Since installation of the sensors a measurement is collected every half an hour. This yields in a time series of over one year. Every location has different soil and vegetation conditions.

During an 8-week fieldwork in June and July 2018, 342 volumetric soil moisture measurements were collected. Volumetric soil moisture measurements are sampled at every sensor location on the same depth with the use of Kopecky rings. After quality control on dry bulk density, 329 samples were used for validation with in-situ soil moisture sensor data at the same date and time. The best correlation between volumetric soil moisture measurements and in-situ soil moisture sensor data is found at nest 1 and the worst at nest 2. This is because at nest 2 the soil is saturated and at nest 1 the soil is very suitable to collect reliable volumetric soil moisture samples. Root mean square errors range between 0.01 and 0.29 m^3/m^3. From the 25 sensors, 10 exceed the threshold value of 0.05 m^3/m^3 used for validation of SMAP satellites (Colliander et al., 2017).

Time series of over one year in-situ soil moisture sensor data from every nest are validated with VanderSat soil moisture X and L-band. The best correlations for the X and L-band are found at nest 5, probably because this nest has the highest representation of the surrounding environment. Root mean square errors range between 0.07 and 0.16 m^3/m^3 for X-band, and 0.06 to 0.23 m^3/m^3 for L-band. The X and L-band both exceed the threshold value of 0.05 m^3/m^3 used for validation of SMAP satellites (Colliander et al., 2017).

From the comparison of volumetric soil moisture measurements with in-situ soil moisture sensor data and the VanderSat soil moisture product during the monsoon period can be concluded that the X-band displays the best correlation and the L-band overestimates soil moisture content.

Acknowledgements

I want to thank Teije van der Horst for his supervision and the weekly meetings for my research at the office of VanderSat. Steven de Jong for his feedback and supervision, to give me permission to do my Master thesis at a commercial Earth observation company. VanderSat to gain relevant work experience next to my studies. I would like to thank VP Delta for making it possible to travel to Myanmar and funding a part of my fieldwork, with attention to Marjan Kreijns, Veronique van der Varst and Lindsey Schwidder for arranging hospitality, flight tickets and invitation letters. Many thanks go to ITC Bago, who helped me arrange everything during the fieldwork and the kitchen ladies who took care of me with lovely food. Sai Wunna, you provided me with a pleasant stay in your office and made me feel home soon. Many thanks to Aung Kyaw Myo, who drove me around in Myanmar, showed directions and assisted me with taking soil samples. Thank you all for this great experience.

Table of contents

Chapter 1: Introduction

1.1 Introduction

This chapter will start with an introduction to soil moisture, satellite obtained soil moisture and vegetation optical depth (VOD). After the introduction the importance of measuring in-situ soil moisture is explained. The scientific relevance and social relevance of this research are presented, followed by the objective and research questions. Chapter 2 continues on the study area and climate.

This research continues on work of Nina Kattler (2017), a previous intern from VanderSat. She set up a small soil moisture sensor network with help of Ebe Gremmer in the Bago region of Myanmar, during the summer of 2017. The main aim of this research is to use this network to validate satellite obtained soil moisture in tropical regions. Remote sensing is a valuable tool for monitoring soil moisture in remote areas, such as Bago in this research. Core validations with in-situ soil moisture measurements on location are necessary to verify the outcome of remote sensing data. This is done by collecting new volumetric soil moisture measurements in the field. Volumetric soil moisture measurements are sampled next to each soil moisture sensor nest to determine the volumetric water content (m^3/m^3) in the soil up to 20cm depth. This data will allow to validate the soil moisture sensor network and eventually the VanderSat satellite obtained soil moisture (VdS SM) product over the tropical region. The fieldwork comprises of a quality assessment of the soil moisture products (both network and satellite products) and includes a field study, maintenance of ground stations and analysis of both the field stations and satellite products.

1.2 Soil moisture

Soil moisture is usually defined as the water contained in the unsaturated soil zone, which is located between the soil surface and the ground water level. (e.g. Fredlund and Rahardjo, 1993; Hillel, 1998; Robock et al., 2000; Seneviratne et al., 2010). Although soil moisture is a small component of the hydrological cycle, it plays an essential role in understanding hydrology. Soil moisture is often an initial condition or boundary condition in relevant hydrologic models, with applications in e.g. weather forecasting, water resources management, drought prediction and ecosystem health monitoring (SMAP handbook, Entekhabi et al., 2014). Soil moisture is an important link between the exchange of water and energy at the soil atmosphere interface (Gouweleeuw., 2000). Soil moisture is also a hydrological state variable that affects global, regional and local scales. On global and regional scales, soil moisture plays an important role on weather and climate systems. Therefore the Global Climate Observing System initiative (2010) has identified soil moisture as an essential climate variable (Benninga et al., 2018).

The most common definition of soil moisture is volumetric soil moisture, expressed as the volumetric water present over a defined soil depth [m^3 water per m^3 soil] or as the depth of a column of water contained in a given depth of soil [mm water per mm soil] (Dorigo et al., 2011). Soil moisture content can also be expressed as a fraction of saturation. Soils contain pores which are usually less than 50% of the soil volume. These pores are filled with organic matter, air and water (or a combination of them). When all the pores are filled with water, the soil is fully saturated and soil moisture content reached its maximum. The saturation ratio varies between 0 (no soil moisture content) and 1 (maximum soil moisture content). Volumetric water fraction [m^3/m^3] is the most common unit for the saturation ratio (Dorigo et al., 2011). Essential for the definition of soil moisture is the characterization of the soil depth. Soil moisture content is not distributed homogeneously and varies vertically, horizontally and depends on soil depth. Soil moisture values can range between 0.0–1.0 m^3/m^3, whereas in practice they do not exceed 0.6 m^3/m^3 (de Jeu et al., 2008).

1.3 Satellite obtained soil moisture

Remote sensing systems and techniques are becoming more advanced to monitor Earth resources, one which is soil moisture. In this research passive microwave technology is used from SMAP (soil moisture active passive) and AMSR-E (Advanced Microwave Scanning Radiometer – Earth Observing System). AMSR-E is a passive microwave radiometer on board of the Aqua satellite that measures precipitation rates, cloud water, water vapor, sea surface winds, sea surface temperature, ice, snow and soil moisture (https://aqua.nasa.gov/amsr-e). SMAP is an Earth satellite mission that measures and maps Earth's soil moisture content and freeze/thaw state (https://smap.jpl.nasa.gov/). The advantage of passive microwave technology is that it relies on natural microwave emission from the Earth rather than reflected sunlight. Furthermore, passive microwaves are less affected by sun-sensor geometry issues, clouds and aerosols (Liu et al., 2018).

SMAP's passive microwave techniques, in particular L-band frequencies (1-2GHz, wavelength 15-30cm) have shown good promise for global mapping of near surface (0-5cm) soil moisture at a spatial resolution between 25-40km and temporal resolution of 2 to 3d (Mohanty et al., 2017). Soil moisture data can also be obtained from e.g. C (4-8 GHz, wavelength 3.8-7.5cm) and X-bands (8-12GHz, wavelength 2.5-3.8cm). The L-band is considered to be the most optical frequency to derive soil moisture because at lower frequencies radiation emitted from the soil becomes more sensitive to water content (Crow et al., 2012). The penetration depth of passive microwave signals is in general one tenth of the wavelength but might increase up to one third of the wavelength for dryer soils and increasing surface roughness (Karthikeyan et al., 2017). The X-band has a penetration depth up to

1 cm into the soil, the L-band has a penetration depth up to 5 cm into the soil and P-band has a penetration depth up to 10-20 cm into the soil (Garrison et al., 2017).

Thermal radiation is emitted by all natural surfaces, due to the land surface and atmosphere. Passive microwave technology does not measure soil moisture directly, but measure observed brightness temperatures. Brightness temperatures are a measure of microwave radiation emitted from the soil surface through the atmosphere. The microwave radiation is polarized into horizontal and vertical oscillation. The land parameter retrieval model (LPRM) algorithm uses the vertical and horizontal oscillation to resolve the radiation originating from the soil and vegetation simultaneously with input of temperature data (Owe et al., 2001; Owe et al., 2008). The LPRM is a simple radiative transfer equation in an iterative forward modelling approach that links surface geophysical variables (i.e. soil moisture, vegetation water content, and soil/canopy temperature) to the observed brightness temperatures and derives vegetation optical depth (VOD) (de Jeu et al., 2008; van der Schalie, 2017). Surface temperatures are derived with a separate retrieval algorithm that uses vertical polarization measurements (Meesters et al., 2005). The LRPM can be applied at all microwave frequencies, and only needs soil texture information as external data source. The soil texture maps are obtained from the Food and Agricultural Organization (FAO) (de Jeu et al., 2017).

The theory for measuring soil moisture at microwave frequencies lies in the contrast between the dielectric properties of liquid water (~80) and dry soil material (~4). The large dielectric constant of water is the result of the water molecule's alignment of its permanent electric dipole in response to an applied electromagnetic field (de Jeu et al., 2008). When water is added to a soil matrix, the dielectric constant of the soil increases strongly (Hipp 1974). This results in a big range of dielectric properties of soil-water mixtures (4-40) and is the result of the natural microwave emission from the soil (Schmugge et al., 1986). The dielectric constant is a complex number, the real part determines the propagation of energy as it passes upward through the soil, while the imaginary part determines the energy loss. Factors that influence the dielectric constant are due to temperature, salinity, soil texture and wavelength (de Jeu et al., 2008).

The ability to measure soil moisture with satellites depend on specifications of the sensor, the assumptions and parameter values adopted from the retrieval algorithms, the soil and vegetation cover conditions, sloped terrain, open water bodies and ice (e.g. Burgin et al., 2017; Chan et al., 2016; Das et al., 2014; Kerr et al., 2016; Pathe et al., 2009).

1.4 Vegetation optical depth (VOD)

Vegetation cover influences soil moisture obtained from the microwave spectrum and is one of the major factors that affects satellite obtained soil moisture in tropical areas. Vegetation absorbs or scatters the radiation emitted from the soil. On the other part, vegetation itself also emits radiation. These two effects counteract each other. Soil emission will decrease in dense vegetation while radiation emitted from the vegetation increases. In very dense vegetated areas the emission from the soil is completely masked out. The resulting emission is therefore due to the vegetation cover (de Jeu et Al., 2008).

Vegetation optical depth (VOD) represents the canopy water content dynamics. The optical depth is a measure of how opaque a medium (the canopy) is to radiation passing through it. The optical depth is directly related to the vegetation water content and dielectric properties of water, and is also a function of the incidence angle and the radiometric frequency (Meesters et al., 2005). In this research VOD data is obtained from brightness temperatures derived from X and L-band. Microwave signals are also strongly related to the temperature of the emitting surface, which may include both the soil and the vegetation canopy. The advantage of VOD is that the signal remains sensitive to variations in relatively high biomass density (Zhou et al., 2014). Over closed canopy rainforest, VOD retrievals can be assumed to represent water content dynamics at the canopy level, including the leaves and branches (Guglielmetti et al., 2007; Jones et al., 2011; Jones et al., 2014). Shorter wavelengths tend to be more sensitive due to vegetation influences. Soil moisture and VOD retrieved from C, L and X-bands are subject to scattering and absorption and therefore require some correction.

1.5 In-situ soil moisture sensor nests in relation to satellite obtained soil moisture

In-situ soil moisture sensor nests can be used to evaluate satellite obtained soil moisture data. However, evaluation of in-situ soil moisture sensor data has received little attention in literature (Dorigo et al., 2013). Several soil moisture testbeds with in-situ sensors are developed over the past years, e.g. terrestrial environmental observatories (TERENO) in Germany and Marena Oklahoma In-Situ Sensor Testbed (MOISST) Oklahoma. These sites extensively evaluate the outcome of satellite soil moisture data. In-situ soil moisture measurement networks need a long-term perspective to evaluate long time series such as provided by the European Space Agency Climate Change Initiative (CCI) soil moisture product (Liu et al., 2012; Dorigo et al., 2015).

In-situ soil moisture content provides valuable data for calibrating and validating satellite-obtained soil moisture retrievals (Dorigo et al., 2011). In-situ soil moisture data also provides information on spatial

and temporal variability of soil moisture at different scales, because soil moisture conditions vary in space and time. The spatial variability of soil moisture conditions depends on the scale of considered observation. In-situ soil moisture measurements are accurate and have high temporal resolution, but have small spatial support (van der Schalie et al., 2018). This is one of the main problems of in-situ soil moisture validation to satellite data; one measures a point well supported in time and the other a spatially well covered signal with few temporal points.

VanderSat developed a downscaling technique to reduce the spatial resolution of satellite obtained soil moisture. Due to patents (WO2017216186), little is published about the methods of the VanderSat satellite obtained soil moisture product (VdS SM). In this research VdS SM X and L-band are used. Both are sampled at 100m grid size which is a very good improvement compared to spatial resolutions of SMOS (35-50km) and SMAP (36km). Most agricultural, hydrological, meteorological and land-use applications need representation of small scale spatial heterogeneity while traditional soil moisture retrievals are in the order of kilometres (Mohanty et al., 2017). The volumetric soil moisture measurements and in-situ soil moisture sensor nests in Myanmar contribute valuable data to validate the output of the downscaling technique of the VdS SM product, because this data is the first of its kind taken in the tropical region of Myanmar.

1.6 Scientific relevance

Soil moisture is one of the best indicators of agricultural droughts (Mo, 2008; Sheffield & Wood, 2007). Soil moisture measurements in the tropics are relatively unexplored and validation is an important and challenging aspect of satellite obtained soil moisture retrievals. The most direct form of validation is to compare the soil moisture retrievals with in-situ station observations (Al Bitar et al., 2012; Karthikeyan et al., 2017). In-situ soil moisture measurements provide a reference for validating Earth observation retrievals and land process models. The LPRM which VanderSat uses is challenged by limitations in tropical environments due to dense vegetation. The combination of the soil moisture sensor network, satellite obtained soil moisture and volumetric soil moisture measurements are essential to validate reliable soil moisture estimation in Myanmar.

1.7 Social relevance

Water plays an important role in daily life and livelihood in Myanmar. Myanmar is subject to a highly variable monsoon climate with distinct dry and wet seasons, changing rivers systems and dynamic coastlines. The economy of Myanmar is largely dependent on agriculture and over 65 percent of the population is employed in this sector. Myanmar lacks integrated water management structures. This

is mainly because the country was subjected to a military rule until 2011. Ever since Integrated Water Resources Management (IWRM) strategies are being developed but are still in an early stage. VanderSat cooperates with the RVO (Rijksdienst voor Ondernemend Nederland) subsidized “Partners for Water” project by VP Delta. Several start-ups in the program of VP Delta are experimenting on smart innovation solutions in Myanmar. Myanmar is a very suitable country to test new water management strategies and can be implemented if successful. These strategies are necessary for themes as erosion, sedimentation, rainfall, water (quality), irrigation and subsidence. VanderSat can use their technology to investigate how much water is present in the soil. In-situ soil moisture measurements need core validations with satellite data and in turn improve the VdS SM signal. With reliable satellite obtained soil moisture data advise can be given to farmers on irrigation schemes and successful harvesting, but also provide useful data to insurance companies in case of draughts and/or failed harvesting.

1.8 Objective

The objective of this research is to validate satellite obtained soil moisture derived from the X and L-band in Bago, Myanmar and ultimately to develop a high spatial and temporal soil moisture dataset in the tropical region. To achieve this more in-situ soil moisture sensor measurements and volumetric soil moisture samples are collected and a cross validation is done. The cross-validation results in a better understanding of satellite obtained soil moisture, sampled at 100m grid size in tropical areas with dense vegetation.

1.9 Research questions

The main question in this research is: How do volumetric soil moisture samples, in-situ soil moisture sensor measurements and satellite obtained soil moisture from X and L-bands in Bago, Myanmar compare to each other?

Three minor research questions are investigated to answer the main research question:

- How does the in-situ soil moisture sensor data compare with volumetric soil moisture measurements?
- How does the in-situ soil moisture sensor data compare with VanderSat satellite obtained soil moisture X-band?
- How does the in-situ soil moisture sensor data compare with the VanderSat satellite obtained soil moisture L-band?

Chapter 2: Study area and climate of Bago, Myanmar

The climate of Myanmar is mainly determined by its geographical position. Myanmar is located in the South of the Asiatic continent and separated from neighbouring countries by high mountain walls. In the far North lies the Himalaya, in the Northwest the jungle hills near Bangladesh, while the Chin Hills and the Yomas are separating Myanmar from India (Zin, 2017). The country is significantly shaped by the presence of the Ayerwady river and consists of big lowland plains. Because of the diversity in relief, strong differences in precipitation are present. The central part of Myanmar receives 762mm per year while certain coastal regions receive up to 5080mm per year. The mean annual rainfall is 2341mm per year (Naing, 2005). The climate of Myanmar can be roughly divided into 4 different regions: the dry zone, the coastal zone, the Shan plateau and the Irrawady river delta. Bago is located in the Irrawady river delta area of Myanmar. Bago has a tropical climate with three distinct seasons: the cool period from November to February, the hot period from March to May and the monsoon period from late May to October. During the monsoon period, intense rainfall takes place which contributes up to 90% of the annual rainfall (Naing, 2005). The arrival and departure of the monsoon over Myanmar is displayed in Figure 1 and 2. Bago corresponds with the 23rd of May arrival line. Monthly normal rainfall and temperature data are given in Figure 3 and 4. During the cool and hot period, it is unlikely that precipitation takes place.

Figure 1: Monsoon onset date (Zin, 2017)

Figure 2: Monsoon offset date (Zin, 2017)

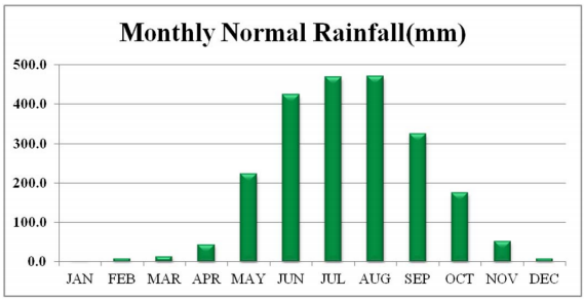

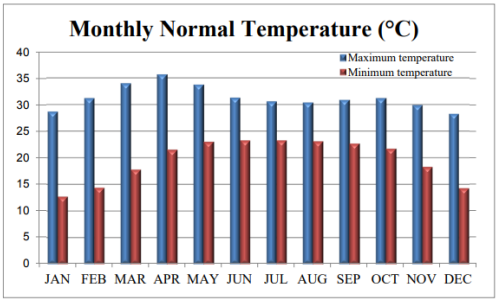

Figure 3: Monthly normal rainfall (Zin, 2017). *Figure 4: Monthly normal temperature (Zin, 2017).*

An 8-week fieldwork has been carried out from the beginning of June until the end of July 2018 in the Bago region of Myanmar. A soil moisture sensor network was installed here in June 2017 by Nina Kattler and Ebe Gremmer (former interns of VanderSat). The soil moisture sensor network consists of five analogue data loggers at different locations (Figure 6, Table 1) in a radius of 15-20 km from nest 1. Each data logger consists of five sensors measuring in-situ soil moisture content at 0, 10 and 20 cm depth. For calibration and validation volumetric soil moisture measurements are sampled next to these sensors. More detailed information about each sensor nest can be found in Appendix 9.1. In the next chapter more is explained about the sensors and sampling method.

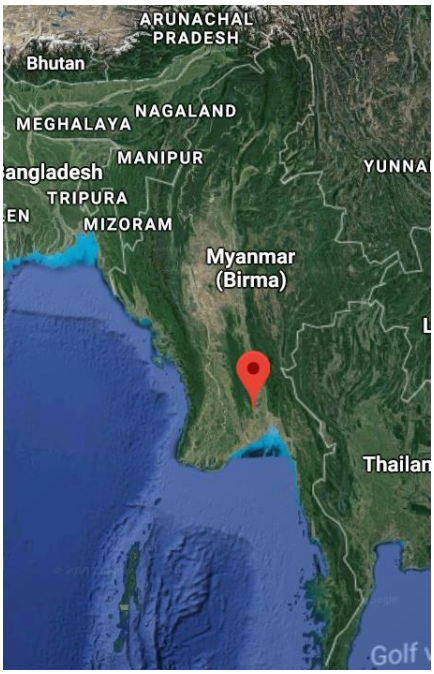

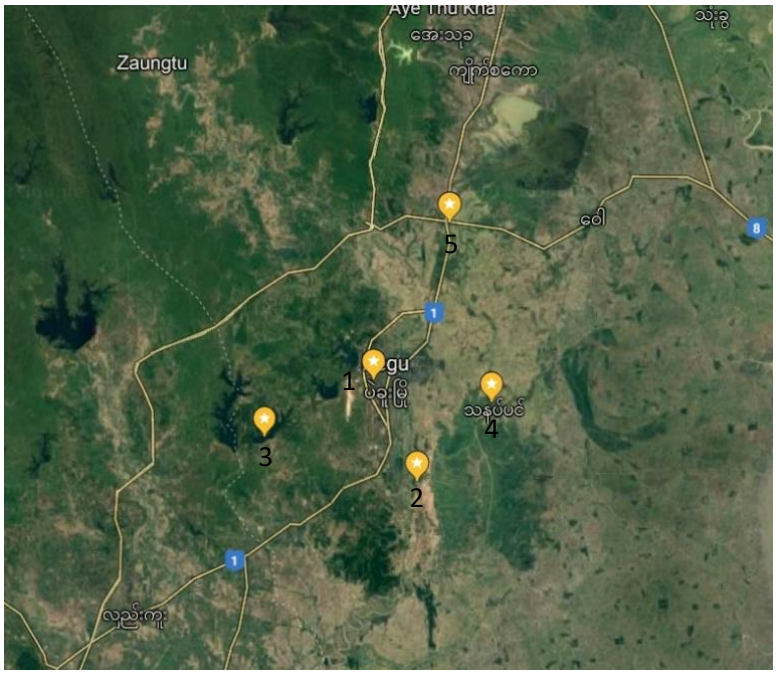

Figure 5: Myanmar, red arrow indicates Bago. *Figure 6: The locations of the five sensor nests, source: Google maps.*

Location	Latitude	Longitude
Nest 1	17°18’50 N	96°27’12 E
Nest 2	17°12’56 N	96°29’52 E
Nest 3	17°15’31 N	96°20’33 E
Nest 4	17°17’31 N	96°34’23 E
Nest 5	17°27'58 N	96°31'49 E

Table 1: The locations of the sensor nests with latitude and longitude.

Chapter 3: Methods

3.1 Introduction

This chapter explains the methods used in this research. The soil sampling method is explained, how volumetric soil moisture samples are collected in the field and how the data processing is done. The next part is explains how the quality of samples is considered based on bulk density and statistical outliers. There is explained how the data loggers and sensors measure and record in-situ soil moisture content. More is explained about the VanderSat satellite obtained X and L-band data. Techniques as root mean square errors and Pearson correlations that have been used to validate volumetric soil moisture samples with in-situ soil moisture sensor data and satellite obtained soil moisture data are explained. There is also explained how each dataset is compared to another.

3.2 Volumetric soil moisture sampling

Volumetric soil moisture measurements were taken near each sensor (within 2 meters) according to the gravimetric method (Dorigo et al., 2011). Kopecky rings were used with a fixed volume of 100 cm^3 to sample the soil. Sampling of the soil was done with care, error samples were removed in the field and taken again. Soil samples were taken at the same depth as the soil moisture sensors. One sample was taken at 0 cm, three samples at 10 cm and two samples at 20 cm depth. This was done for every visit at a sensor nest. Date, time and depth were written down on each sample. The collected samples were brought to the lab at ITC Bago for processing (Figure 7 and 8). The wet samples were weighed and oven dried at 105 °C for 24 hours. After 24 hours the samples were weighted again and the mass of water (volumetric water content) was calculated by subtracting the wet weight from the dry weight.


Figure 7: Weighing the samples and storing the data. Figure 8: The wet samples before going in the oven. Stacked columns from left to right: nest 1, nest 3, nest 4 and nest 5.

Dry bulk density and porosity were calculated to evaluate the sampling method of the volumetric soil moisture measurements. In this research especially to do a quality assessment on them to see if each sample was suitable for validation to in-situ soil moisture measurements. The dry bulk density is determined as the weight of the soil after it is dried in the oven and defined by Formula 1.

$$\textit{Formula 1: } Dry\ bulk\ density\ (g/cm^3) = \frac{Dried\ soil\ weigth\ (g)}{Volume\ of\ soil\ (cm^3)}$$

The porosity is inversely related to the dry bulk density and defined by Formula 2.

$$\textit{Formula 2: } Porosity\ (\%) = 1 - \frac{Bulk\ density\ (\frac{g}{cm^3})}{Particle\ density\ (\frac{g}{cm})} * 100\ \%$$

In Formula 2 the quartz particle density is used for porosity calculations.

$$\textit{Formula 3: } Partice\ density = 2650\ g/cm^3$$

The volumetric water content is defined by Formula 4.

$$\textit{Formula 4: } Volumetric\ water\ content\ (m^3/m^3) = \frac{Volume\ of\ water * 100\%}{Total\ volume}$$

3.3 Quality assessment of volumetric soil moisture samples

For each nest at each depth of 0, 10 and 20cm, the data quality of the volumetric soil moisture samples was reviewed. First selection consists of a visual interpretation in the field, if the soil samples are properly filled and do not contain pebbles or trash. Second selection is done by plotting box plots of

every nest to compare the dry bulk density. For example, if one volumetric soil moisture sample at nest 1 at 10cm depth is significantly different in bulk density from the others, it is considered a statistical outlier, and it will be removed for further analysis.

3.4 In-situ soil moisture sensor network, sensors and loggers

The soil moisture sensor network consists of five locations and thus five Decagon Em50 Analog Data Loggers. The Em50 data logger (Figure 9) is a five channel, self-contained data recorder designed for use with any ECH$_2$O sensor. The Em50 can store over 36000 data scans and is suitable to last in extreme weather from -40 to 60°C and up to 100% relative humidity (Decagon services, 2015). To each data logger five Decagon GS1 Ruggedized soil moisture sensors are connected. Two sensors at 20cm depth, two sensors at 10cm depth and one sensor at surface level. The sensors have a VWC resolution of 0.001 m^3/m^3 and ± 0.03 m^3/m^3 accuracy (3%). The data logger is set to take a soil moisture measurement every 30 minutes in the local time zone (UTC +6:30 hours). The Em50 is configured by plugging a laptop into the com port. Sai Wunna, staff officer at the Irrigation Technology centre in Bago, Myanmar, visits the data loggers once a month to extract the data and sends it by e-mail to VanderSat.

Figure 9: Data logger of nest 2 with 5 connected sensors. The comport is used for connection with a laptop.

3.5 VanderSat satellite soil moisture X and L-band

VanderSat processed the satellite obtained soil moisture data. Two different datasets are used for validation, X-band and L-band data sampled at 100 m grid size. The X-band is based on AMSR-E satellite data. The L-band is based on SMAP and AMSR-E satellite data. SMAP has an orbit repeat cycle of 8 days, while AMSR-E has an orbit repeat cycle of 16 days. The satellite data is non-vegetated corrected, which means presence and influence of vegetation is not taken into account of the algorithm. At each location of a sensor nest the data is extracted with the use of an application programming interface (API). This results in a time series of over one year starting in June 2017 until July 2018 for both X and L-band. Not every day contains of a measurement. For the X-band a minimum of 195 and maximum of 254 measurements are used. For the L-band a minimum of 97 and a maximum of 134 measurements. Another data column is calculated by the algorithm which is called X or L-band average. This dataset contains a measurement every day. The X-band descending satellite overpass time is approximately 01:30 a.m. and L-band at 06:00 a.m. in Myanmar time zone (UTC +6:30 hours). The X-band can measure soil moisture content up to 1cm depth and L-band up to 5cm depth depending on soil dryness.

3.6 Root mean square error

To validate volumetric soil moisture measurements with in-situ soil moisture sensor data and with satellite obtained soil moisture X and L-band, root mean square errors (RMSE) are calculated for each sensor. The RMSE (Formula 5) is a measure of how much deviation there is between two datasets. It indicates how spread out the data is compared to a best line of fit (Y=X). RMSE values of 0.05 m^3/m^3 and lower are considered good for validation of SMAP satellites (Colliander et al., 2017).

Formula 5: $RMSE = \sqrt{\frac{1}{n}\sum(xi - \dot{x}i)^2}$

Root mean square error, xi is the GTM and $\dot{x}i$ *the corresponding in-situ soil moisture sensor measurement and n the sample size.*

3.7 Pearson correlation

To validate volumetric soil moisture measurements with in-situ soil moisture sensor data and with satellite obtained soil moisture X and L-band, Pearson correlations coefficient are calculated for each sensor. The Pearson correlation coefficient (Formula 6) is a measurement of linear correlation between two datasets. The correlation coefficient ranges from -1 to 1. A Pearson value of 1 indicates a perfect correlation between the two datasets, where all data point are present on a linear (Y=X) line (Maidment, 1993). When X increases, Y increases. A negative value indicates that all datapoints for Y

decreases as X increases. When the Pearson correlation equals 0 no correlation is present between the datasets.

Formula 6: Pearson correlation $= \frac{n(\Sigma xy) - (\Sigma x)(\Sigma y)}{\sqrt{[n(\Sigma x^2) - (\Sigma x)^2][n(\Sigma y^2) - (\Sigma (y)^2]}}$

Pearson correlation coefficient, n indicates the pairs of data that need to be compared, X and Y are the two variables, for example volumetric soil moisture measurements and in-situ soil moisture measurements.

3.8 Volumetric soil moisture samples compared to in-situ soil moisture sensor data

Volumetric soil moisture samples are validated with in-situ soil moisture sensor data at the same day, time and depth. Since the sampling method yields that there are three volumetric soil moisture measurements at 10 cm depth and two at 20 cm depth, these are averaged at each depth. Scatter plots of volumetric soil moisture measurements are compared to in-situ soil moisture sensor measurements for every nest and every sensor. A linear regression line (R^2) is plotted in these datasets. The root mean square errors and the Pearson correlations are calculated between the datasets. These values are stored in tables to give insight in the performance of each sensor at each nest. Finally, a time series is plotted for visualization.

3.9 In-situ soil moisture sensor data compared to VanderSat satellite soil moisture X & L-band

In-situ soil moisture sensor data is validated with VanderSat satellite obtained soil moisture by creating a dataset which contains only in-situ sensor measurements at the same time of the satellite overpass for both X and L-band. Scatter plots of in-situ soil moisture compared to satellite obtained soil moisture are made for each nest and each sensor. A linear regression line (R^2) is plotted in these datasets. The same analysis as in volumetric soil moisture measurements compared to in-situ sensor data is performed. Root mean square errors and Pearson correlations are calculated between the datasets and stored in tables. Time series are plotted for visualization.

Chapter 4: Results

4.1 Introduction

The objective of this MSc thesis is to validate the in-situ soil moisture sensor network in Bago, Myanmar with the use of volumetric soil moisture samples collected in the field and the VanderSat satellite obtained soil moisture X and L-band. This chapter will display the results found in this research and starts with the volumetric soil moisture samples that were collected. The next results focus on the in-situ soil moisture sensor measurements: the trends that are observed and their response to wet and dry seasons. These results are followed by a calibration of the sensors that measure in-situ soil moisture content. Then the results are given for comparing volumetric soil moisture measurements to in-situ soil moisture sensor measurements. The results are given for in-situ soil moisture sensor measurements of a time period of one year are compared to the VanderSat satellite soil obtained moisture X and L-band. Finally, a comparison is made between volumetric soil moisture samples, in-situ soil moisture sensor measurements and the VanderSat satellite obtained soil moisture X and L-band during the fieldwork period of 8 weeks in the wet monsoon period.

4.2 Volumetric soil moisture samples and quality assessment

During the 8 weeks of fieldwork in June and July 2018, 342 volumetric soil samples were collected. After quality control on bulk density 329 samples remained for validation with in-situ soil moisture sensor data. An example is given in Figure 10, two outliers are present at the volumetric soil moisture measurements sampled at 10cm depth, these are removed for further analysis. The total samples before and after quality control are displayed in Table 2. All other box plots are visualized in Appendix 9.2.

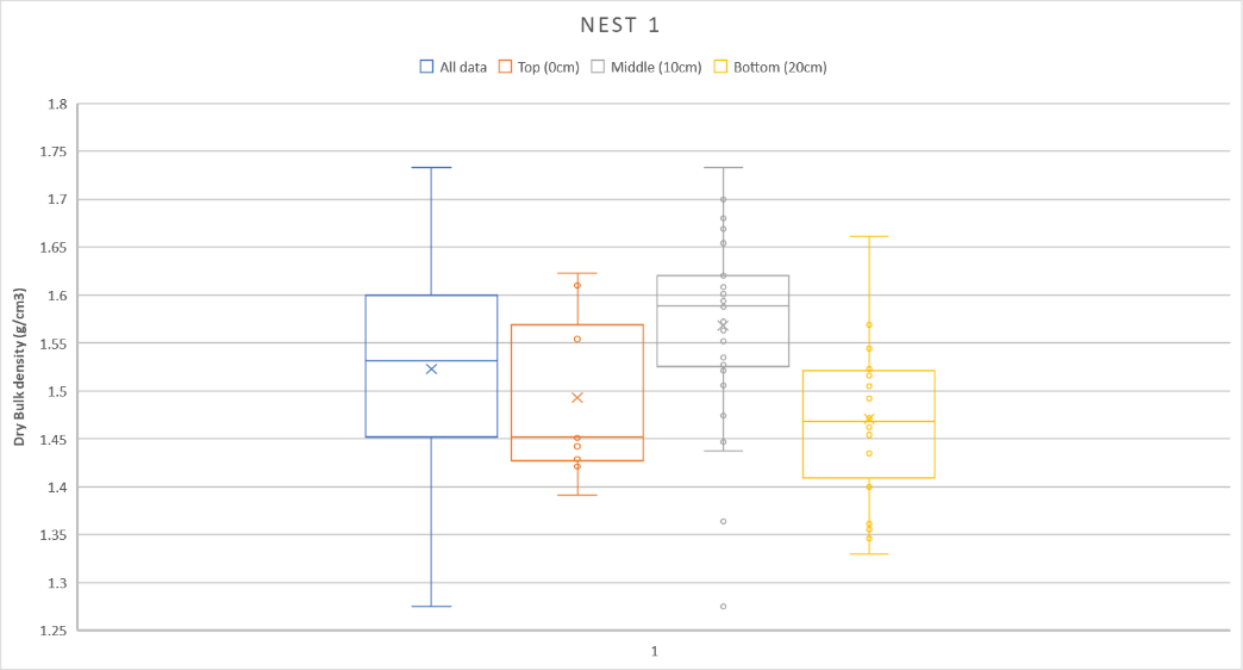

Figure 10: Nest 1: Dry bulk density of volumetric soil moisture measurements sampled at 0, 10 and 20cm depth. Two outliers are present in the 10cm volumetric soil moisture measurements at 1.364 and 1.275 g/cm^3. These two outliers are removed.

Location	Volumetric soil moisture measurements	Volumetric soil moisture measurements used for validation
Nest 1	60	58
Nest 2	72	68
Nest 3	60	60
Nest 4	72	65
Nest 5	78	78

Table 2: The five different soil moisture sensor nests, it's locations and the amount of measurements.

In Figure 11 and Table 3 can be observed that bulk density varies between 1.21 and 1.75 g/cm^3, which corresponds with silty clay (Maidment, 1993). The variation in bulk density is because each sensor nest contains differences in soil texture, compaction, porosity and soil moisture content. Some nests consist of clay material compared to silty and sandy soils found at other nests. From Table 3 can be obtained that porosity varies between 0.34 and 0.54. The volumetric water content varies between 0.16 and 0.48 m^3/m^3. Nest 3 has the highest bulk density on average, while porosity and volumetric water content are the lowest on average.

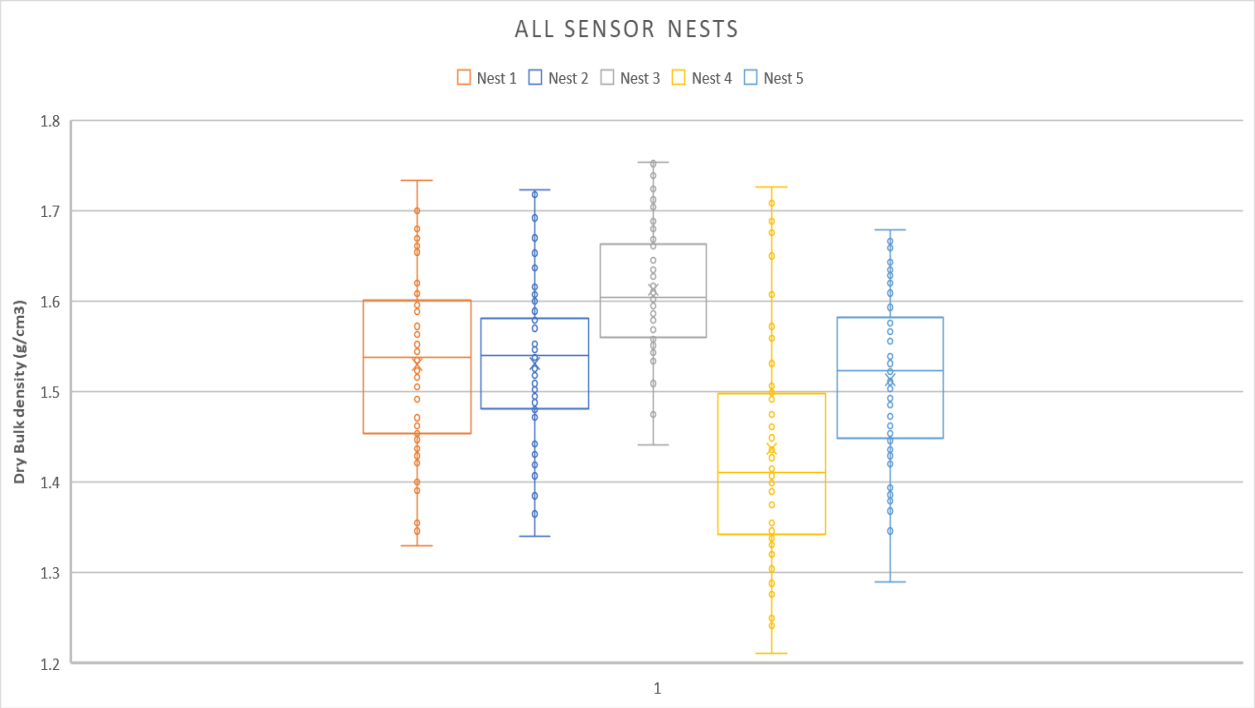

Figure 11: Box plots of all the volumetric soil moisture measurements at the five sensor nests, the outliers are removed.

Bulk density (g/cm^3)	**Nest 1**	**Nest 2**	**Nest 3**	**Nest 4**	**Nest 5**
Min	1.33	1.34	1.44	1.21	1.29
Max	1.73	1.72	1.75	1.73	1.68
Range	0.40	0.38	0.31	0.52	0.39
Mean	1.53	1.53	1.61	1.44	1.51
Porosity	**Nest 1**	**Nest 2**	**Nest 3**	**Nest 4**	**Nest 5**
Min	0.35	0.35	0.34	0.35	0.37
Max	0.50	0.49	0.46	0.54	0.51
Range	0.15	0.15	0.12	0.19	0.15
Mean	0.42	0.42	0.39	0.46	0.43
Volumetric water content (m^3/m^3)	**Nest 1**	**Nest 2**	**Nest 3**	**Nest 4**	**Nest 5**
Min	0.16	0.25	0.19	0.25	0.28
Max	0.37	0.48	0.27	0.46	0.42
Range	0.21	0.24	0.09	0.21	0.15
Mean	0.28	0.36	0.22	0.38	0.35

Table 3: Bulk density, porosity and volumetric water content of the sampled volumetric soil moisture measurements.

4.3 In-situ soil moisture sensor measurements

Figure 12 displays the average volumetric water content over 20cm depth for all five nests. Nest 2 and nest 4 are the wettest during monsoon conditions (June-November). This corresponds with observations and volumetric soil moisture measurements sampled in the field. The pattern of nest 2 can be ignored for the period of November 2017 until June 2018 due to errors in the sensor data. When the data of nest 2 is averaged over 20cm depth, it will not display a true result. The general trend observed is that the wet season starts in May and half October the dry period starts which corresponds with the monsoon onset and offset given in Figure 1 and 2.

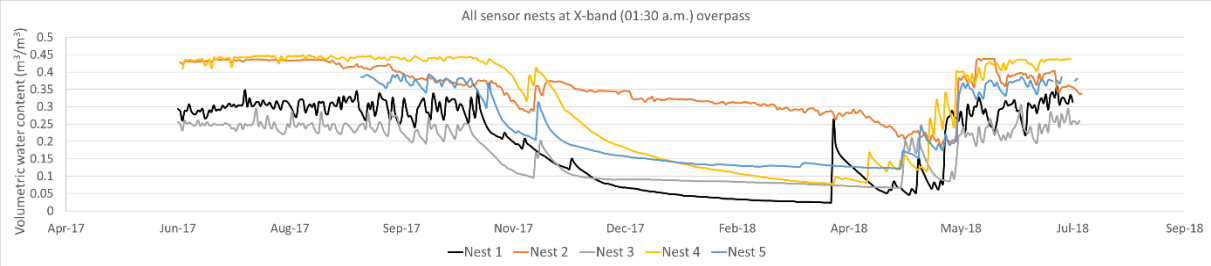

Figure 12: Time series of in-situ soil moisture content (m^3/m^3) at 01:30 a.m. satellite overpass for the five sensor nests. Each line displays the average measurement over 20cm depth.

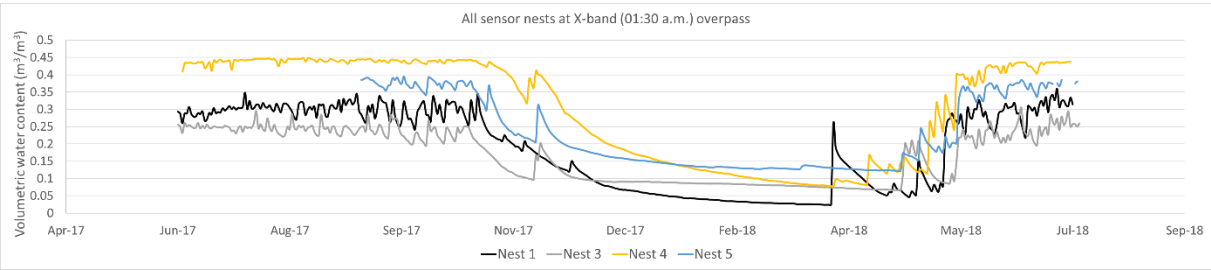

Figure 13: Same as Figure 12, but nest 2 is excluded.

A trend that can be observed in Figure 14 and Appendix 9.3 that sensor 1 in all nests which are located at surface level, displays the biggest variation in volumetric water content. The sensors at 10 and 20cm depth display less variation in volumetric water content. This is due to the fact that soil moisture content at surface level strongly depends on precipitation and evaporation. Another observation is that the sensors at 10 and 20cm depth measure more soil moisture compared to the surface sensor at the start of the dry period (late October). There is a clear delay in time before the soil is almost dried up to 20cm depth. Furthermore can be observed that for example in November a few precipitation events take place which do not always penetrate up to 20cm depth. This means that this water will evaporate before reaching deeper soils. These trends are only visible for the surface sensors. At the

start of the rain season in in May 2018 can be observed that so much rain falls that the sensors at 10 and 20cm depth measure the increased soil moisture content in the soil. This means the water has no time to evaporate.

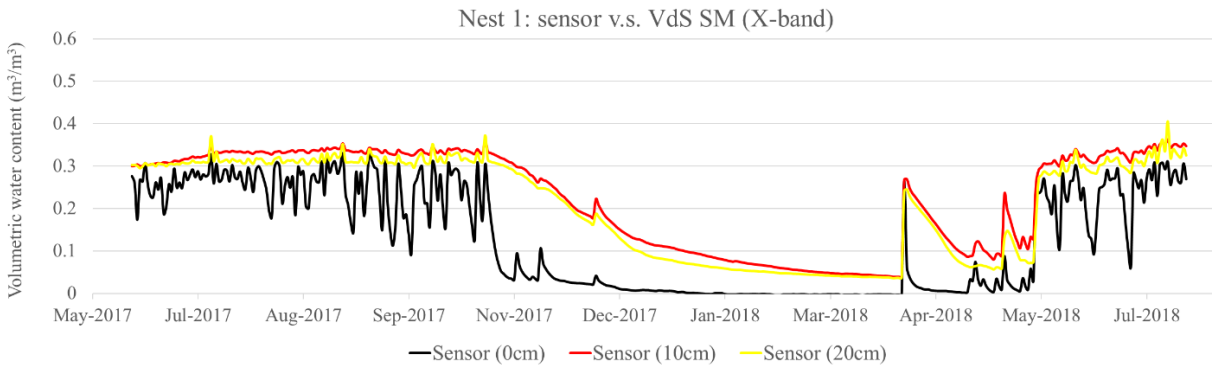

Figure 14: Nest 1: In-situ soil moisture sensor data at 0, 10 and 20cm depth at X-band time overpass (01:30 a.m.) The measurements of the two sensors at 10 and 20cm depth are averaged.

4.4 Sensor calibration

The almost horizontal line in Figure 12 at nest 2 and nest 4 during the period June-September 2017 indicates that the soil is almost fully saturated and is an indicator for sensor calibration. When the soil is fully saturated, all pores are filled with water and the ratio between them is 1. The average sensor measurements at 20cm depth for nest 2, sensor 4 and 5 are 0.446 and 0.429 m^3/m^3 respectively. The porosity of volumetric soil moisture measurements sampled in the field at the same depth is on average 0.422. When the average porosity is divided by the average volumetric water content the results are 1.056 for sensor 4 and 1.016 for sensor 5. This means more water is measured by the in-situ soil moisture sensors compared to the available pore space calculated in the lab. The overestimation is 5.6% for sensor 4 and 1.6% for sensor 5. Decagon provided an accuracy of 3% which seems fair considered that the volumetric soil samples are sampled within 2 meters from the sensors. The difference in sensor 4 is probably the result of a small error in the sampling method. There can be concluded that these sensors work properly.

4.5 Volumetric soil moisture samples compared to in-situ soil moisture sensor measurements

All volumetric soil moisture samples are compared with in-situ soil moisture sensor measurements (Appendix 9.4). In Figure 15 and Figure 16 can be observed that the scattered datapoints are close to the linear Y=X line. For nest 1 can be concluded that there is a good correlation based on the R^2, RMSE and Pearson correlation over depth. Especially at 20cm depth the best correlations are found, see

Figure 17, 18 and Table 4. The volumetric water content displays less variation at deeper depths compared to surface measurements, which is also indicated by the spread in scattered data points present at surface level measurements (Figure 15 and Figure 16).

Table 4 displays all the results for the calculated root mean square errors, Pearson correlations and R^2 correlations. In general, the volumetric soil moisture measurements correspond well to the sensor measurements, again mainly for volumetric soil moisture measurements collected at 10 and 20cm depth. Nest 2 displays the worst results of all nests, this is due to the fact that sensor 2 and sensor 3 were broken for a period of several months, which results in no data. Furthermore there were difficulties with the sensors and logger at this nest at during the fieldwork period, but have been replaced with new equipment.

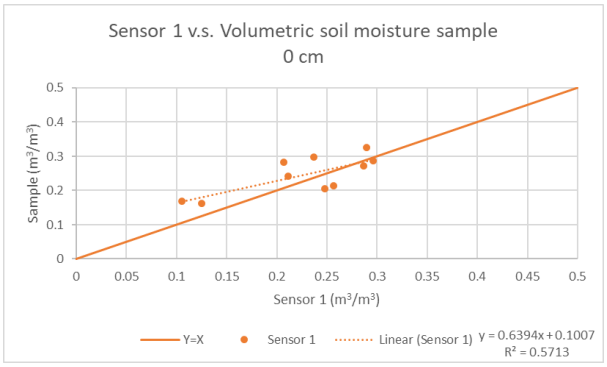

Figure 15: Scatter plot of nest 1, sensor 1 (0 cm).

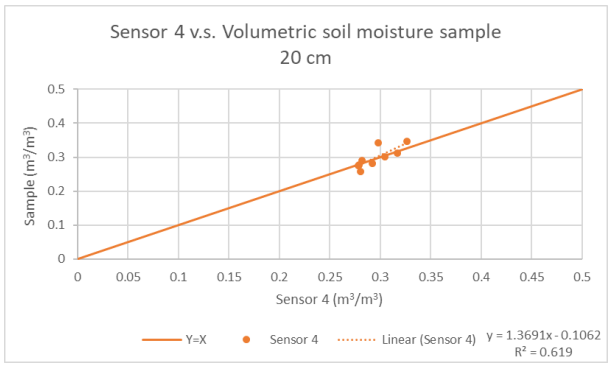

Figure 16: Scatter plot of nest 1, sensor 5 (20 cm).

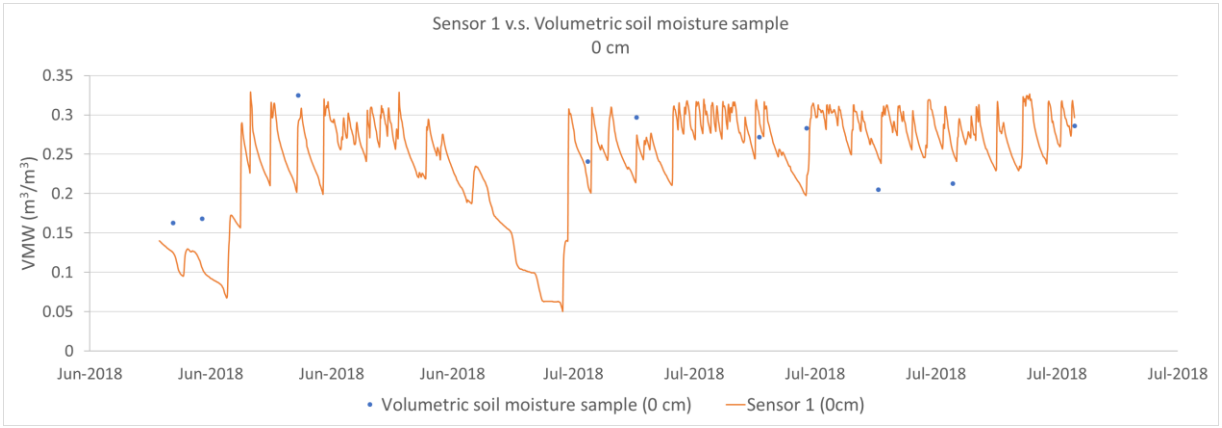

Figure 17: Time series of the nest 1 sensor 1 (0 cm), volumetric soil moisture sample compared to in-situ soil moisture sensor data.

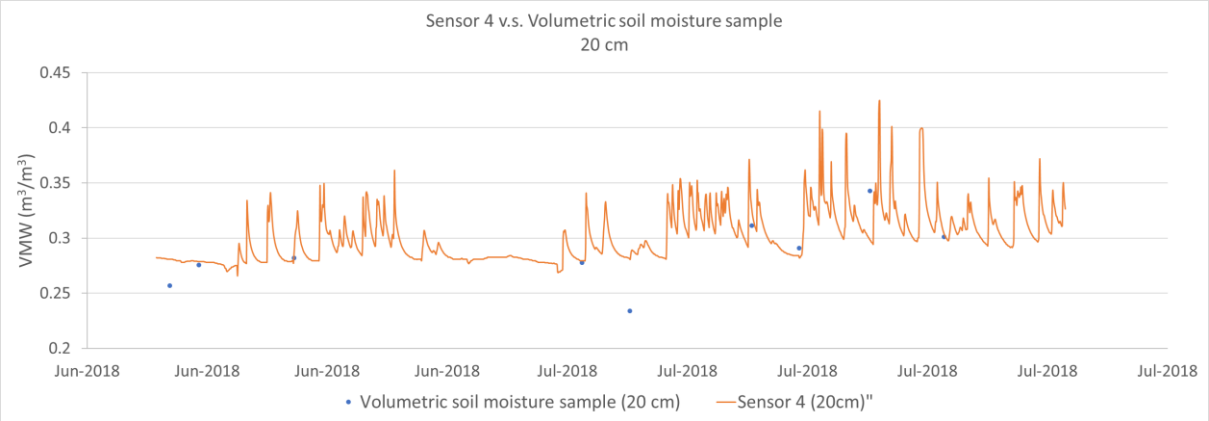

Figure 18: Time series of the nest 1 sensor 4 (20 cm), volumetric soil moisture sample compared to in-situ soil moisture sensor data.

Nest 1	Sensor 1	Sensor 2	Sensor 3	Sensor 4	Sensor 5
Pearson	0.755849	0.753095	0.776223	0.786786	0.846899
RMSE	0.045699	0.06469	0.046758	0.019029	0.027941
R-square	0.5713	0.5672	0.6025	0.619	0.7172
Nest 2	Sensor 1	Sensor 2	Sensor 3	Sensor 4	Sensor 5
Pearson	-0.315	-0.11597	-0.39206	-0.75974	-0.60636
RMSE	0.038117	0.07675	0.075766	0.052704	0.052803
R-square	0.0992	0.0134	0.1537	0.5772	0.3677
Nest 3	Sensor 1	Sensor 2	Sensor 3	Sensor 4	Sensor 5
Pearson	0.216472	0.4683	0.561683	0.704222	0.713111
RMSE	0.035411	0.021115	0.022652	0.011389	0.024749
R-square	0.0469	0.2193	0.3155	0.4959	0.5085
Nest 4	Sensor 1	Sensor 2	Sensor 3	Sensor 4	Sensor 5
Pearson	0.129134	0.13195	0.12095	0.459873	0.362821
RMSE	0.28809	0.036739	0.057633	0.097966	0.102549
R-square	0.0167	0.0174	0.0146	0.2115	0.2075
Nest 5	Sensor 1	Sensor 2	Sensor 3	Sensor 4	Sensor 5
Pearson	0.40438	0.698705	0.73422	0.561835	0.424318
RMSE	0.033913	0.020688	0.026481	0.045339	0.059168
R-square	0.261	0.2832	0.3511	0.3157	0.18

Table 4: Pearson correlations, root mean square errors and R-square correlations. Sensor 1 is at surface level, sensor 2 & 3 at 10cm depth and sensor 4 & 5 at 20cm depth. The colour bar displays the highest correlations in green and the lowest correlations in red.

From Table 4 can be observed that nest 1 displays the best correlations for volumetric soil moisture measurements compared to in-situ soil moisture sensor measurements. Very high Pearson, RMSE and R^2 values are found and especially sensor 5 displays a near perfect fit. Ten out of twenty-five sensors from all nests exceed the RMSE threshold of 0.05 m^3/m^3 for the validation of SMAP satellites

(Colliander et al., 2017). The explanation of a lack of strong correlation is probably the result of the difficulty of collecting reliable volumetric soil moisture samples and the spatial variability between the sensors and the samples. Combined with the calibration done in Chapter 4.4 the sensors monitor in-situ soil moisture content properly, except for nest 2.

4.6 In-situ soil moisture sensor measurements compared to VanderSat satellite soil moisture X & L-band

In-situ soil moisture sensor measurements are validated with VanderSat satellite soil moisture X and L-band (Appendix 9.5). In Figures 19, 20 and 21 the in-situ soil moisture sensor data are displayed for 0, 10 and 20cm depth against VdS SM X and L-band for nest 1. For nest 1 can be observed that the X-band displays the best correlation with the sensor data and the L-band overestimates the soil moisture content (Figure 21). Especially the range and offset match best between X-band and in-situ sensor measurements.

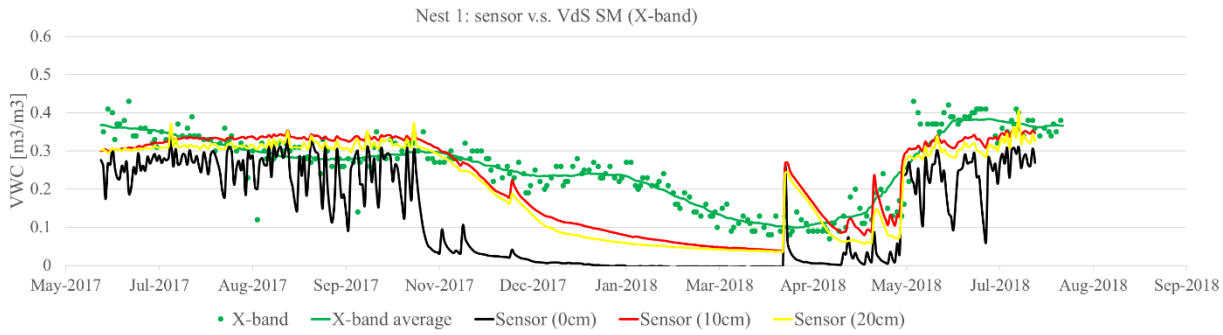

Figure 19: Nest 1: In-situ soil moisture sensor data at 0, 10 and 20 cm depth compared to X-band.

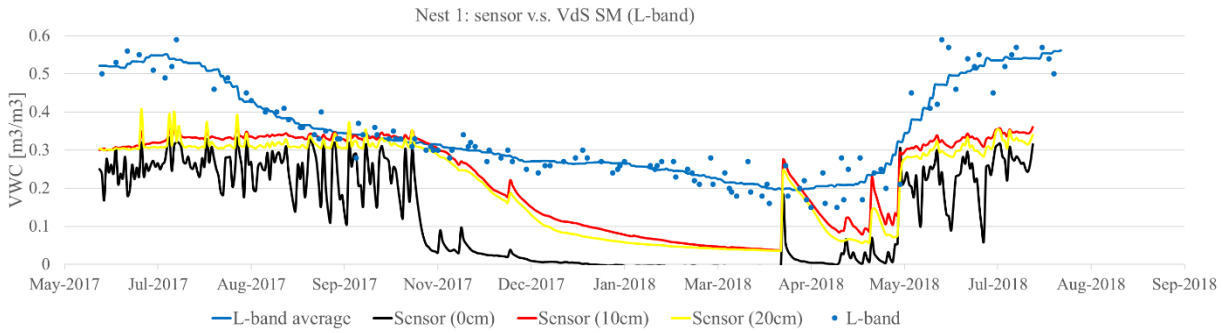

Figure 20: Nest 1: In-situ soil moisture sensor data at 0, 10 and 20 cm depth compared to L-band.

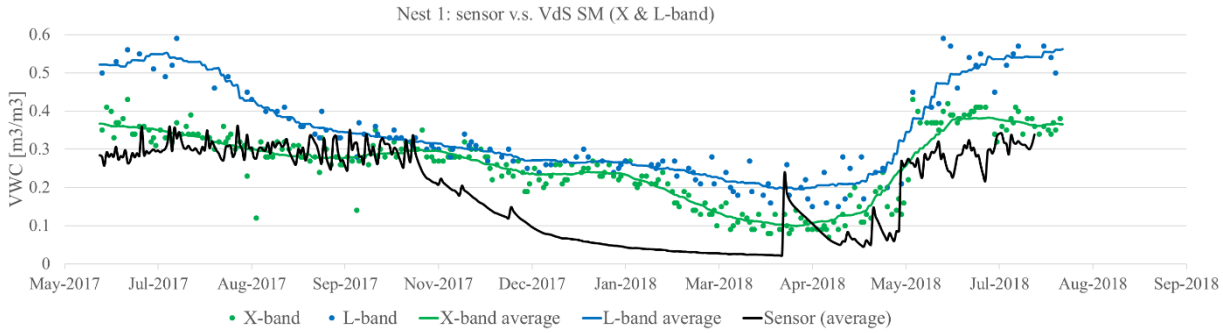

Figure 21: Nest 1: In-situ sensor data averaged over 20 cm depth compared to X and L-band.

Another observation is the that there are outliers present in the X-band scattered data (Figure 21, period of August to September 2017). These values are located significantly far away from the other measurements and the calculated average. Furthermore can be observed that during the cool and hot period from October to January, the X and L-band come close to each other in measuring soil moisture content. During the dry period almost no precipitation takes place, in contrast to the monsoon period. During the monsoon period the X and L-band diverge from each other.

In Figure 22, 23 and 24 the other in-situ soil moisture sensor nest data are displayed against the X and L-band. The same trend can be spotted, during wet monsoon period the L-band diverges from the X-band and measures more soil moisture content. Over the whole year period, the L-band overestimates soil moisture content compared to the X-band. Another observation is the time delay when the drying period starts in late October. The in-situ soil moisture sensor data rapidly decreases and the X and L-band do not match this trend. Nest 5 may be the only exception, where both X and L-band display the same pattern and good response at the transition from dry to wet and vice versa.

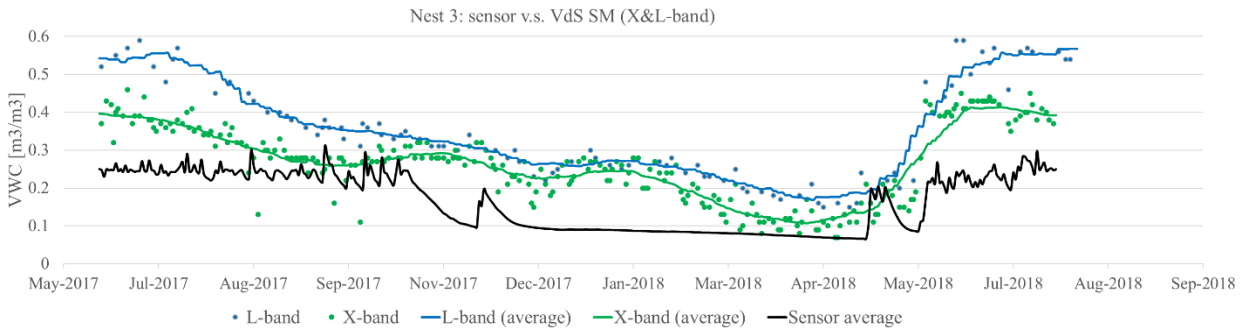

Figure 22: Nest 3 In-situ sensor data averaged over 20cm depth compared to X and L-band measurements.

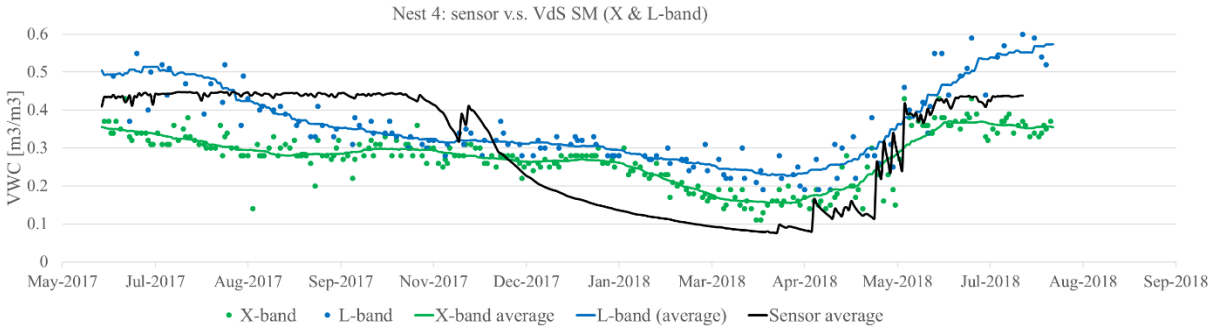

Figure 23: Nest 4 In-situ sensor data averaged over 20 cm depth compared to X and L-band measurements.

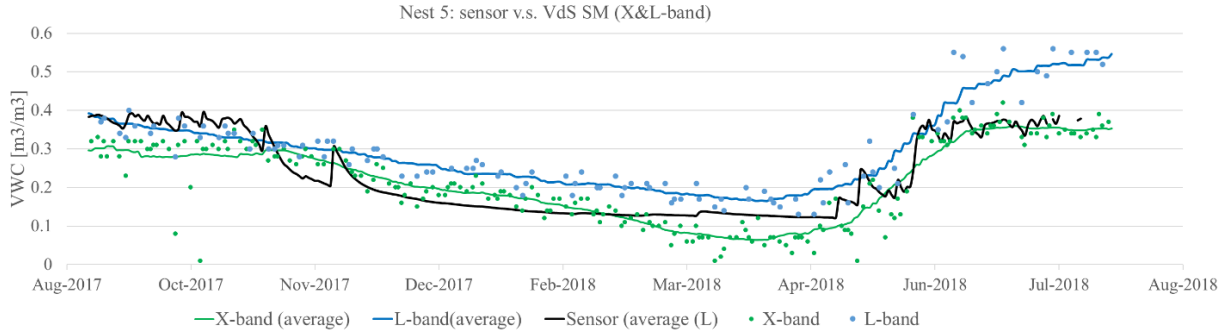

Figure 24: Nest 5 In-situ sensor data averaged over 20 cm depth compared to X and L-band measurements.

In Table 5 all Pearson correlations, root mean square errors and R-square correlations are given for each nest and sensor. From the comparison of all the sensor nests is observed that the highest correlations are found in nest 5 and the lowest correlations in nest 2. All the sensors exceed the critical RMSE of $0.05m^3/m^3$ as given by Colliander et al., 2017 to validate SMAP satellites. The low correlations in nest 2 are again due to noise and missing data in the timeseries of in-situ soil moisture sensor measurements. For nest 5 both the X and L-band indicate very good correlations which can be explained due to the fact that this nest has the highest representation for the environment.

Nest 1	Sensor 1	Sensor 2	Sensor 3	Sensor 4	Sensor 5
Pearson X	0.7029	0.760955	0.769035	0.755937	0.775813
RMSE X	0.15608	0.082543	0.078153	0.096156	0.082542
R-Square X	0.4941	0.5791	0.5914	0.5714	0.6019

Nest 1	Sensor 1	Sensor 2	Sensor 3	Sensor 4	Sensor 5
Pearson L	0.77763	0.723082	0.742335	0.744079	0.752672
RMSE L	0.23037	0.13946	0.14102	0.164793	0.144539
R-Square L	0.6047	0.5228	0.5391	0.5247	0.5569

Nest 2	Sensor 1	Sensor 2	Sensor 3	Sensor 4	Sensor 5
Pearson X	0.64423	0.527572	0.608404	0.43269	0.432688
RMSE X	0.0928	0.102975	0.079336	0.136157	0.120449
R-Square X	0.415	0.2783	0.3702	0.1872	0.1872

Nest 2	Sensor 1	Sensor 2	Sensor 3	Sensor 4	Sensor 5
Pearson L	0.63339	0.693436	0.688964	0.51955	0.543665
RMSE L	0.10333	0.081583	0.086272	0.097751	0.088975
R-Square L	0.232	0.4809	0.4747	0.2699	0.2956

Nest 3	Sensor 1	Sensor 2	Sensor 3	Sensor 4	Sensor 5
Pearson X	0.76006	0.74983	0.723398	0.766614	0.751597
RMSE X	0.13787	0.125462	0.110866	0.117221	0.106625
R-Square X	0.5777	0.5622	0.5233	0.5877	0.5649

Nest 3	Sensor 1	Sensor 2	Sensor 3	Sensor 4	Sensor 5
Pearson L	0.83078	0.827903	0.777046	0.810918	0.810569
RMSE L	0.21322	0.205872	0.190425	0.199127	0.187444
R-Square L	0.6902	0.5881	0.6038	0.6576	0.657

Nest 4	Sensor 1	Sensor 2	Sensor 3	Sensor 4	Sensor 5
Pearson X	0.75927	0.769444	0.771952	0.752851	0.763863
RMSE X	0.12295	0.093251	0.107273	0.113418	0.095315
R-Square X	0.5765	0.592	0.5959	0.5668	0.5835

Nest 4	Sensor 1	Sensor 2	Sensor 3	Sensor 4	Sensor 5
Pearson L	0.7101	0.711288	0.721617	0.710517	0.710908
RMSE L	0.1341	0.091056	0.107293	0.137029	0.108371
R-Square L	0.5042	0.5059	0.5207	0.5048	0.5054

Nest 5	Sensor 1	Sensor 2	Sensor 3	Sensor 4	Sensor 5
Pearson X	0.83112	0.822004	0.846084	0.838072	0.829298
RMSE X	0.06708	0.068318	0.073126	0.06796	0.07178
R-Square X	0.6908	0.6757	0.7159	0.7024	0.6877

Nest 5	Sensor 1	Sensor 2	Sensor 3	Sensor 4	Sensor 5
Pearson L	0.85192	0.838281	0.849456	0.863713	0.845501
RMSE L	0.1052	0.06453	0.05663	0.061715	0.068803
R-Square L	0.7258	0.7027	0.7216	0.746	0.7149

Table 5: Left: X-band. Right: L-band. Pearson correlations, root mean square errors and R-square correlations. Sensor 1 is at surface level, sensor 2 & 3 at 10 cm depth and sensor 4 & 5 at 20 cm depth. The green colour displays the highest correlations, red colour displays the lowest correlations.

4.7 Volumetric soil moisture measurements compared to in-situ soil moisture sensor measurements and VanderSat satellite soil moisture X & L-band

The following results reflect the 8 weeks fieldwork performed during June and July 2018 (see Appendix 9.6). For nest 1, 2 and 3 can be observed in Appendix 9.6 that both the X and L-band measure more soil moisture compared to volumetric soil moisture samples and in-situ soil moisture sensor data. The X-band for these nests is located closer to the volumetric soil moisture measurements and in-situ sensor data. For nest 4 can be observed in Appendix 9.6 that the X-band measures less soil moisture content compared to the in-situ sensor data. The L-band data overestimates the soil moisture content. The X-band of nest 5 has the best correlations with volumetric soil moisture measurements and in-situ sensor measurements, as can be observed in Figure 25 and Figure 26. For the fieldwork period during monsoon conditions can be concluded that the X-band displays better correlations with volumetric soil moisture measurements and in-situ sensor data compared to the L-band.

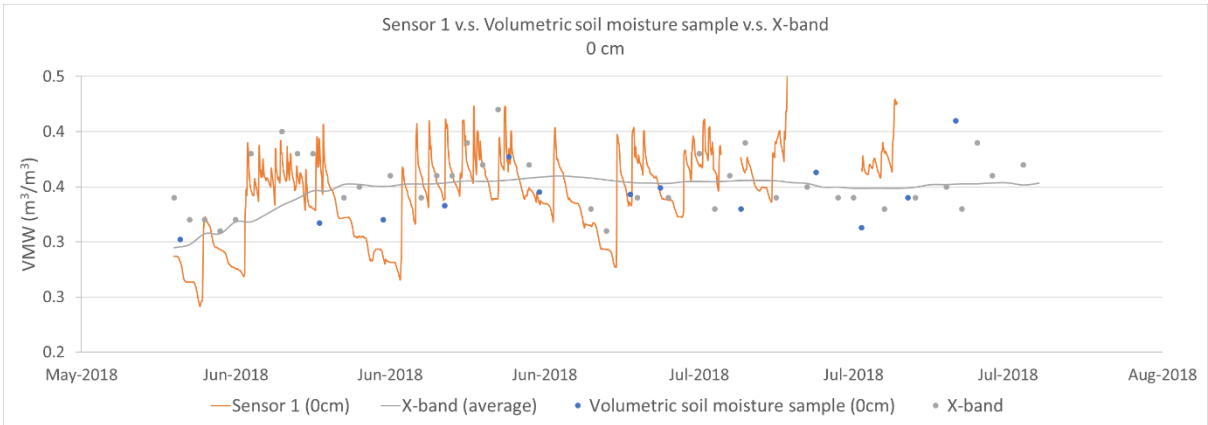

Figure 25: Nest 5 sensor 1 (0 cm): In-situ sensor measurement v.s. volumetric soil moisture sample v.s. X-band

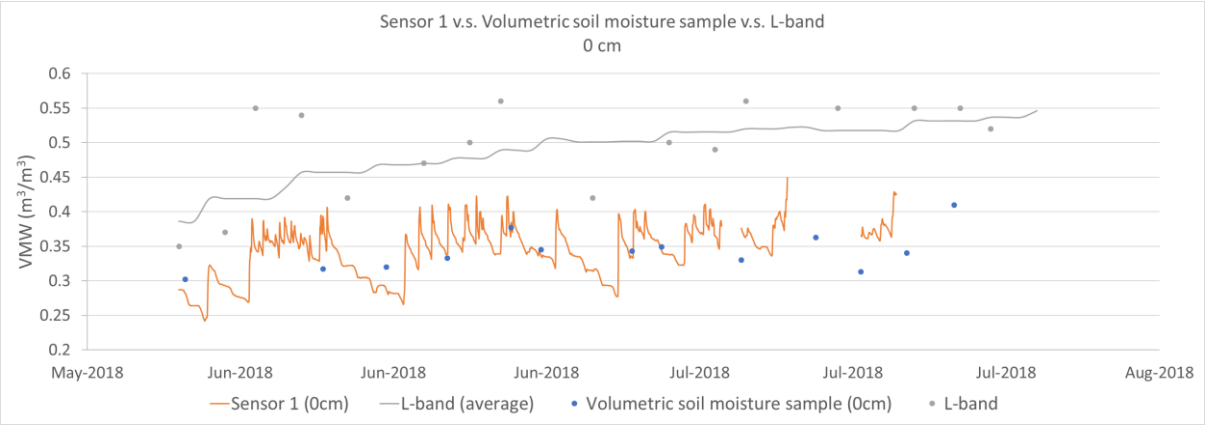

Figure 26: Nest 5 sensor 1 (0 cm): In-situ sensor measurement v.s. volumetric soil moisture sample v.s. L-band

4.8 Vegetation optical depth compared to in-situ soil moisture content and VanderSat satellite soil moisture

In Figure 27 and Figure 28 vegetation optical depth (VOD) is plotted against average in-situ soil moisture content and VanderSat satellite soil moisture X-band for nest 1. The visualizations of all other sensor nests can be found in Appendix 9.7. As discussed before VOD is an indicator for the vegetation water content. During the onset of the wet monsoon period in May VOD and X-band are located far away from each other (Figure 27). When the dry period starts at the end of October, VOD is still increasing and reaches an almost flat line. This indicates that the signal is saturated. This saturation trend can be best observed in nest 2 and nest 4. When the dry period ends the VOD decreases again. The X-band seems to be very sensitive to changes in vegetation water content, and displays a questionable result during the dry period.

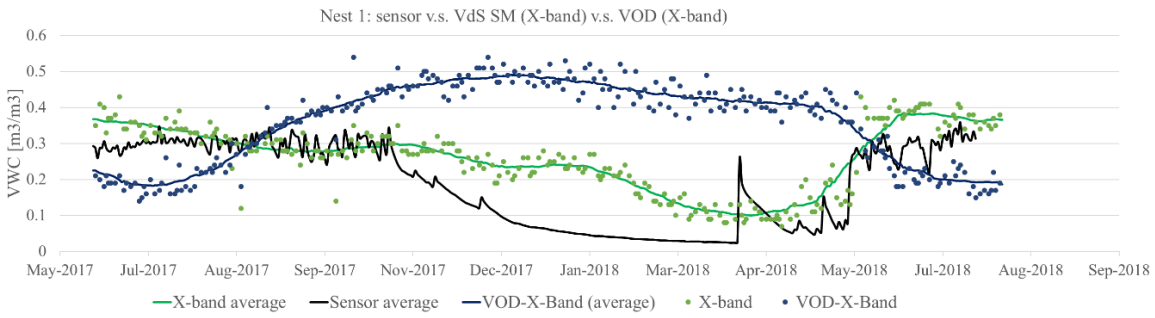

Figure 27: Nest 1: In-situ average soil moisture sensor measurement (0-20cm) compared to VOD and VanderSat X-band. Note: VOD is dimensionless.

For the L-band (Figure 28) the VOD is also very low compared to the L-band. However, during the monsoon period it continues decreasing until the beginning of October. After this period VOD increases over time until a maximum is reached at the end of December and follows a similar pattern compared to the L-band until the monsoon period starts. Saturation is not observed in VOD of the L-band. At the start of the monsoon period in 2018 soil moisture content increases in both sensor data and satellite data, but the VOD does not respond. At the beginning of the monsoon period, high soil moisture content in present in the soil. An explanation could be that it takes quite some time before this moisture is taken up by the vegetation.

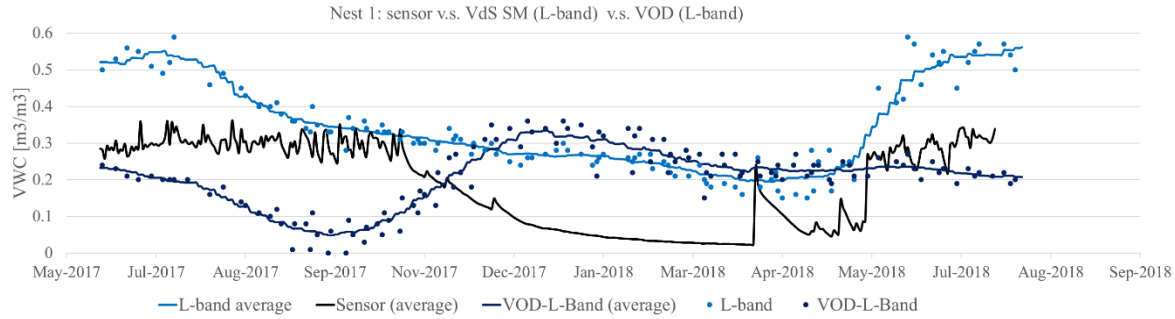

Figure 28: Nest 1: In-situ average soil moisture sensor measurement (0-20cm) compared to VOD and VanderSat L-band. Note: VOD is dimensionless.

In Figures 29, 30, 31 and 32 VOD is plotted for both X and L-band. There can be observed that VOD X and L-band display the same pattern for nest 1, 3 and 4. The main difference observed is the delay in time before VOD L-band increases during the monsoon period compared to the VOD X-band. Nest 5 displays the least variation between X-band and L-band. This is probably because this nest has highest representation for the environment compared to the other sensor nests.

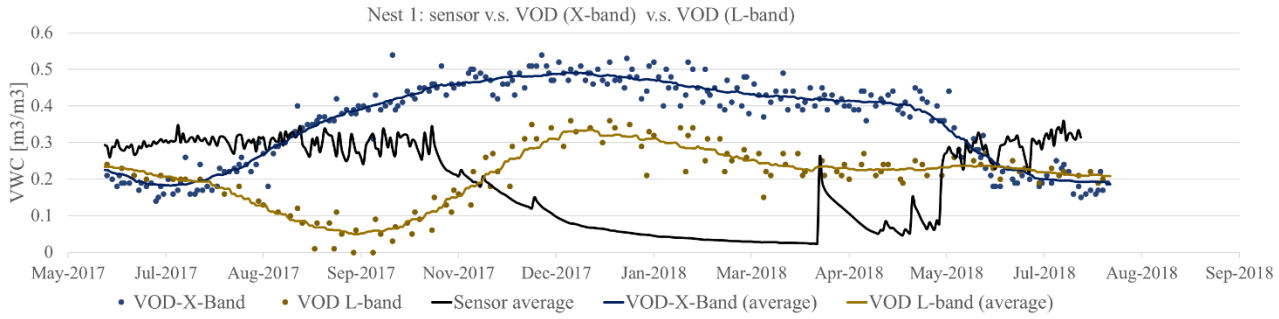

Figure 29: Nest 1: In-situ average soil moisture sensor measurement (0-20cm) compared to VOD X & L-band. Note: VOD is dimensionless.

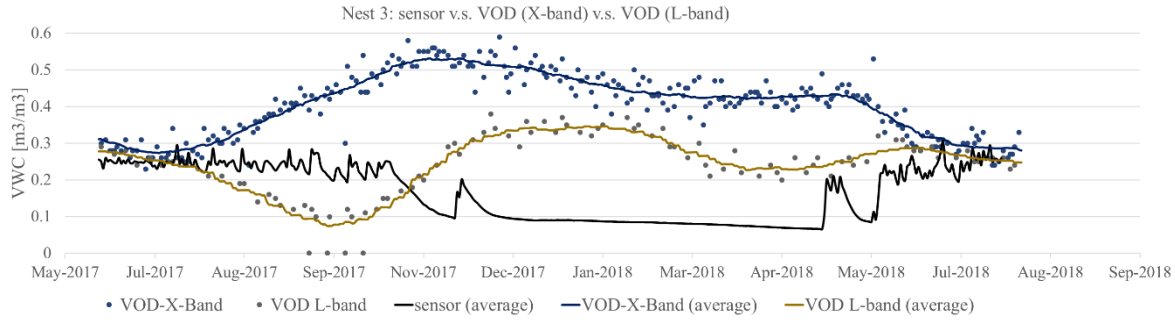

Figure 30: Nest 3: In-situ average soil moisture sensor measurement (0-20cm) compared to VOD X & L-band. Note: VOD is dimensionless.

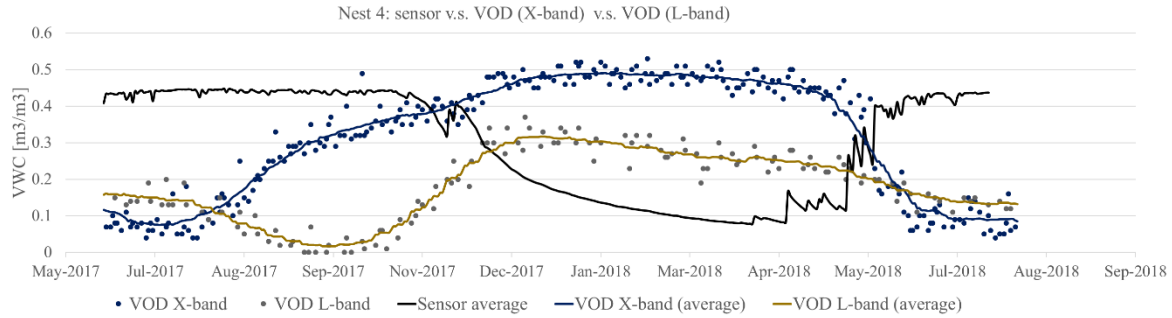

Figure 31: Nest 4: In-situ average soil moisture sensor measurement (0-20cm) compared to VOD X & L-band. Note: VOD is dimensionless.

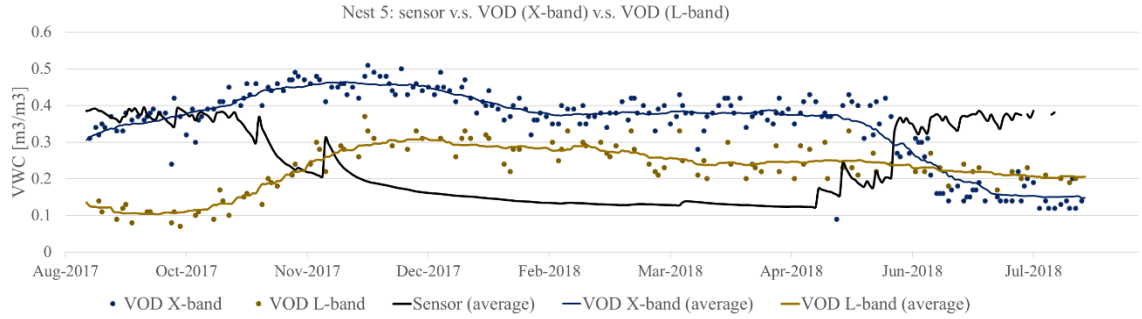

Figure 32: Nest 5: In-situ average soil moisture sensor measurement (0-20cm) compared to VOD X & L-band. Note: VOD is dimensionless.

Chapter 5: Discussion

This chapter focuses on the discussion part of this research. The first part takes the sampling method, collected soil samples, in-situ sensor nests and representativeness of the area into account. The second part focuses on our results compared to other studies. The last part focuses on VOD, NDVI, vegetation (greenness) and satellite obtained soil moisture in contrast to wet and dry seasons.

The sampling method applied during the fieldwork to collect volumetric soil moisture samples was always executed in the same manner, but small differences have been found between samples. An explanation for this could be that volumetric soil moisture measurements were never sampled on the same location as the sensor measures in-situ soil moisture content. The soil was considered spatially uniform within 2 meters distance of the sensors. However, soil moisture content varies due to spatial variations, soil texture, topography and land cover.

Sometimes the Kopecky rings to take soil samples were not completely filled with soil and slipped through the applied quality control. Plastic, roots or pebbles were occasionally present in the volumetric soil samples. Although all samples were visually interpreted in the field and lab, these small uncertainties could not be prevented. Another uncertainty occurred because samples were collected during monsoon season. Heavy showers come and go, monsoon season made collecting reliable volumetric soil moisture measurements difficult.

Only five sensor nests are located in the Bago area. These five sensor nests indicate the quality of satellite obtained soil moisture data. According to Dorigo et al., 2013 the quality of in-situ soil moisture measurements depends on representativeness of an area (does the location of the sensors truly represent the area), the changes that take place in the surrounding environment (like soil compaction) and the sensor system itself (sensitivity due to temperature). More sensor nests with a higher representativeness for the surrounding could give better insight in the validation of the satellite soil moisture data in Bago. Other research found that in-situ soil moisture measurements strongly depend on climate, distinct mean, spatial variability and skewness observed in each climate zone (Li and Rodell, 2013). Spatial variability is also observed in this research. In-situ soil moisture content is measured with 2 sensors at 10cm depth and 2 sensors at 20cm depth. These sensors never measure exactly the same volumetric water content, although they are located close (~30cm) to each other. This means soil moisture varies spatially on decimeter scale.

The difficulty of comparing volumetric soil moisture measurements with in-situ soil moisture sensor data to validate satellite data is mainly the upscaling of point data (volumetric samples and in-situ soil moisture) to a bigger area (satellite obtained soil moisture). Therefore validation of satellite obtained soil moisture data includes scaling errors.

Cui et al., 2017 validated in-situ soil moisture in Genhe, China with LPRM C and X-band with a bias of 0.261–0.576 m^3/m^3. In the same research SMAP resulted in a RMSE of 0.039–0.063 m^3/m^3 compared to in-situ soil moisture measurements. Bindlish et al., 2017 found RMSE of 0.094 m^3/m^3 for LPRM validation with in-situ reference data. The RMSE of Bago for in-situ soil moisture compared to X-band range from 0.067 to 0.156 m^3/m^3 and for L-band 0.0566 to 0.230 m^3/m^3. The results of this research are somewhat lower. This is probably the result of differences in (dense) vegetation, dynamic water bodies, representativeness of the area or a combination of them. To investigate this theory satellite obtained soil moisture is compared with vegetation optical depth and satellite images.

During the onset of monsoon period VOD displays a decreasing trend for X-band. This trend is strange because there would be expected that the water content in the vegetation will increase after a severe time of drought. The VOD L-band displays a decreasing trend during the onset of monsoon and rapidly increases at the end of September. This pattern is more reliable compared to the VOD X-band but there is a time lag observed before the water in taken up by the vegetation. An explanation for this could be the sensitivity of the VOD and model parameters of LPRM. The LPRM becomes severely challenged in areas with dense vegetation. VOD is spatially sampled at 100m, but the algorithm takes the surrounding area into account up to kilometers. Differences in vegetation cover, vegetation density and differences in land use over the year could explain this. Farmers in Myanmar grow rice during the monsoon period and their rice paddies are filled with water. During the dry period the rice paddies are converted into agricultural fields for growing beans and pulses.

A difference in vegetation cover and greenness is observed in satellite obtained images from LANCE Rapid Response MODIS system (NASA) and given in Figure 33. The left part of Figure 33 displays the satellite image of 2015 at the end of the Monsoon period while the right part displays the image at the end of the dry period. There can be observed that at the end of the dry period, vegetation is significantly less in greenness and suffers from the drought. At the end of the monsoon period vegetation is very green and the covered area increased. Figure 34 displays the NDVI (Normalized Difference Vegetation Index) for the research area including all five sensor nests for the period of June 2017 until July 2018. There can be observed that the onset of the monsoon period NDVI rapidly

increases until the end of the monsoon period. During the dry period NDVI keeps decreasing until the start of next monsoon period. The NDVI images corresponds with the satellite images displayed in Figure 33 and Appendix 9.8. The high contrast in greenness between the wet season and dry season also observed and used to discriminate monsoon forests from other forests by combining maximum and minimum annual NDVI (Sen and Ronggao, 2016). These observations are contrasting with the observed vegetation water content (VOD) predicted by the LPRM and therefore more research should be done on this part.

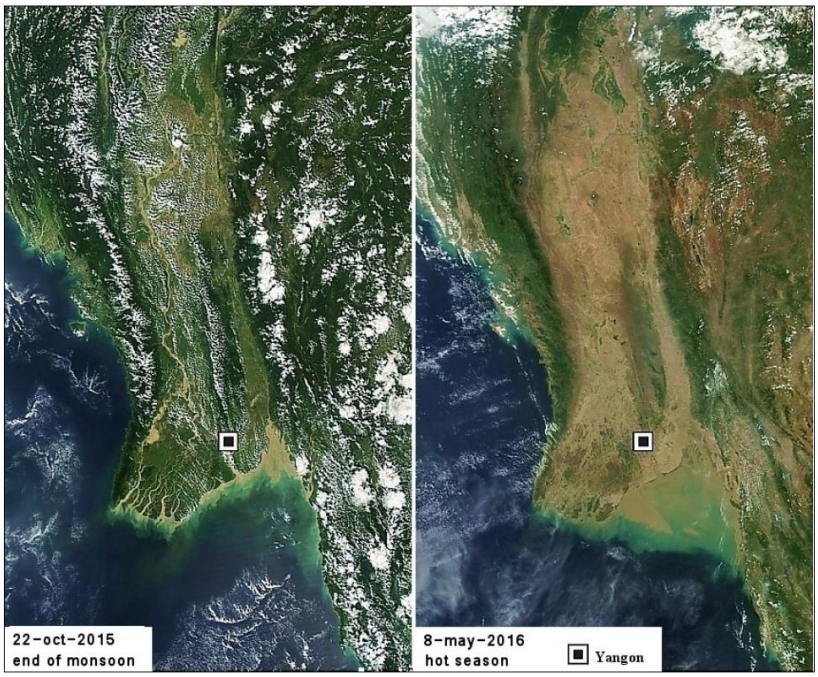

Figure 33: Satellite images obtained from LANCE Rapid Response MODIS system (NASA). Bago is located ~70 km North-East of Yangon.

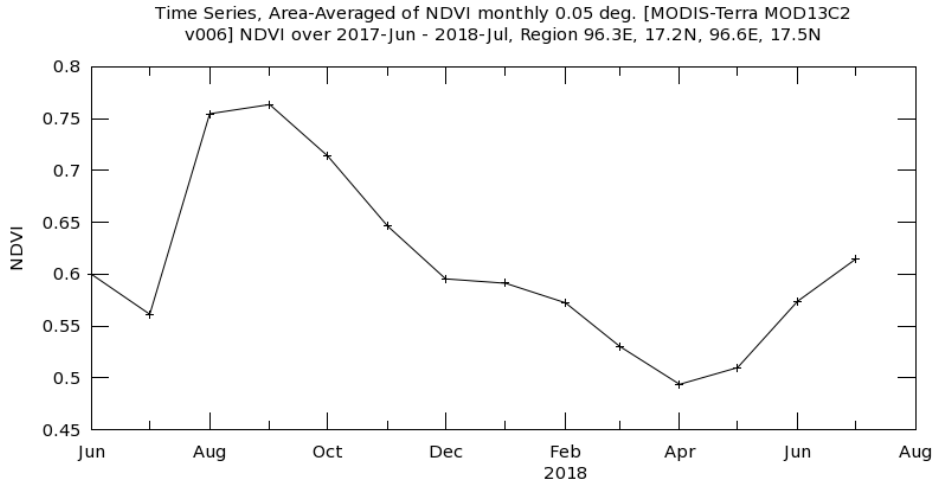

Figure 34: NDVI time series for the period June 2017-July 2018 obtained from Giovanni, NASA.

Chapter 6: Conclusions

In this research volumetric soil moisture samples are validated with in-situ soil moisture sensor data. There can be observed in for example nest 1 (Figure 17 and Figure 18) that volumetric soil samples satisfy the outcome of the in-situ sensor data. Volumetric soil moisture sample measurements are close to the sensor measurement and follow the trend of an increase or decrease in soil moisture content. There can be concluded that RMSE ranges from 0.011 to 0.288 m^3/m^3. From the 25 sensors monitoring in-situ soil moisture content, 10 exceed the critical RMSE threshold value of 0.05 m^3/m^3 used for validation of SMAP satellites (Colliander et al., 2017). The RMSE less than 0.05 m^3/m^3 is exceeded for nest 1 (sensor 2), nest 2 (sensor 2, 3, 4, 5), nest 4 (sensor 1, 3, 4, 5) and nest 5 (sensor 5). The Pearson correlation is found negative for nest 2 and positive for the other nests. Especially nest 1 has very high correlations up to 0.846. Nest 4 has a moderate correlation especially sensor 1, 2 and 3. R^2 correlation ranges from 0.013 to 0.717. The lowest correlations are found in nest 2 and nest 4 sensor 1, 2 and 3. Overall nest 1 displays the highest correlation followed by nest 5. The lack of a decent correlation in nest 2 is the combination of a loss of a lot of in-situ soil moisture sensor data, the completely saturated soil and sensors that did not work properly.

In this research in-situ soil moisture sensor data is validated with VanderSat satellite obtained soil moisture (X and L-band). For the X-band can be concluded that RMSE ranges from 0.067 to 0.156 m^3/m^3. The Pearson correlation ranges from 0.433 to 0.846 and R^2 correlation from 0.1872 to 0.716. For the L-band can be concluded that RMSE ranges from 0.0566 to 0.230 m^3/m^3. The Pearson correlation from 0.519 to 0.864 and the R^2 correlation from 0.232 to 0.746. Both the X and L-band exceed the RMSE threshold value of 0.05 m^3/m^3 used in validations of SMAP satellites (Colliander et al., 2017). Nest 5 displays the highest correlations with in-situ soil moisture sensor data compared to VdS SM X and L-band. This nest has probably the highest representation for the surrounding environment (Appendix 9.1). Nest 1,3 and 4 display also good correlations, especially the X-band. Another conclusion that can be drawn is that L-band predicts higher soil moisture content compared to the X-band. During the wet periods, the difference between X and L-band is higher compared to the dry periods. Especially in November-January the X and L-band come quite close to each other.

From the comparison of volumetric soil moisture measurements with in-situ soil moisture sensor data and VdS SM X and L-band can be concluded that the L-band overestimates soil moisture content during the monsoon period. The X-band displays the best correlations.

In this research satellite obtained soil moisture from the X and L-band is validated over the tropical region of Bago, Myanmar with the use of in-situ soil moisture sensor data and volumetric soil moisture samples. In general, the correlation between satellite obtained soil moisture, in-situ soil moisture sensor data and volumetric soil moisture samples is acceptable. The explanation for a lack of strong correlation is due to the dynamic and complex tropical regio; the representativeness of each sensor nest to the surrounding area, vegetation influences and changes in land use during the year.

Chapter 7: Recommendations

The first recommendation would be to do another fieldwork in the dry period (November-January) because the fieldwork in this research is only done during the wet period. Core validations during the dry and wet period are essential to calculate a better correlation for Pearson, RMSE and R^2. The scatter plots indicate already good correlations but the spread in data will be much higher.

The second recommendation would be to move nest 2 to another location, this nest displays the largest errors in data, the soil at 10 and 20cm depth is fully saturated during monsoon conditions and it is located too close to a big canal (approximately 20m). This is not a reliable condition for validating in-situ soil moisture data to the satellite obtained soil moisture. This is mainly because this product is spatially sampled at 100m and the algorithm takes the surrounding area into account although water bodies are filtered out their presence still influences the signal.

The third recommendation would be to leave the other sensor nests in place to measure for at least 2 more years. This results in a better statistical distribution as recommended by Jackson et al., 2012. Also, the behaviour of the drying period and the start of the monsoon can be compared over the years.

The fourth recommendation would be to verify in-situ soil moisture sensor data with precipitation and temperature data. Sensors are available on the market that measure soil moisture content and temperature data simultaneously. Curious spikes in soil moisture content can be verified with precipitation data.

The fifth recommendation would be to investigate the behaviour of soil moisture, VOD and the influence of vegetation. The model parameters of the LRPM have to be checked on sensitivity and the used soil texture maps from the FAO. Satellite obtained soil moisture is sometimes higher compared to calculated pore space obtained from volumetric soil moisture samples collected in the field. For

future research it is also highly recommended to select more representative areas to install in-situ soil moisture sensors to validate satellite obtained soil moisture.

The sixth and last recommendation would be to instruct some employees of ITC Bago how to collect volumetric soil moisture measurements and send them a soil sampling kit. This way soil sampling can be done for example once a week at every nest and a yearly timeseries can be captured. Labour is cheap in Myanmar and the sampling method not too difficult to explain.

Chapter 8: References

Al Bitar, A., Leroux, D., Kerr, Y. H., Merlin, O., Richaume, P., Sahoo, A., & Wood, E. F. (2012). Evaluation of SMOS soil moisture products over continental U.S. Using the SCAN/SNOTEL network. *IEEE Transactions on Geoscience and Remote Sensing*, *50*(5 PART 1), 1572–1586. https://doi.org/10.1109/TGRS.2012.2186581

Benninga, H. J. F., Carranza, C. D. U., Pezij, M., Van Santen, P., Van Der Ploeg, M. J., Augustijn, D. C. M., & Van Der Velde, R. (2018). The Raam regional soil moisture monitoring network in the Netherlands. *Earth System Science Data*, *10*(1), 61–79. https://doi.org/10.5194/essd-10-61-2018

Bindlish, R., Cosh, M. H., Jackson, T. J., Koike, T., Fujii, H., Chan, S. K., … Coopersmith, E. J. (2017). GCOM-W AMSR2 Soil Moisture Product Validation Using Core Validation Sites. *IEEE Journal of Selected Topics in Applied Earth Observations and Remote Sensing*, 1–11. https://doi.org/10.1109/JSTARS.2017.2754293

Burgin, M. S., Colliander, A., Njoku, E. G., Chan, S. K., Cabot, F., Kerr, Y. H., … Yueh, S. H. (2017). A Comparative Study of the SMAP Passive Soil Moisture Product with Existing Satellite-Based Soil Moisture Products. *IEEE Transactions on Geoscience and Remote Sensing*, *55*(5), 2959–2971. https://doi.org/10.1109/TGRS.2017.2656859

Chan, S. K., Bindlish, R., O'Neill, P. E., Njoku, E., Jackson, T., Colliander, A., … Kerr, Y. (2016). Assessment of the SMAP Passive Soil Moisture Product. *IEEE Transactions on Geoscience and Remote Sensing*, *54*(8), 4994–5007. https://doi.org/10.1109/TGRS.2016.2561938

Colliander, A., Jackson, T. J., Bindlish, R., Chan, S., Das, N., Kim, S. B., … Yueh, S. (2017). Validation of SMAP surface soil moisture products with core validation sites. Remote Sensing of Environment, 191(March), 215–231. https://doi.org/10.1016/j.rse.2017.01.021

Crow, W. T., Berg, A. A., Cosh, M. H., Loew, A., Mohanty, B. P., Panciera, R., … Walker, J. P. (2012). Upscaling Sparse Ground-Based Soil Moisture Observations for the Validation of Coarse-Resolution Satellite Soil Moisture Products. Reviews of Geophysics, 50, 1–20. https://doi.org/10.1029/2011RG000372.1.INTRODUCTION

Cui, C., Xu, J., Zeng, J., Chen, K. S., Bai, X., Lu, H., … Zhao, T. (2018). Soil moisture mapping from satellites: An intercomparison of SMAP, SMOS, FY3B, AMSR2, and ESA CCI over two dense network regions at different spatial scales. *Remote Sensing*, *10*(1). https://doi.org/10.3390/rs10010033

Das, N. N., Entekhabi, D., Njoku, E. G., Shi, J. J. C., Johnson, J. T., & Colliander, A. (2014). Tests of the SMAP combined radar and radiometer algorithm using airborne field campaign observations and simulated data. *IEEE Transactions on Geoscience and Remote Sensing*, *52*(4), 2018–2028. https://doi.org/10.1109/TGRS.2013.2257605

Decagon Devices, I. (2015a). Em50 Digital Data Logger. Retrieved November 5, 2017, from https://www.decagon.com/en/data-loggers-main/data-loggers/em50-digitalanalog-datalogger/ Decagon Devices, I. (2015b). GS1 VWC | Soil Moisture Sensor | Decagon Devices. Retrieved November 5, 2017, from https://www.decagon.com/en/soils/volumetric-water-contentsensors/gs1/

Decagon Devices, I. (2015b). GS1 VWC | Soil Moisture Sensor | Decagon Devices. Retrieved November 5, 2017, from https://www.decagon.com/en/soils/volumetric-water-contentsensors/gs1/

De Jeu, R. A. M., Dorigo, W., van der Schalie, R., Chung, D., Wagner, W., & Kidd, R. (2017). ESA Climate Change Initiative Phase II - Soil Moisture: Algorithm Theoretical Baseline Document (ATBD), (Version 03.2), 1–25.

De Jeu, R. A. M., Holmes, T. R. H., Parinussa, R. M., & Owe, M. (2014). A spatially coherent global soil moisture product with improved temporal resolution. *Journal of Hydrology*, *516*, 284–296. https://doi.org/10.1016/j.jhydrol.2014.02.015

De Jeu, R. A. M., & de Nijs, A. (2017). Evaluatie van hoge resolutie satelliet bodemvochtproducten met behulp van grondwaterstandmetingen. *Stromingen*, *28*(2), 3–14.

De Jeu, R. A. M., Wagner, W., Holmes, T. R. H., Dolman, A.J., Van De Giesen, N.C., Friesen, J. (2008). Global Soil Moisture Patterns Observed by Space Borne Microwave Radiometers and Scatterometers, 399–420. https://doi.org/10.1007/s10712-008-9044-0

De Lange, W. J., Prinsen, G. F., Hoogewoud, J. C., Veldhuizen, A. A., Verkaik, J., Oude Essink, G. H. P., … Kroon, T. (2014). An operational, multi-scale, multi-model system for consensus-based, integrated water management and policy analysis: The Netherlands Hydrological Instrument. *Environmental Modelling and Software*, *59*, 98–108. https://doi.org/10.1016/j.envsoft.2014.05.009

Dorigo, W. A., Gruber, A., De Jeu, R. A. M., Wagner, W., Stacke, T., Loew, A., … Kidd, R. (2015). Evaluation of the ESA CCI soil moisture product using ground-based observations. *Remote Sensing of Environment*, *162*, 380–395. https://doi.org/10.1016/j.rse.2014.07.023

Dorigo, W. A., Wagner, W., Hohensinn, R., Hahn, S., Paulik, C., Xaver, A., … Jackson, T. (2011). The International Soil Moisture Network: A data hosting facility for global in situ soil moisture measurements. *Hydrology and Earth System Sciences*, *15*(5), 1675–1698. https://doi.org/10.5194/hess-15-1675-2011

Dorigo, W. A., Xaver, A., Vreugdenhil, M., Gruber, A., Hegyiová, A., Sanchis-Dufau, A. D., … Drusch, M. (2013). Global Automated Quality Control of In Situ Soil Moisture Data from the International Soil Moisture Network. *Vadose Zone Journal*, *12*(3), 0. https://doi.org/10.2136/vzj2012.0097

Entekhabi, D., Njoku, E. G., O'Neill, P. E., Kellogg, K. H., Crow, W. T., Edelstein, W. N., … Van Zyl, J. (2010). The soil moisture active passive (SMAP) mission. *Proceedings of the IEEE*, *98*(5), 704–716. https://doi.org/10.1109/JPROC.2010.2043918

Entekhabi, D., Yueh, Si., O'Neil, P. E., Kellogg, K. H., Allen, A., Bindlish, R., & Administration, N. A. and S. (2014). SMAP Handbook. *Mapping Soil Moisture and Freeze/Thaw from Space*, 192.

Escorihuela, M. J., Chanzy, A., Wigneron, J. P., & Kerr, Y. H. (2010). Effective soil moisture sampling depth of L-band radiometry: A case study. *Remote Sensing of Environment*, *114*(5), 995–1001. https://doi.org/10.1016/j.rse.2009.12.011

Fredlund, D. G. and Rahardjo, H.: Soil mechanics for unsaturated soil., JohnWiley and Sons, New York, 1993.

Garrison, J., Lin, Y. C., Nold, B., Piepmeier, J. R., Vega, M. A., Fritts, M., … Knuble, J. (2017). Remote sensing of soil moisture using P-band signals of opportunity (SoOp): Initial results. *International Geoscience and Remote Sensing Symposium (IGARSS)*, *2017–July*, 4158–4161. https://doi.org/10.1109/IGARSS.2017.8127917

Gouweleeuw, B. T. (2000). Satellite passive microwave surface moisture monitoring. Retrieved from Http://www.hydrology.nl/images/docs/dutch/2000.01.20_Gouweleeuw.pdf

Hillel, D. (1998). Environmental Soil Physics. Academic Press, San Diego. 771 pp.

Hipp J.E. (1974) Soil electromagnetic parameters as functions of frequency, soil density, and soil moisture. In: Proceedings of the IEEE 62:98–103

Jackson, T. J., Bindlish, R., Cosh, M. H., Zhao, T., Starks, P. J., Bosch, D. D., … Leroux, D. (2012). Validation of soil moisture and Ocean Salinity (SMOS) soil moisture over watershed networks in the U.S. IEEE Transactions on Geoscience and Remote Sensing, 50(5 PART 1), 1530–1543. https://doi.org/10.1109/TGRS.2011.2168533 Jackson, T. J., Colliander, A., Kimball, J., Reichle, R., Crow, W., Entekhabi, D., & Neill, P. O. (2012). Soil Moisture Active Passive (SMAP) Mission - Science Data Calibration and Validation Plan. Retrieved from https://smap.jpl.nasa.gov/files/smap2/CalVal_Plan_120706_pub.pdf

Kerr, Y. H., Al-Yaari, A., Rodriguez-Fernandez, N., Parrens, M., Molero, B., Leroux, D., … Wigneron, J. P. (2016). Overview of SMOS performance in terms of global soil moisture monitoring after six years in operation. *Remote Sensing of Environment*, *180*, 40–63. https://doi.org/10.1016/j.rse.2016.02.042

Karthikeyan, L., Pan, M., Wanders, N., Kumar, D. N., & Wood, E. F. (2017). Four decades of microwave satellite soil moisture observations: Part 2. Product validation and inter-satellite comparisons. *Advances in Water Resources*, *109*, 236–252. https://doi.org/10.1016/j.advwatres.2017.09.010

Lakhankar, T., Jones, A., Combs, C., Sengupta, M., Haar, T., & Khanbilvardi, R. (2010). Analysis of Large Scale Spatial Variability of Soil Moisture Using a Geostatistical Method. *Sensors*, *10*(1), 913–932. https://doi.org/10.3390/s100100913

Li, B., & Rodell, M. (2013). Spatial variability and its scale dependency of observed and modeled soil moisture over different climate regions. *Hydrology and Earth System Sciences*, *17*(3), 1177–1188. https://doi.org/10.5194/hess-17-1177-2013

Liu, Y. Y., Dijk, A. I. J. M. Van, Miralles, D. G., Mccabe, M. F., Evans, J. P., Jeu, R. A. M. De, … Restrepo-coupe, N. (2018). Remote Sensing of Environment Enhanced canopy growth precedes senescence in 2005 and 2010 Amazonian droughts. *Remote Sensing of Environment*, *211*(April), 26–37. https://doi.org/10.1016/j.rse.2018.03.035

Liu, Y. Y., Dorigo, W. A., Parinussa, R. M., De Jeu, R. A. M., Wagner, W., McCabe, M. F., … Van Dijk, A. I. J. M. (2012). Trend-preserving blending of passive and active microwave soil moisture retrievals. *Remote Sensing of Environment*, *123*(October 2006), 280–297. https://doi.org/10.1016/j.rse.2012.03.014

Maidment, D. R. (1993). Handbook of Hydrology. New York, no. 28, 1424. https://doi.org/10.1016/0141-4607(86)90100-9

Meesters, A. G. C. A., Jeu, R. A. M. De, & Owe, M. (2005). Analytical Derivation of the Vegetation Optical Depth From the Microwave Polarization Difference Index, *2*(2), 121–123.

Mo, K. C. (2008). Model-Based Drought Indices over the United States. *Journal of Hydrometeorology*, *9*(6), 1212–1230. https://doi.org/10.1175/2008JHM1002.1

Mohanty, B. P., Cosh, M. H., Lakshmi, V., & Montzka, C. (2017). Soil Moisture Remote Sensing: State-of-the-Science. *Vadose Zone Journal*, *16*(1), 0. https://doi.org/10.2136/vzj2016.10.0105

Naing, M. M. (2005). Paddy field irrigation systems in Myanmar. Retrieved from http://www.fao.org/world/regional/rap/publication_catalogue.asp%5Cnhttp://ovidsp.ovid.com/ovidweb.cgi?T=JS&CSC=Y&NEWS=N&PAGE=fulltext&D=caba6&AN=20083287669%5Cnhttp://library.wur.nl/sfx_local?sid=OVID:cabadb&id=pmid:&id=doi:&issn=1014-191X&isbn=&volume=&i

Owe, M., De Jeu, R., & Walker, J. (2001). A methodology for surface soil moisture and vegetation optical depth retrieval using the microwave polarization difference index. IEEE Transactions on Geoscience and Remote Sensing, 39(8), 1643–1654. https://doi.org/10.1109/36.942542

Owe, M., R. D. Jeu, and T. Holmes (2008), Multisensor historical climatology of satellite-derived global land surface moisture, J. Geophys. Res., 113, F01002, doi:10.1029/2007JF000769.

Pathe, C., Wagner, W., Sabel, D., Doubkova, M., & Basara, J. B. (2009). Using ENVISAT ASAR global mode data for surface soil moisture retrieval over Oklahoma, USA. *IEEE Transactions on Geoscience and Remote Sensing*, *47*(2), 468–480. https://doi.org/10.1109/TGRS.2008.2004711

Robock, A., Vinnikov, K. Y., Srinivasan, G., Entin, J. K., Hollinger, S. E., Speranskaya, N. A., et al. (2000). The global soilmoisturedata bank. Bulletin of theAmericanMeteorological Society, 81,1281–1299.

Schmugge TJ, Neil O, Wang PE Jr (1986) Passive microwave soil moisture research. IEEE Trans Geosci Remote Sens 24:12–22. doi:10.1109/TGRS.1986.289584

Sen, L. I. N., & Ronggao, L. I. U. (2016). A Simple Method to Extract Tropical Monsoon Forests Using NDVI Based on MODIS Data: A Case Study in South Asia and Peninsula Southeast Asia, *26*(1), 22–34. https://doi.org/10.1007/s11769-015-0789-3

Seneviratne, S. I., Corti, T., Davin, E. L., Hirschi, M., Jaeger, E. B., Lehner, I., … Teuling, A. J. (2010). Investigating soil moisture-climate interactions in a changing climate: A review. *Earth-Science Reviews*, *99*(3–4), 125–161. https://doi.org/10.1016/j.earscirev.2010.02.004

Sheffield, J., & Wood, E. F. (2007). Characteristics of global and regional drought, 1950-2000: Analysis of soil moisture data from off-line simulation of the terrestrial hydrologic cycle. *Journal of Geophysical Research Atmospheres*, *112*(17), 1–21. https://doi.org/10.1029/2006JD008288

van der Schalie, R., de Jeu, R., Rodríguez-Fernández, N., Al-Yaari, A., Kerr, Y., Wigneron, J. P., … Drusch, M. (2018). The effect of three different data fusion approaches on the quality of soil

moisture retrievals from multiple passive microwave sensors. *Remote Sensing*, *10*(1). https://doi.org/10.3390/rs10010107

World resources institute 2007, Earth Trends: Environmental information, Washington D.C.

Zin, E. E. (2017). Myanmar Climate Report

Zhou, L., Tian, Y., Myneni, R.B., Ciais, P., Saatchi, S., Liu, Y.Y., et al., 2014. Widespread decline of Congo rainforest greenness in the past decade. Nature 509, 86–90.

Chapter 9: Appendix

9.1 Description of sensor nests

Nest 1: ITC (17°18'50 N 96°27'12 E)

This nest is located in the gardens of ITC. The location is on a grass field and surrounded by a big fence. Next to soil moisture sensors are several instruments are present measuring precipitation and evaporation. A rain gauge from Disdro is located here measuring raindrops and intensity. The soil consists of a sandy upper layer of approximately 5cm and below that a relatively uniform silty clay layer. The soil looks clean and no dirt is found.

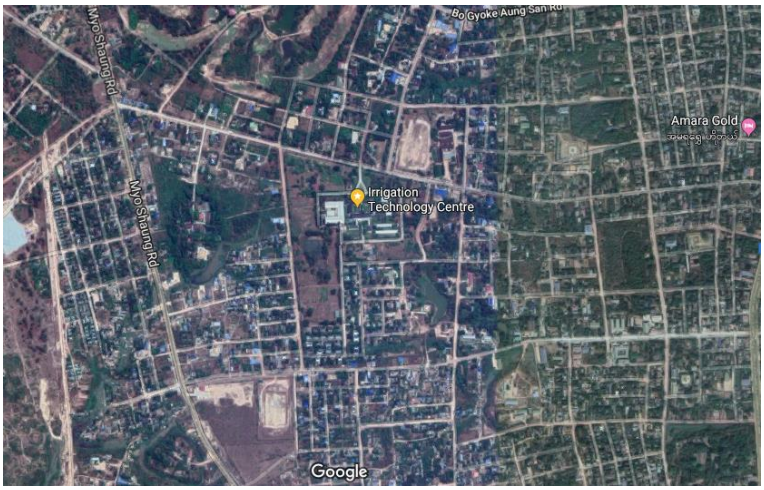

Figure 35: Soil profile of nest 1. Figure 36: Area around nest 1. Yellow point indicates the sensor nest. Source: Google maps.

Nest 2: Tawa (17°12'56 N 96°29'52 E)

This nest is located close (~20m) to a canal that connects to the Bago river. The sensors are located on a grass land and the surrounding consists mainly of rice paddies, farm land and canal. Close to the sensors are instruments to measure rainfall and evaporation. The location is surrounded by a big fence. The soil consists of and sand clay upper layer of 10cm and below a thick clay layer. At 10 and 20cm

depth the soil is very wet and water seeps from the pores. It appears completely saturated.

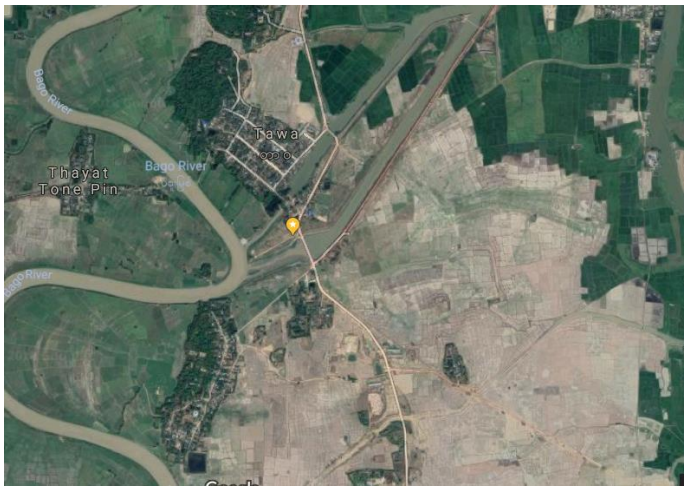

Figure 37: Soil profile of nest 2. Figure 38: Area around nest 2. Yellow point indicates the sensor nest. Source: Google maps.

Nest 3: Alaigni (17°15’31 N 96°20’33 E)

This nest is located close to an artificial reservoir which is used for fresh water storage. The sensors are installed on a property of ITC and covered with a fence. The surrounding environment is densely vegetated with all kinds of threes, bushes and grass. No other instruments are present near the sensors. The soil consists of a uniform layer of silty sand. The soil is relatively dry compared to the other nests.

Figure 39: Nest 3 under a tree. Figure 40: Area around nest 3. Yellow point indicates the sensor nest. Source: Google maps.

Nest 4: Tha Nat Pin (17°17’31 N, 96°34’23 E)

This nest is located in a small village called Tha Nat Pin. The sensors are located in a compound of ITC and several other instruments are present to measure rainfall. The sensors are covered by a fence. The surrounding area consists of many small houses, roads, a small reservoir and many different kinds of vegetation. The soil is very saturated and consist of sandy clay. Plastic trash is abundant and many pieces of gravel or pebbles are found during the soil sampling.

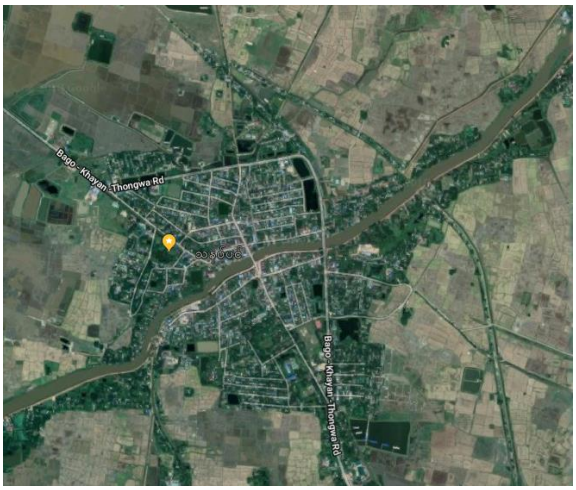

Figure 41: Nest 4. Figure 42: Area around nest 4. Yellow point indicates the sensor nest. Source: Google maps.

Nest 5: Hpa Yar Gyi (17°27'58 N 96°31'49 E)

This nest is located close to the main road from Bago to Hpa Yar Gyi. The sensors are located on a compound of ITC. No other instruments are present monitoring rain data. The sensors are covered by a small bamboo fence and kept safe by people living there. Within a few meters from this nest a big termite mound is present, as well as an artificial lake of approximately 20m by 25m. The surrounding consists of farmland for rice production. The soil consists of silty clay. Many roots are present in the soil.

Figure 43: Me downloading data at nest 5. Figure 44: Area around nest 1. Yellow point indicates the sensor nest. Source: Google maps.

9.2 Bulk density plots (outliers removed)

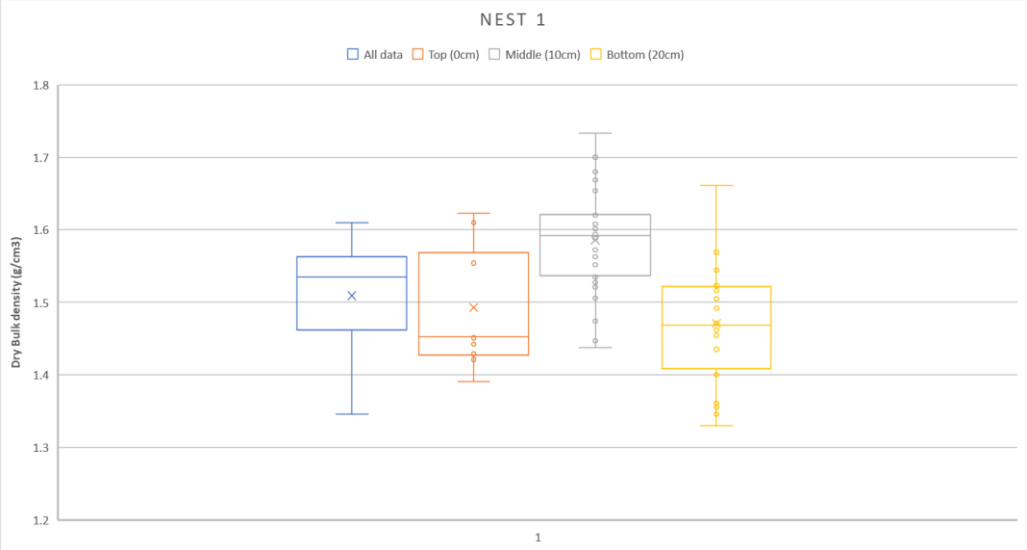

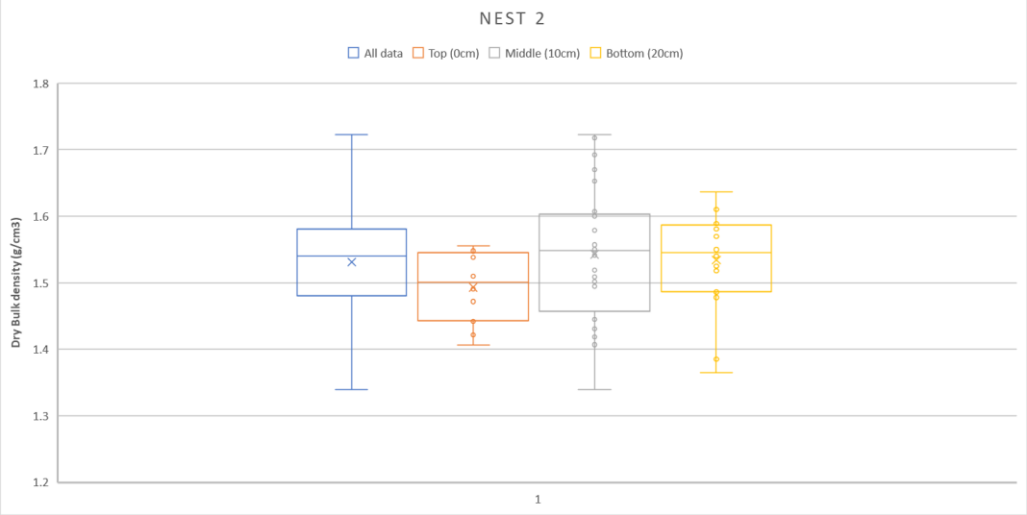

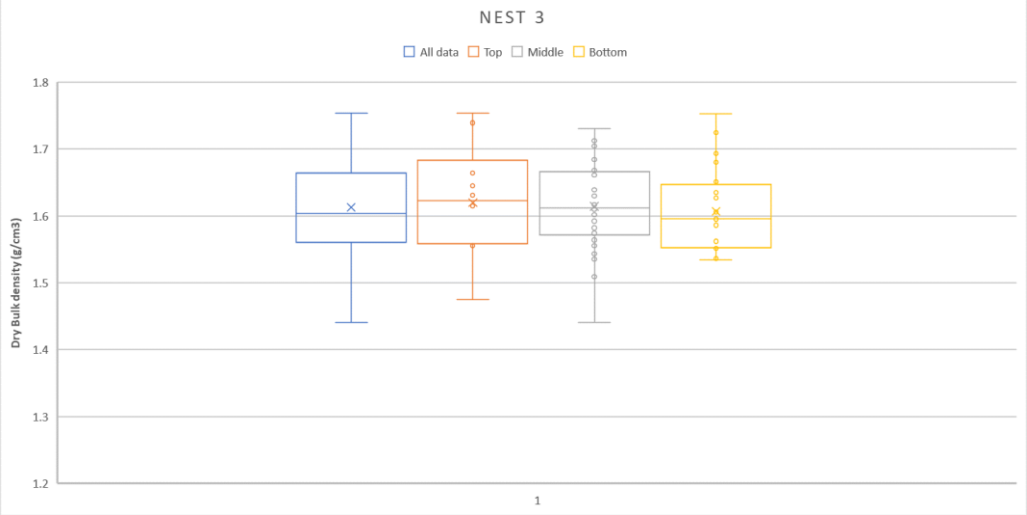

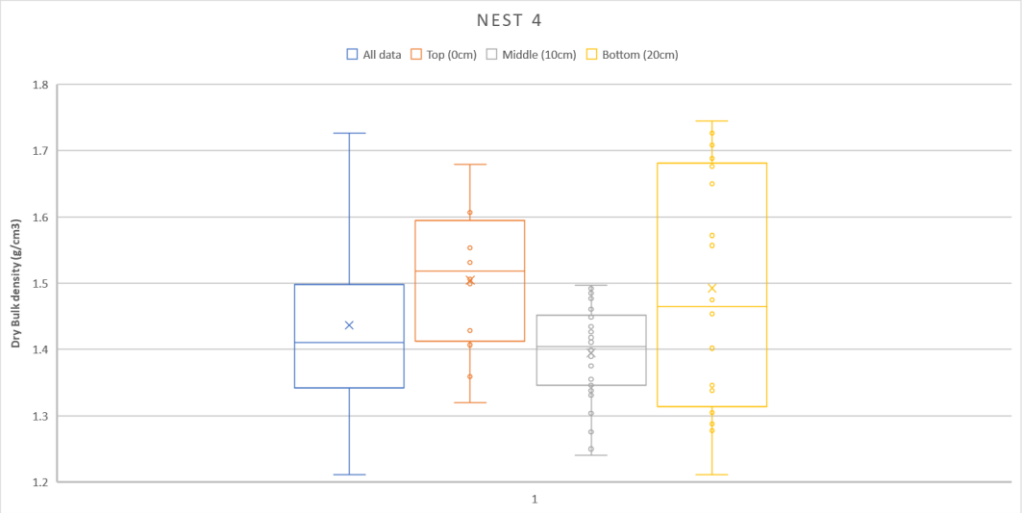
NEST 4
All data
Top (0cm)
Middle (10cm)
Bottom (20cm)
Dry Bulk density (g/cm3)
1.8
1.7
1.6
1.5
1.4
1.3
1.2
1

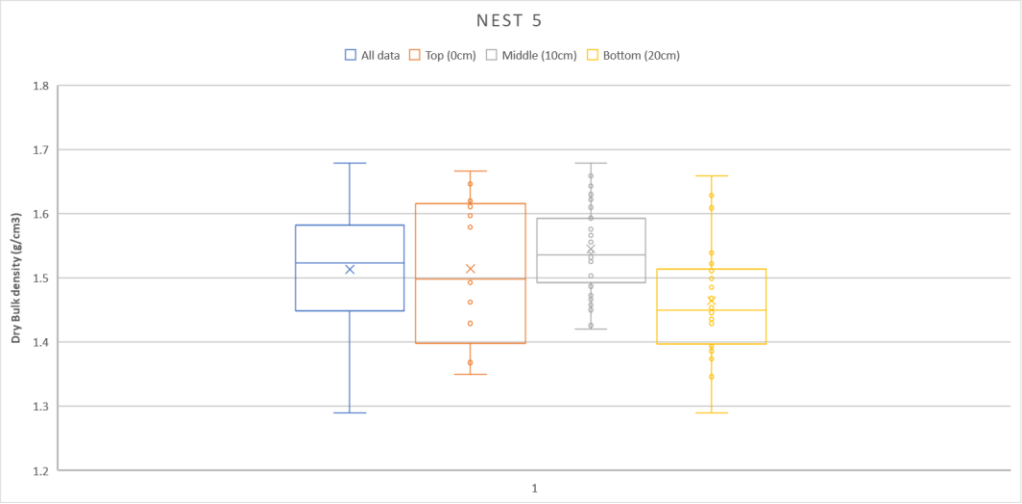
NEST 5
All data
Top (0cm)
Middle (10cm)
Bottom (20cm)
Dry Bulk density (g/cm3)
1.8
1.7
1.6
1.5
1.4
1.3
1.2
1

9.3 In-situ soil moisture sensor data at X-band time overpass (01:30a.m.)

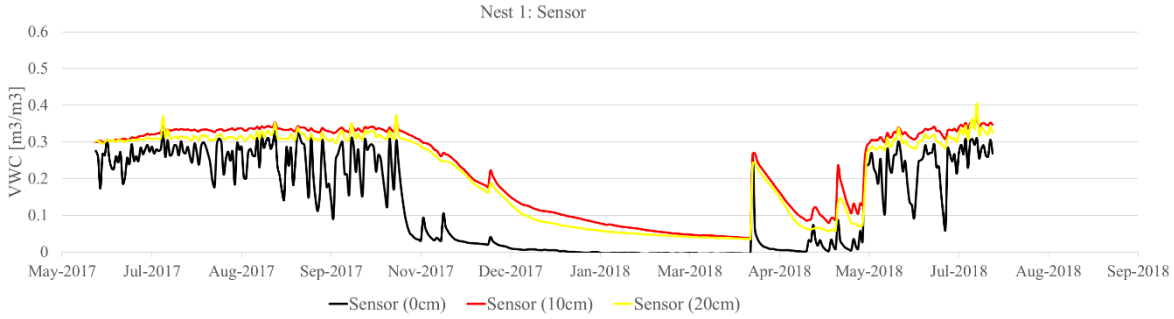

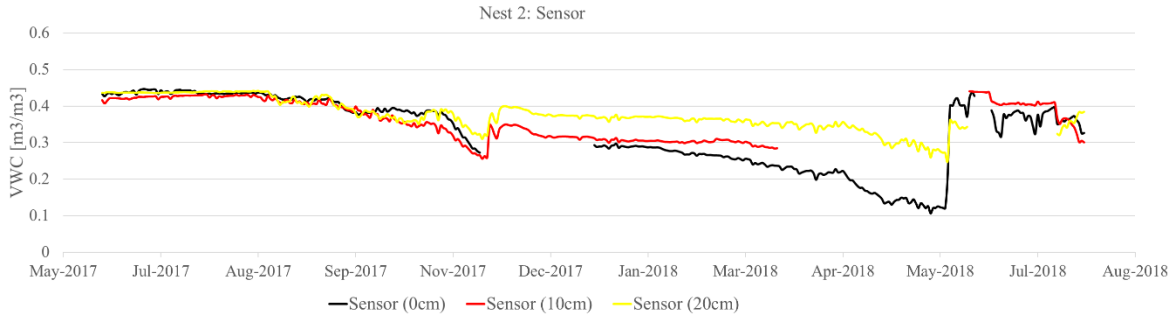

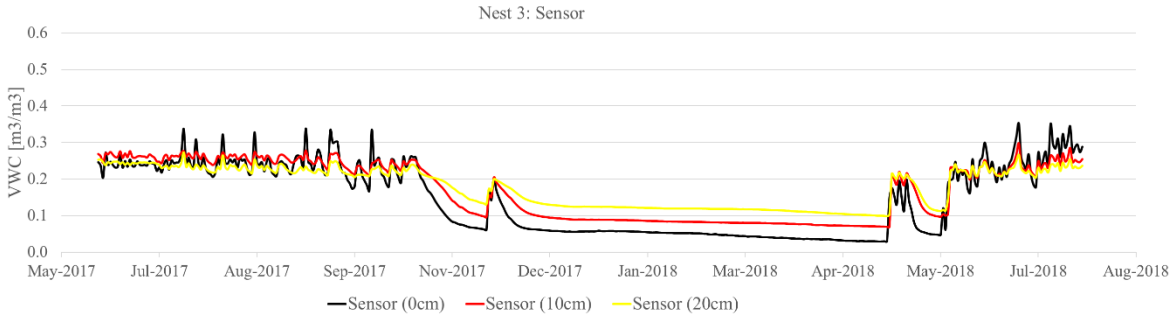

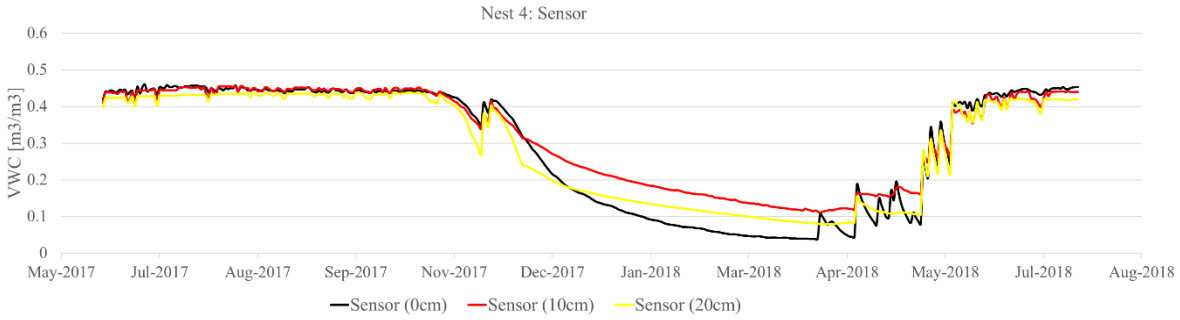

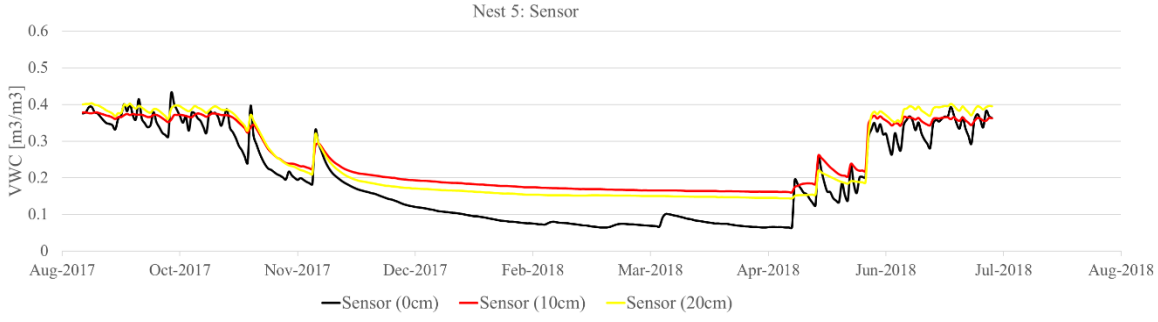

9.4 In-situ soil moisture sensor data compared to volumetric soil moisture measurements

Nest 1: Sensor v.s. Volumetric soil moisture measurements

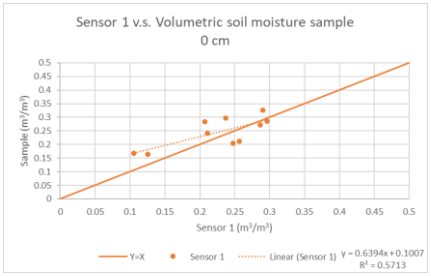

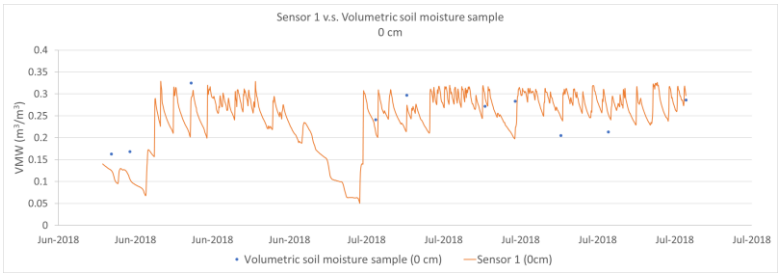

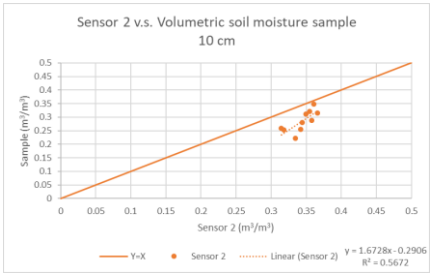

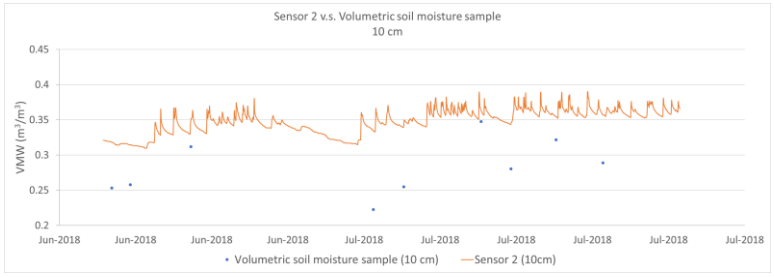

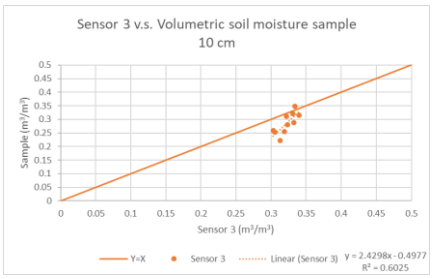

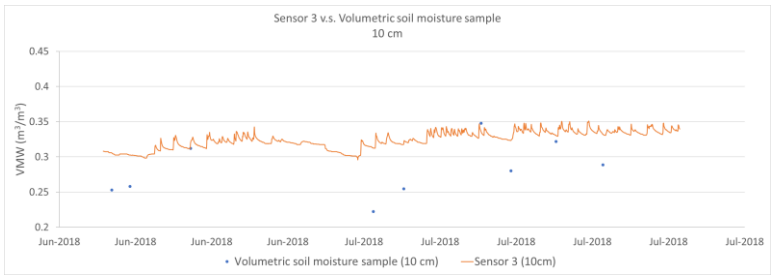

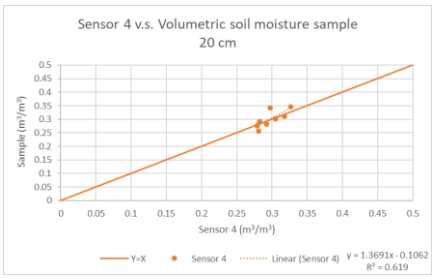

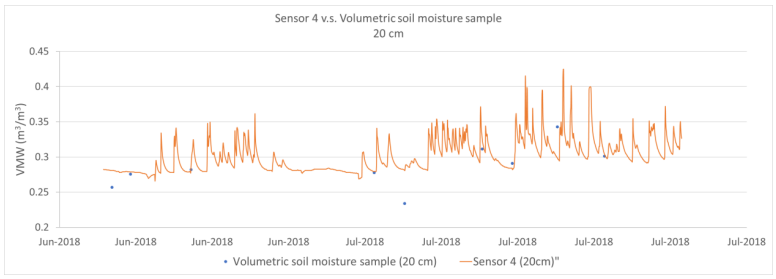

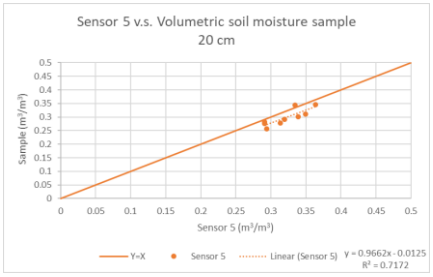

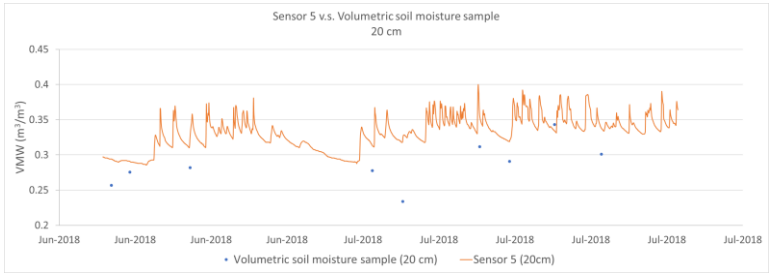

Nest 2: Sensor v.s. Volumetric soil moisture measurements

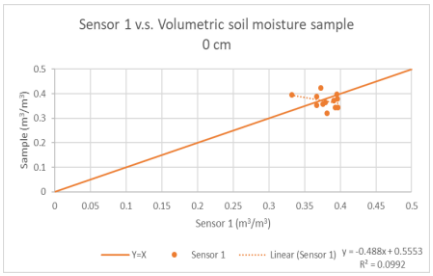

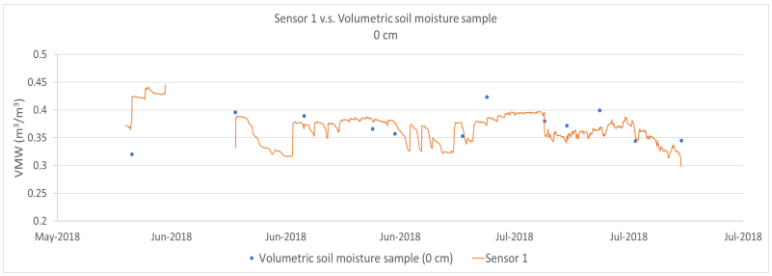

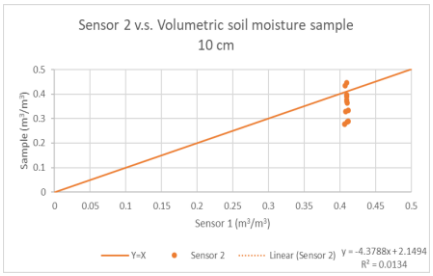

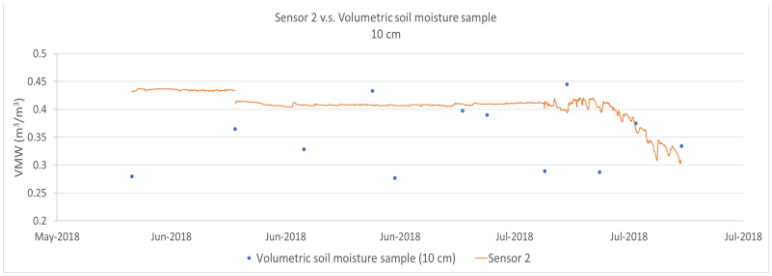

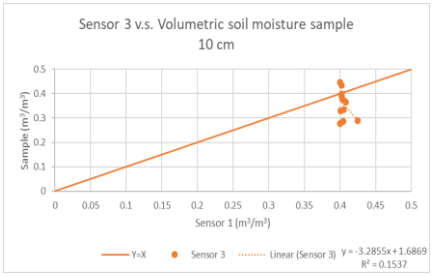

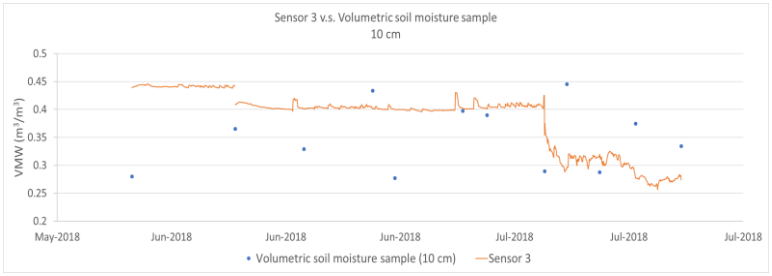

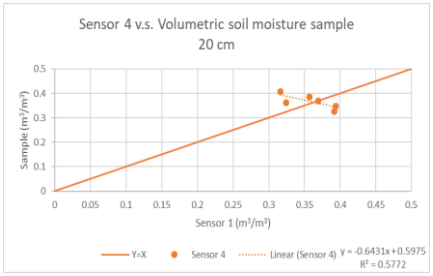

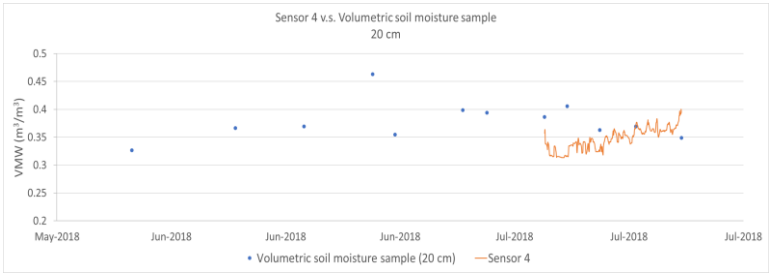

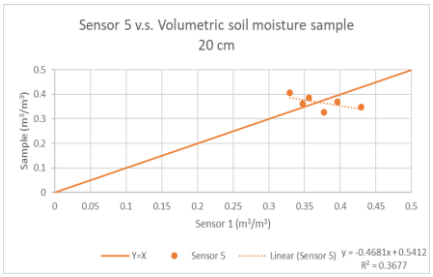

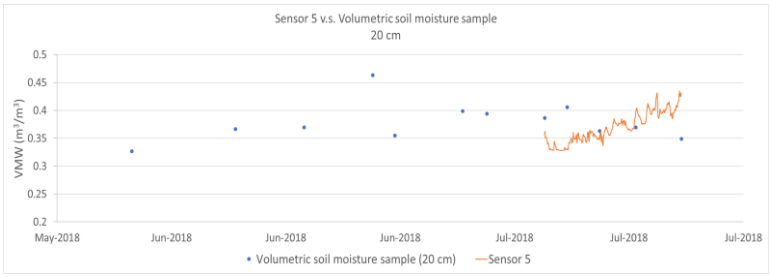

Nest 3: Sensor v.s. Volumetric soil moisture measurements

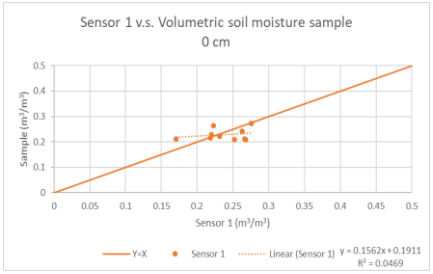

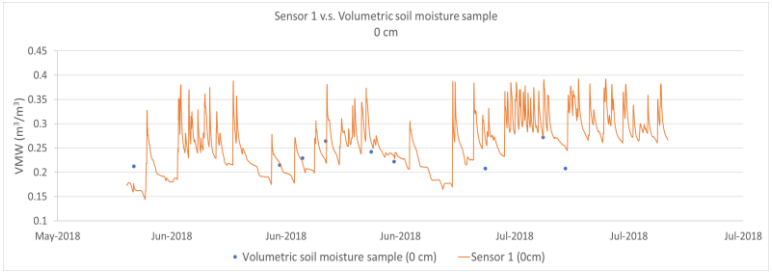

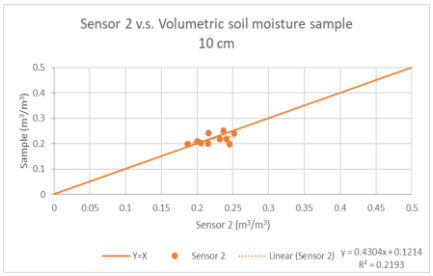

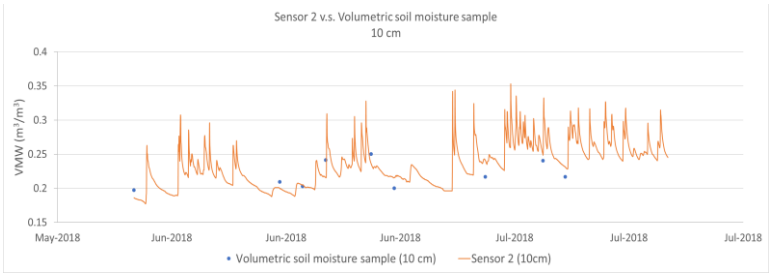

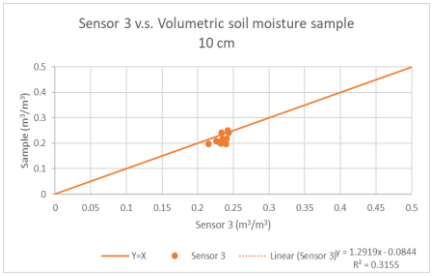

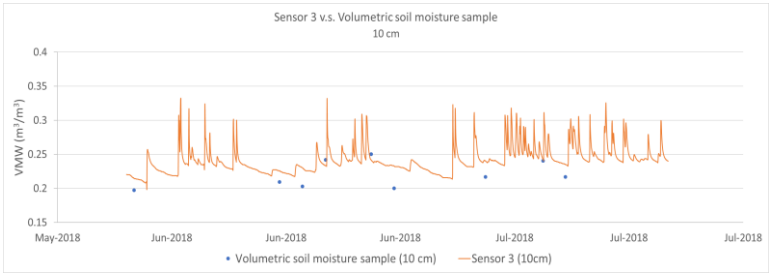

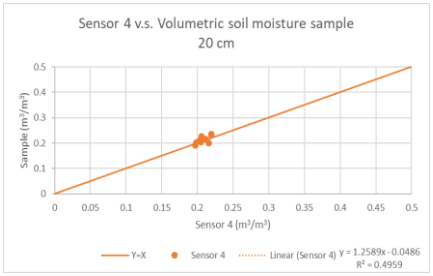

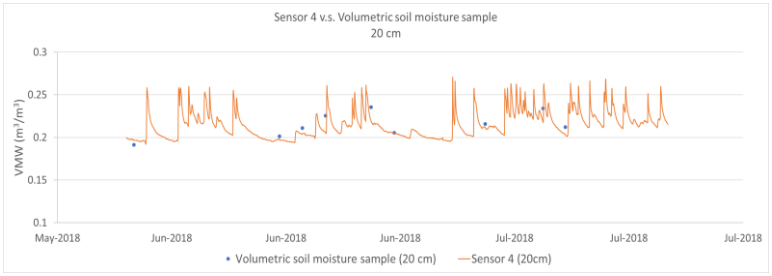

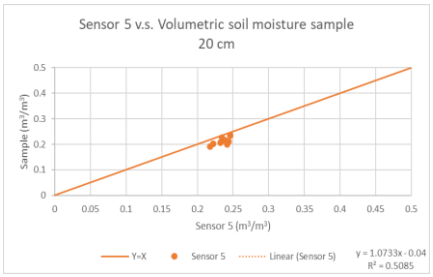

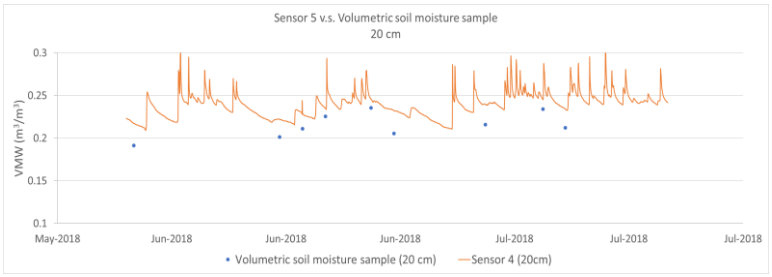

Nest 4: Sensor v.s. Volumetric soil moisture measurements

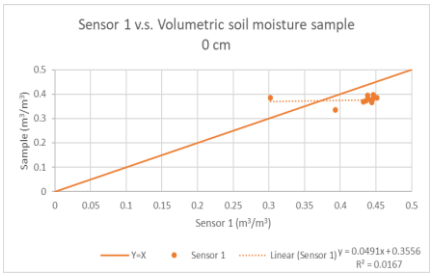

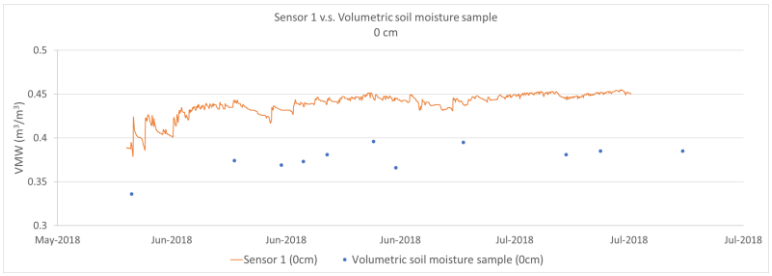

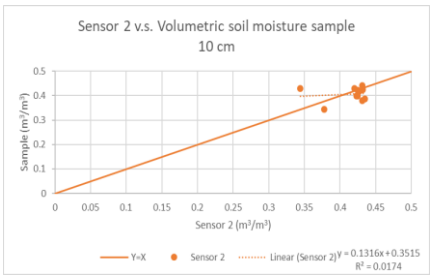

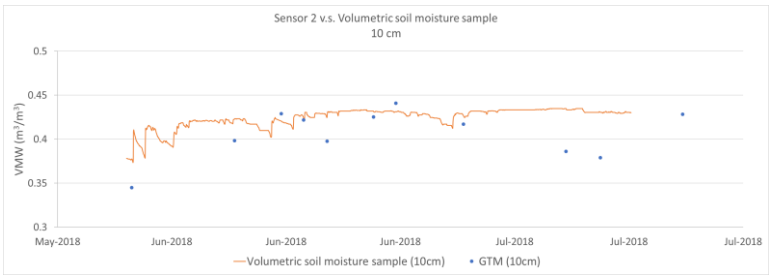

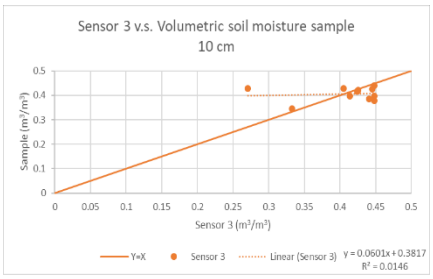

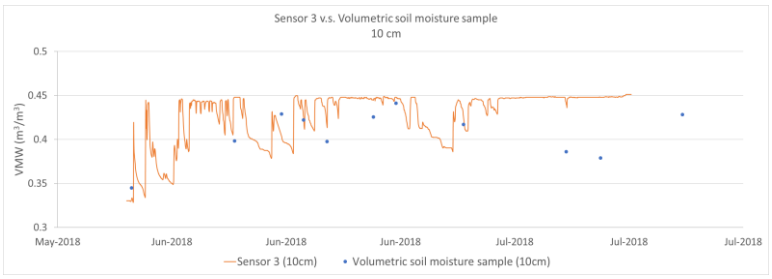

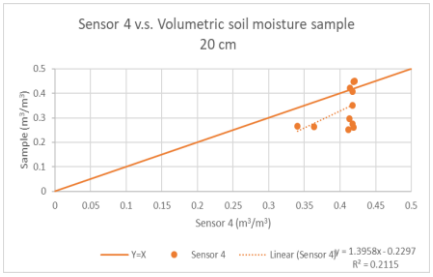

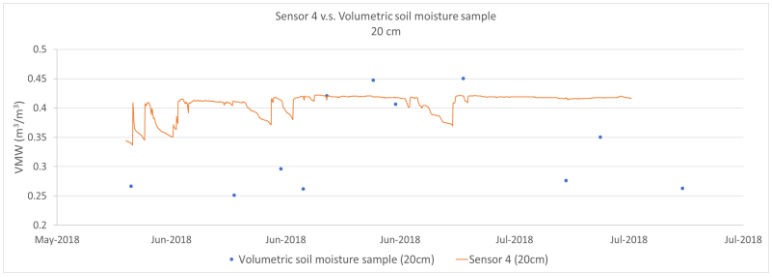

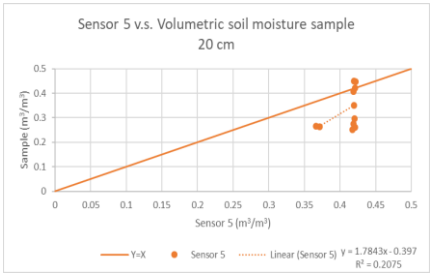

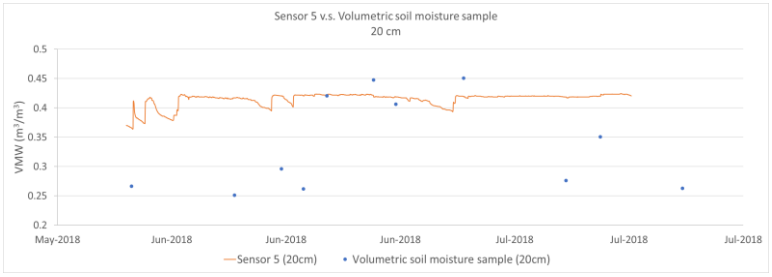

Nest 5: Sensor v.s Volumetric soil moisture measurements

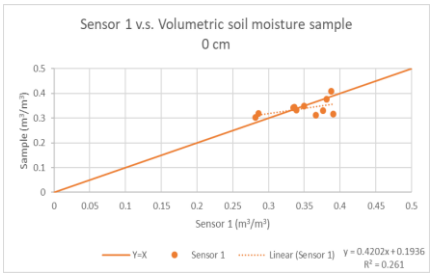

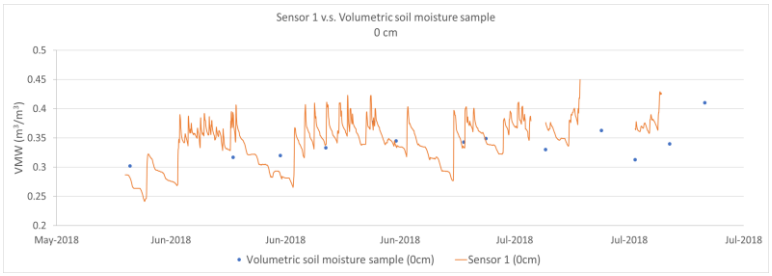

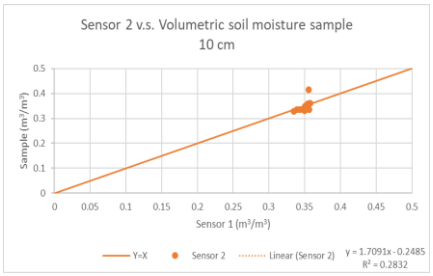

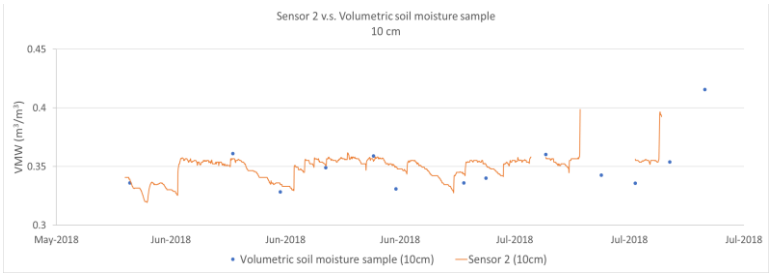

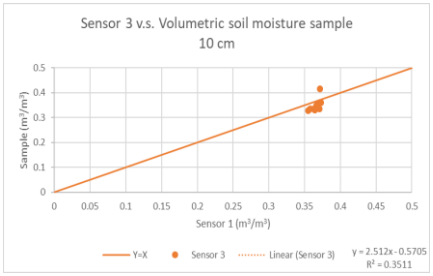

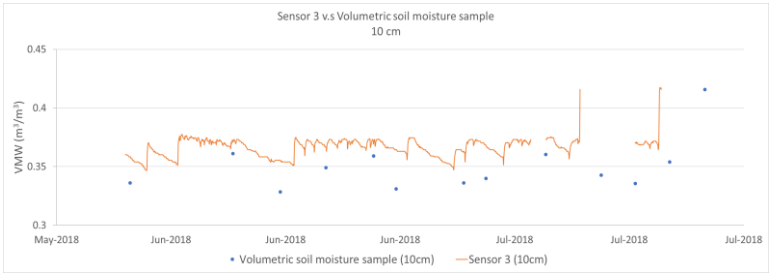

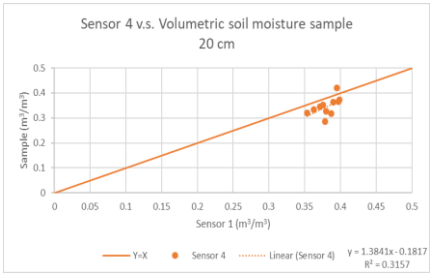

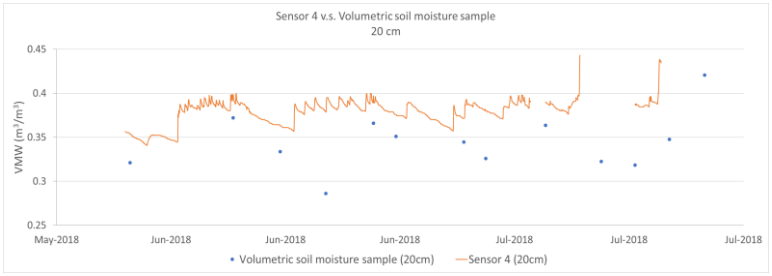

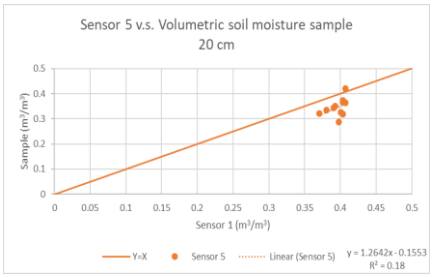

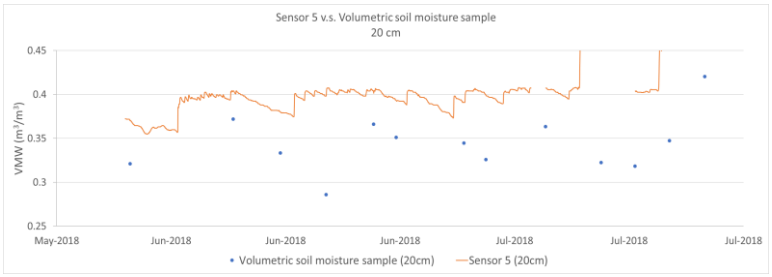

9.5: In-situ soil moisture sensor data compared to VanderSat soil moisture X & L-band

Nest 1: sensor v.s. VdS SM X & L-band

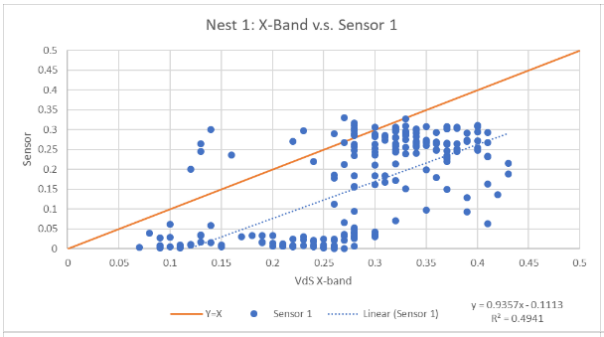

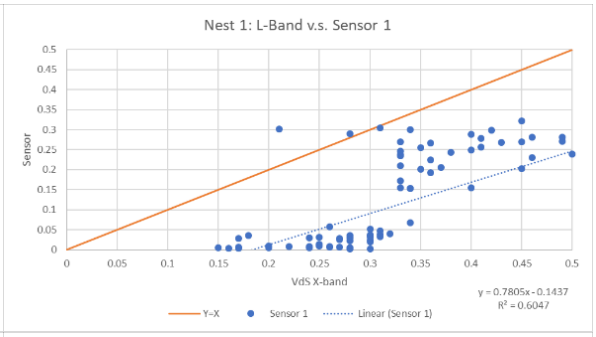

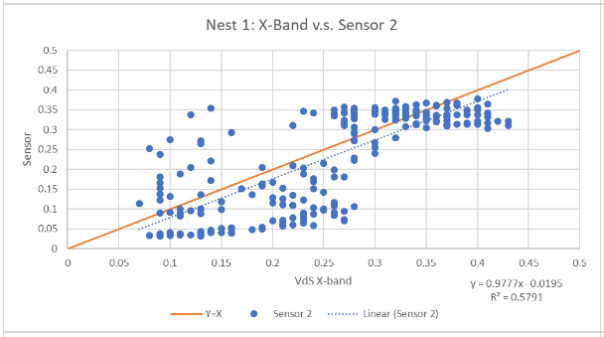

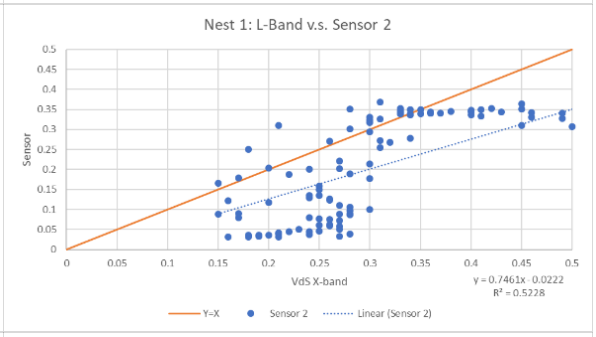

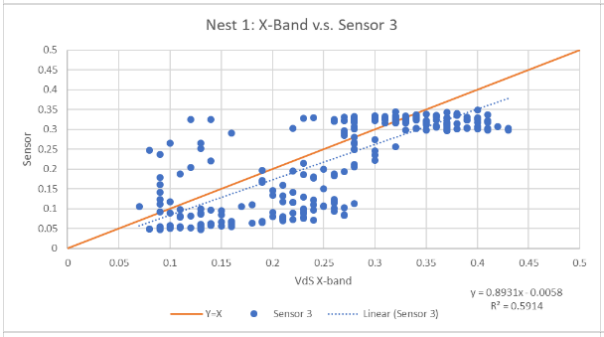

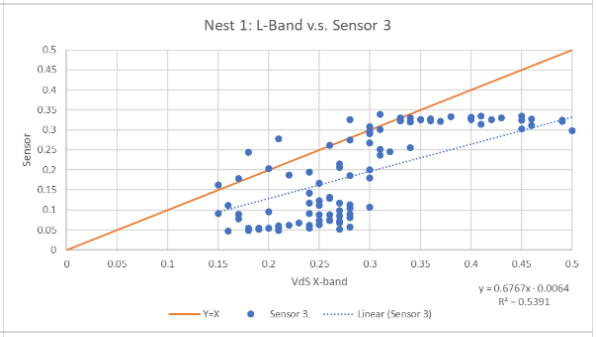

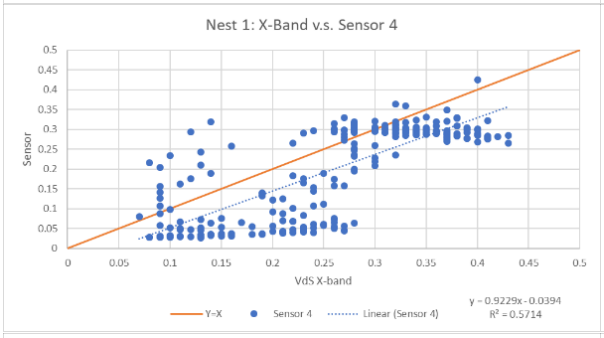

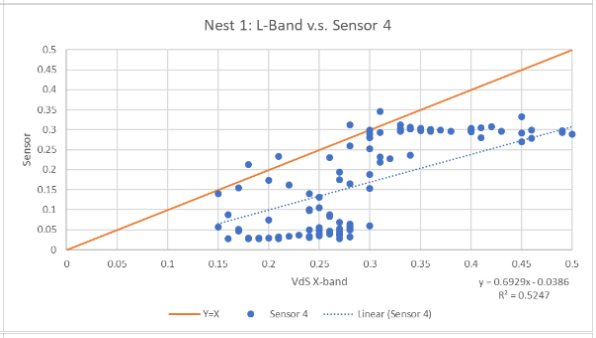

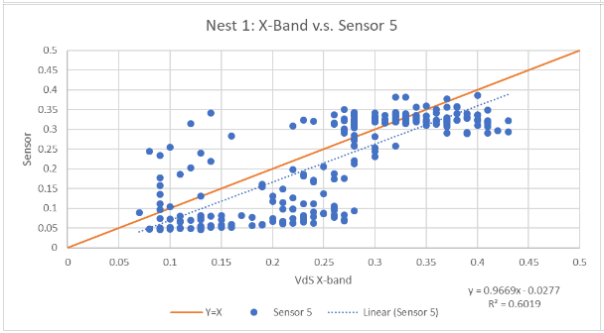

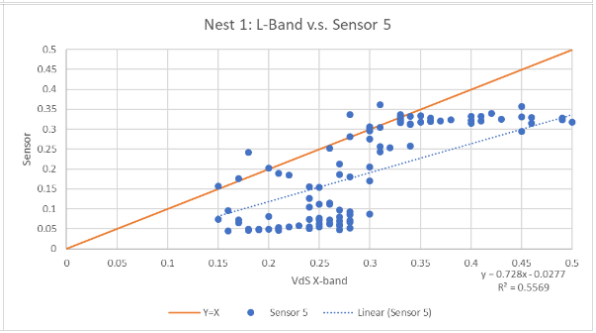

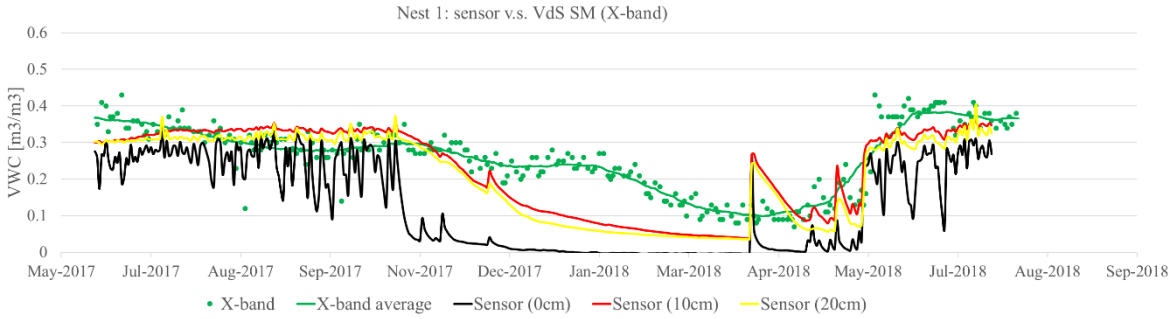
Nest 1: sensor v.s. VdS SM (X-band)
VWC [m3/m3]
0.6
0.5
0.4
0.3
0.2
0.1
0
May-2017
Jul-2017
Aug-2017
Sep-2017
Nov-2017
Dec-2017
Jan-2018
Mar-2018
Apr-2018
May-2018
Jul-2018
Aug-2018
Sep-2018
X-band
X-band average
Sensor (0cm)
Sensor (10cm)
Sensor (20cm)

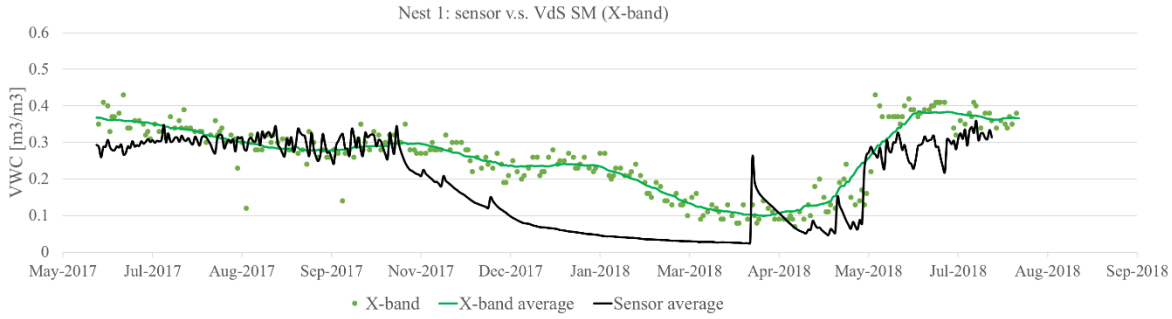
Nest 1: sensor v.s. VdS SM (X-band)
VWC [m3/m3]
0.6
0.5
0.4
0.3
0.2
0.1
0
May-2017
Jul-2017
Aug-2017
Sep-2017
Nov-2017
Dec-2017
Jan-2018
Mar-2018
Apr-2018
May-2018
Jul-2018
Aug-2018
Sep-2018
X-band
X-band average
Sensor average

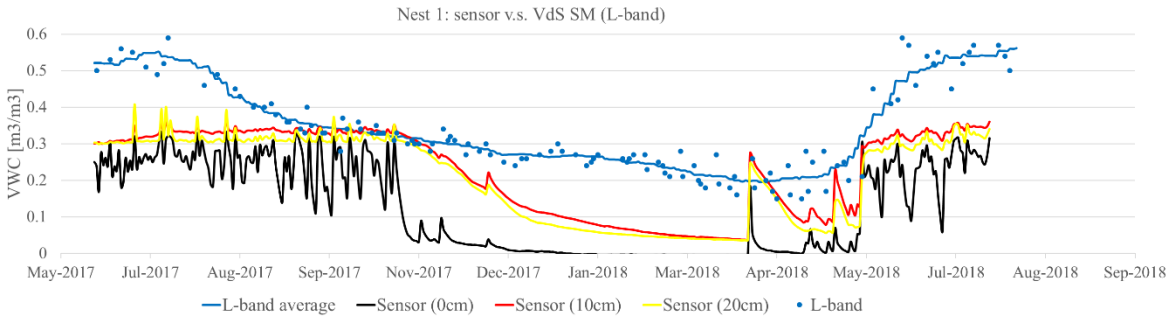
Nest 1: sensor v.s. VdS SM (L-band)
VWC [m3/m3]
0.6
0.5
0.4
0.3
0.2
0.1
0
May-2017
Jul-2017
Aug-2017
Sep-2017
Nov-2017
Dec-2017
Jan-2018
Mar-2018
Apr-2018
May-2018
Jul-2018
Aug-2018
Sep-2018
L-band average
Sensor (0cm)
Sensor (10cm)
Sensor (20cm)
L-band

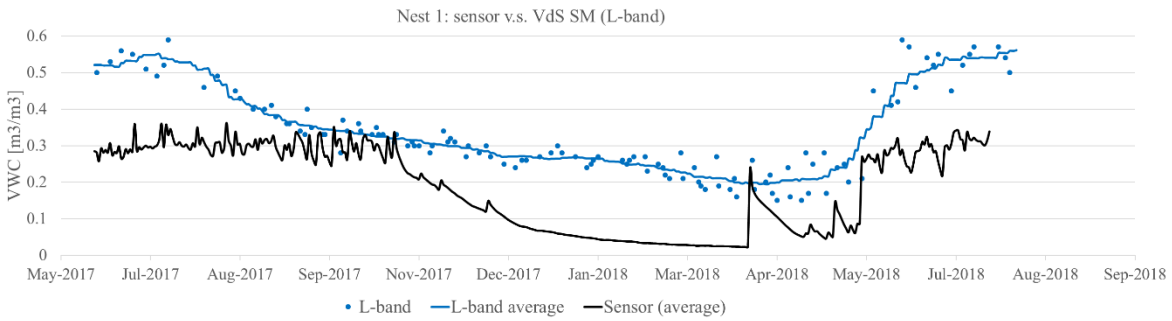
Nest 1: sensor v.s. VdS SM (L-band)
VWC [m3/m3]
0.6
0.5
0.4
0.3
0.2
0.1
0
May-2017
Jul-2017
Aug-2017
Sep-2017
Nov-2017
Dec-2017
Jan-2018
Mar-2018
Apr-2018
May-2018
Jul-2018
Aug-2018
Sep-2018
L-band
L-band average
Sensor (average)

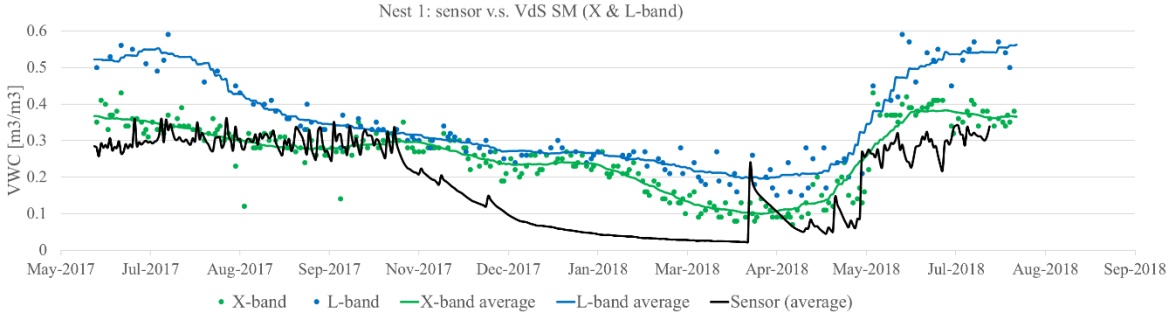
Nest 1: sensor v.s. VdS SM (X & L-band)
VWC [m3/m3]
0.6
0.5
0.4
0.3
0.2
0.1
0
May-2017
Jul-2017
Aug-2017
Sep-2017
Nov-2017
Dec-2017
Jan-2018
Mar-2018
Apr-2018
May-2018
Jul-2018
Aug-2018
Sep-2018
X-band
L-band
X-band average
L-band average
Sensor (average)

Nest 2: sensor v.s. VdS SM X & L-band

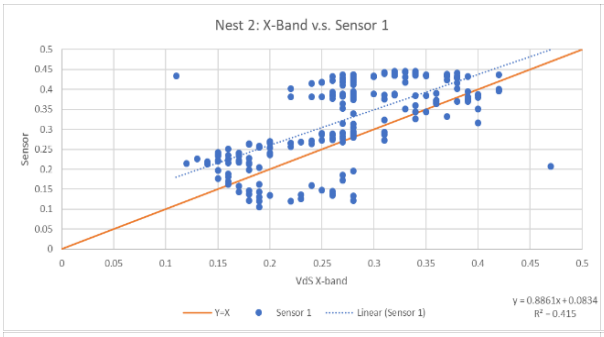

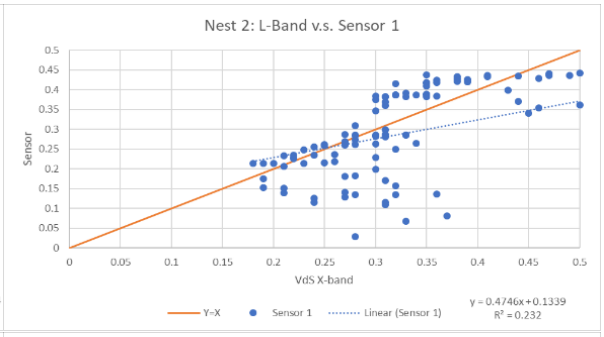

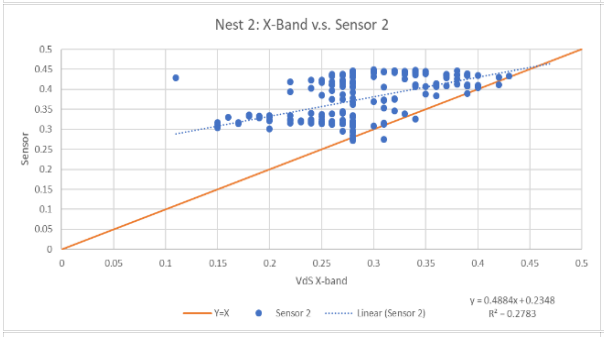

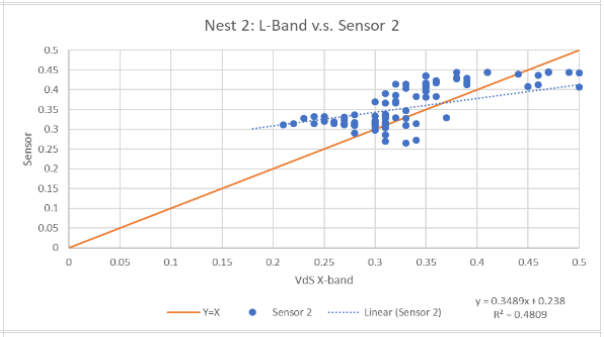

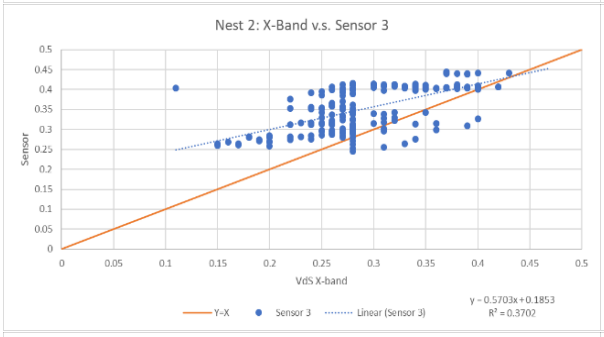

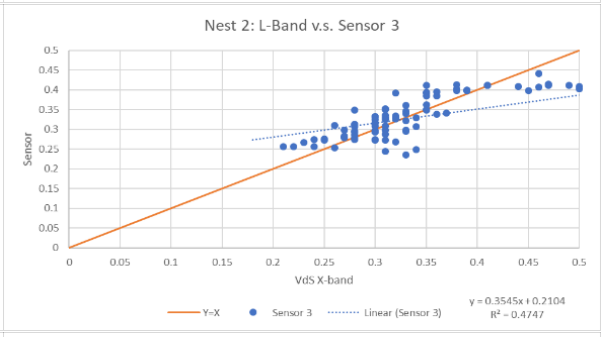

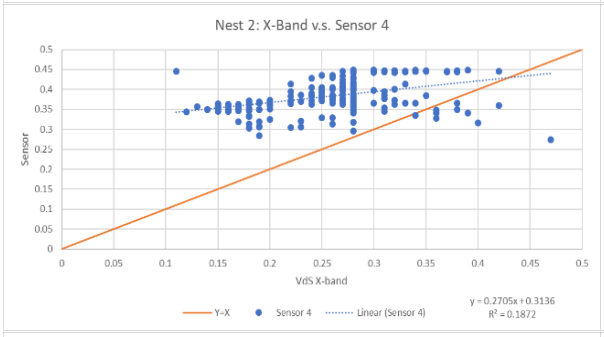

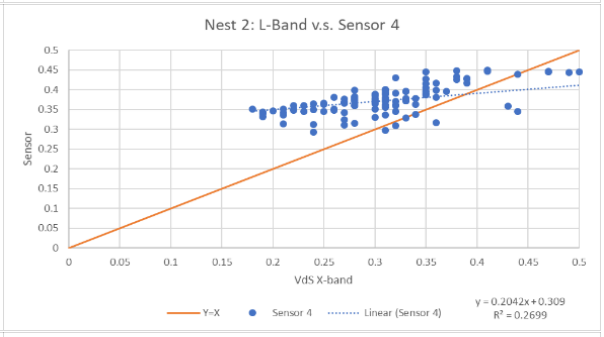

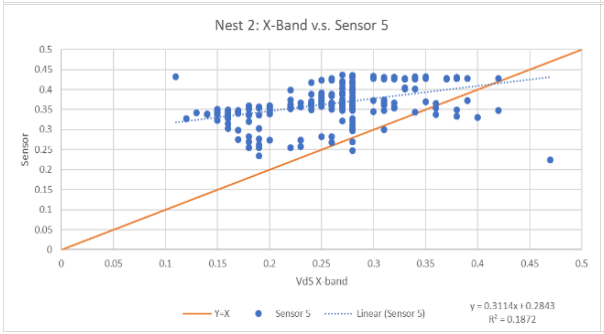

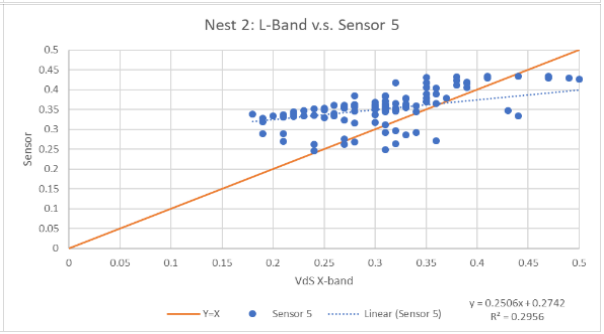

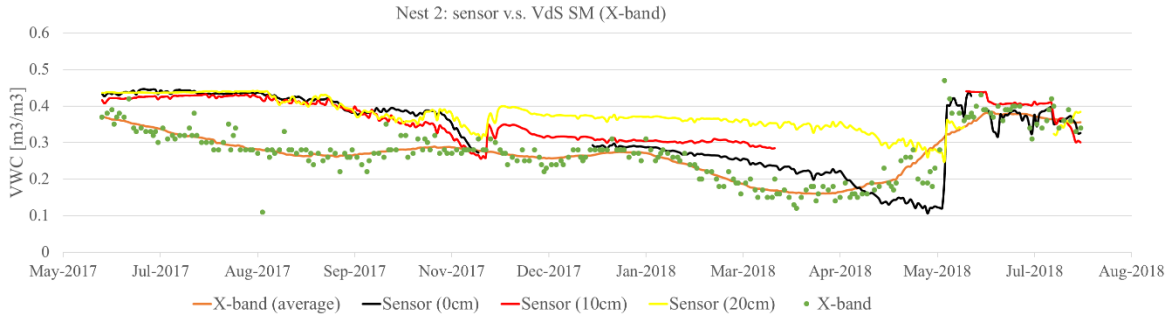
Nest 2: sensor v.s. VdS SM (X-band)
VWC [m3/m3]
0.6
0.5
0.4
0.3
0.2
0.1
0
May-2017
Jul-2017
Aug-2017
Sep-2017
Nov-2017
Dec-2017
Jan-2018
Mar-2018
Apr-2018
May-2018
Jul-2018
Aug-2018
X-band (average)
Sensor (0cm)
Sensor (10cm)
Sensor (20cm)
X-band

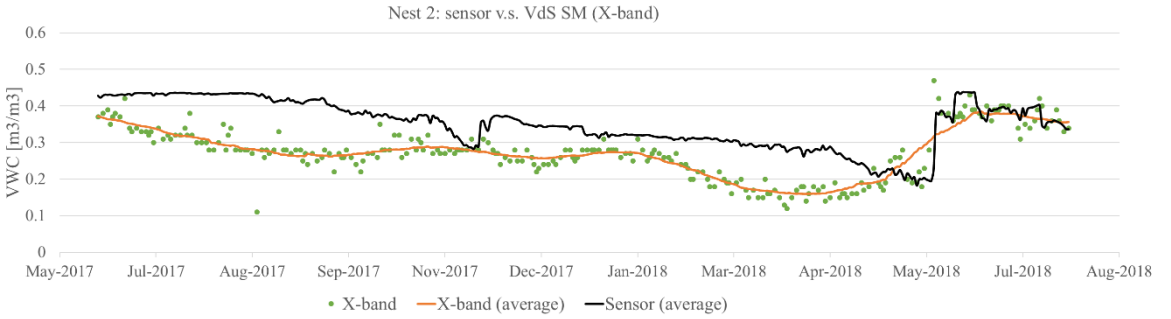
Nest 2: sensor v.s. VdS SM (X-band)
VWC [m3/m3]
0.6
0.5
0.4
0.3
0.2
0.1
0
May-2017
Jul-2017
Aug-2017
Sep-2017
Nov-2017
Dec-2017
Jan-2018
Mar-2018
Apr-2018
May-2018
Jul-2018
Aug-2018
X-band
X-band (average)
Sensor (average)

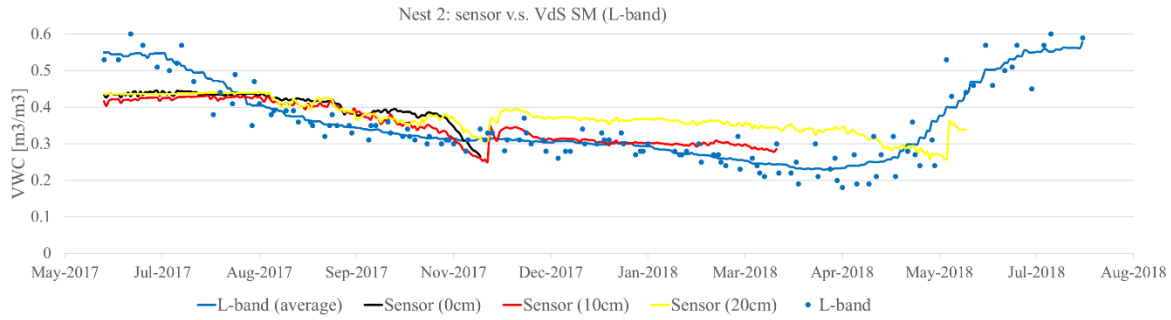
Nest 2: sensor v.s. VdS SM (L-band)
VWC [m3/m3]
0.6
0.5
0.4
0.3
0.2
0.1
0
May-2017
Jul-2017
Aug-2017
Sep-2017
Nov-2017
Dec-2017
Jan-2018
Mar-2018
Apr-2018
May-2018
Jul-2018
Aug-2018
L-band (average)
Sensor (0cm)
Sensor (10cm)
Sensor (20cm)
L-band

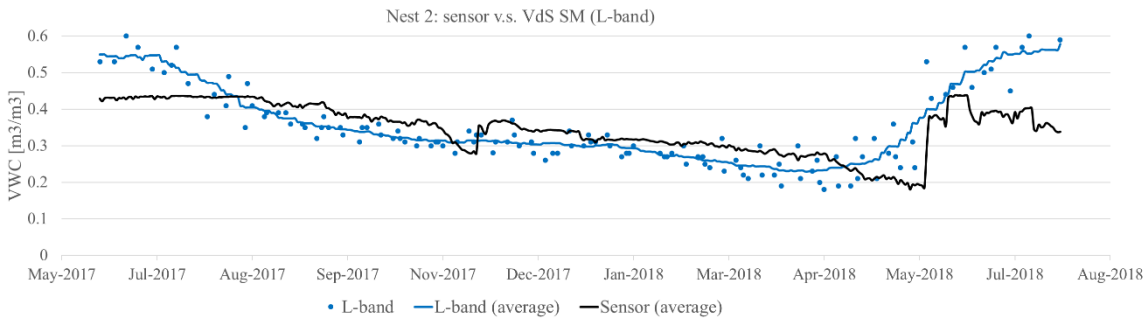
Nest 2: sensor v.s. VdS SM (L-band)
VWC [m3/m3]
0.6
0.5
0.4
0.3
0.2
0.1
0
May-2017
Jul-2017
Aug-2017
Sep-2017
Nov-2017
Dec-2017
Jan-2018
Mar-2018
Apr-2018
May-2018
Jul-2018
Aug-2018
L-band
L-band (average)
Sensor (average)

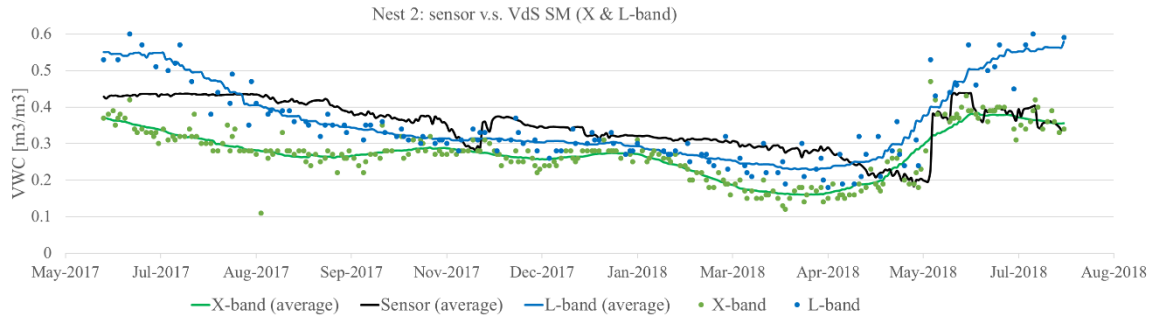
Nest 2: sensor v.s. VdS SM (X & L-band)
VWC [m3/m3]
0.6
0.5
0.4
0.3
0.2
0.1
0
May-2017
Jul-2017
Aug-2017
Sep-2017
Nov-2017
Dec-2017
Jan-2018
Mar-2018
Apr-2018
May-2018
Jul-2018
Aug-2018
X-band (average)
Sensor (average)
L-band (average)
X-band
L-band

Nest 3: sensor v.s. VdS SM X & L-band

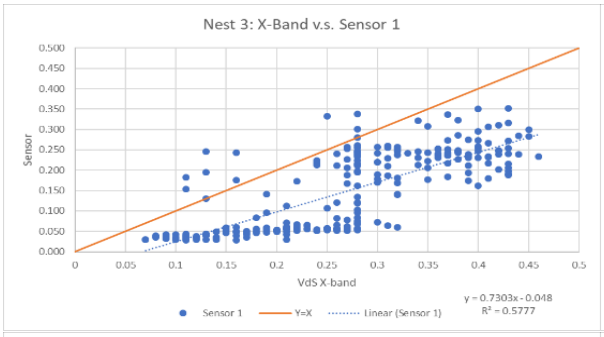

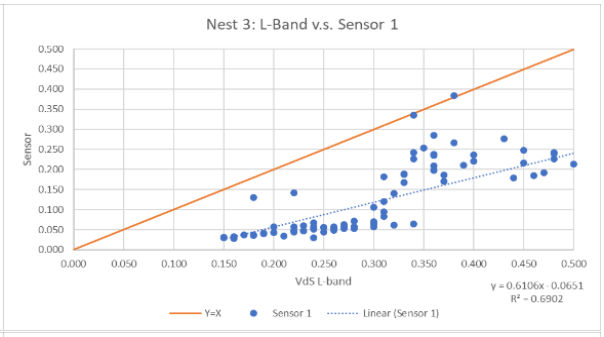

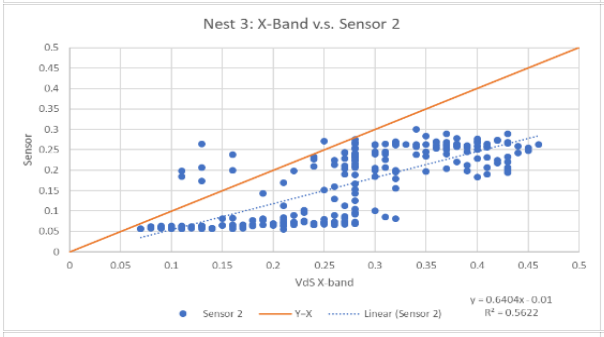

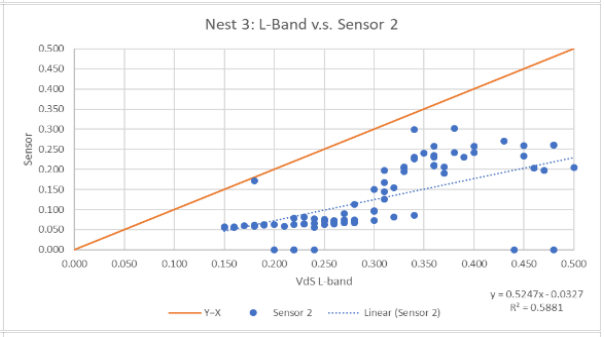

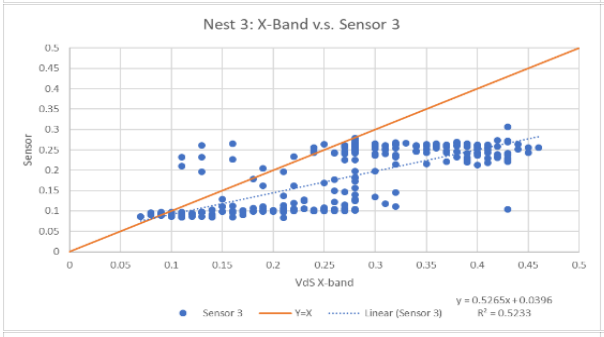

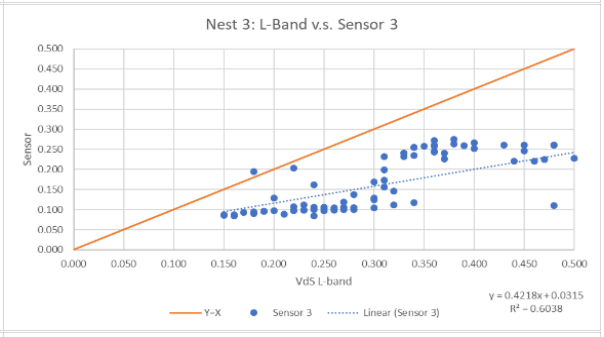

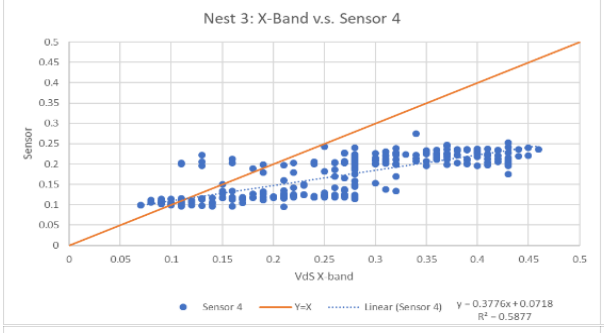

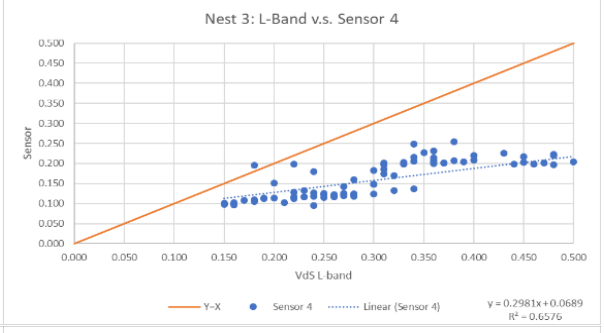

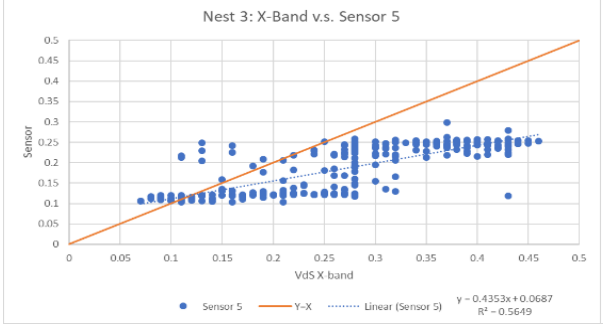

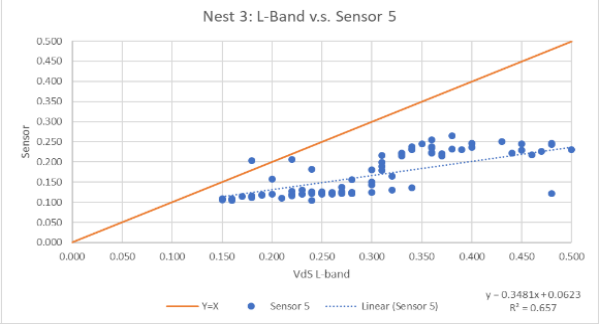

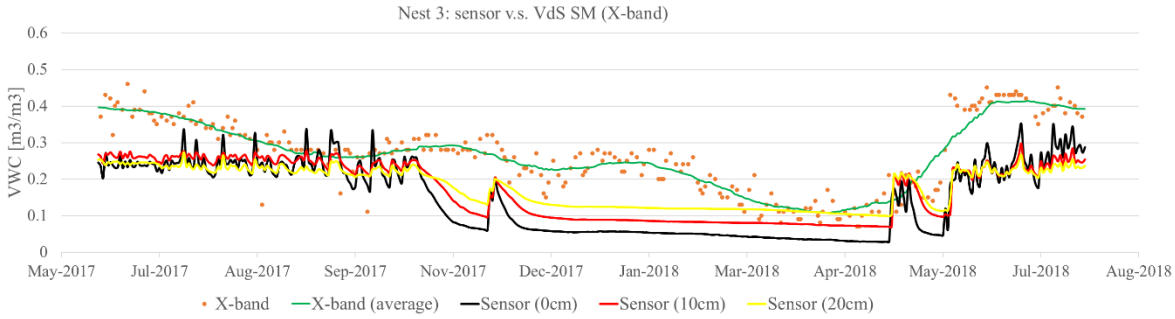
Nest 3: sensor v.s. VdS SM (X-band)
VWC [m3/m3]
0.6
0.5
0.4
0.3
0.2
0.1
0
May-2017
Jul-2017
Aug-2017
Sep-2017
Nov-2017
Dec-2017
Jan-2018
Mar-2018
Apr-2018
May-2018
Jul-2018
Aug-2018
X-band
X-band (average)
Sensor (0cm)
Sensor (10cm)
Sensor (20cm)

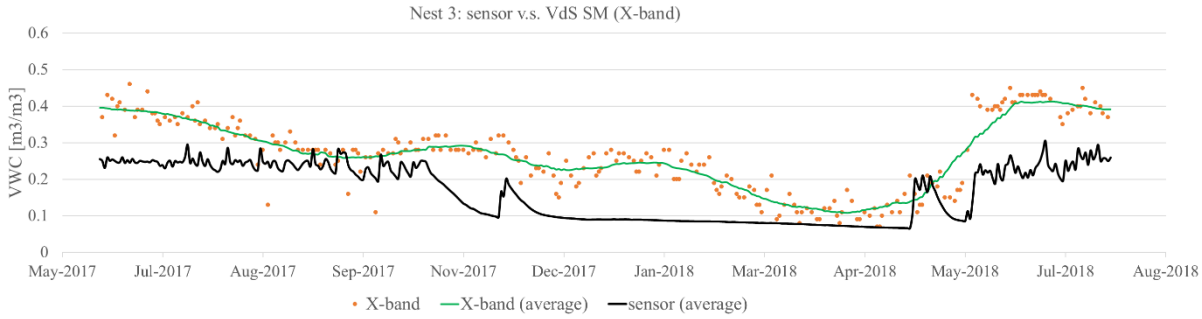
Nest 3: sensor v.s. VdS SM (X-band)
VWC [m3/m3]
0.6
0.5
0.4
0.3
0.2
0.1
0
May-2017
Jul-2017
Aug-2017
Sep-2017
Nov-2017
Dec-2017
Jan-2018
Mar-2018
Apr-2018
May-2018
Jul-2018
Aug-2018
X-band
X-band (average)
sensor (average)

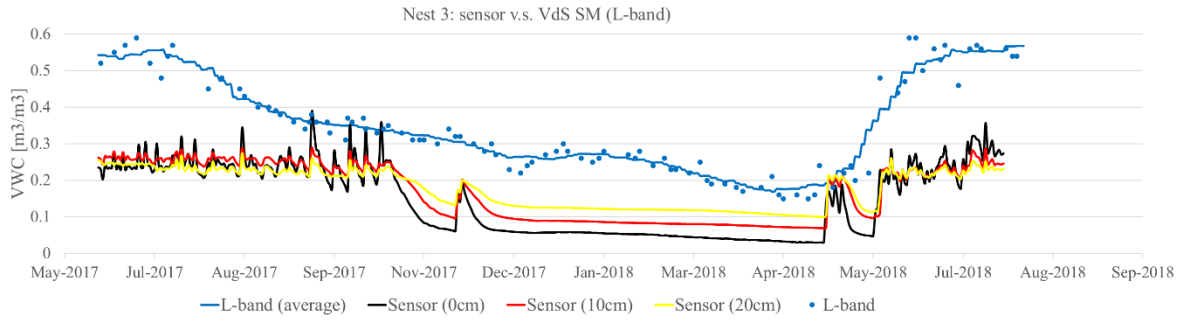
Nest 3: sensor v.s. VdS SM (L-band)
VWC [m3/m3]
0.6
0.5
0.4
0.3
0.2
0.1
0
May-2017
Jul-2017
Aug-2017
Sep-2017
Nov-2017
Dec-2017
Jan-2018
Mar-2018
Apr-2018
May-2018
Jul-2018
Aug-2018
Sep-2018
L-band (average)
Sensor (0cm)
Sensor (10cm)
Sensor (20cm)
L-band

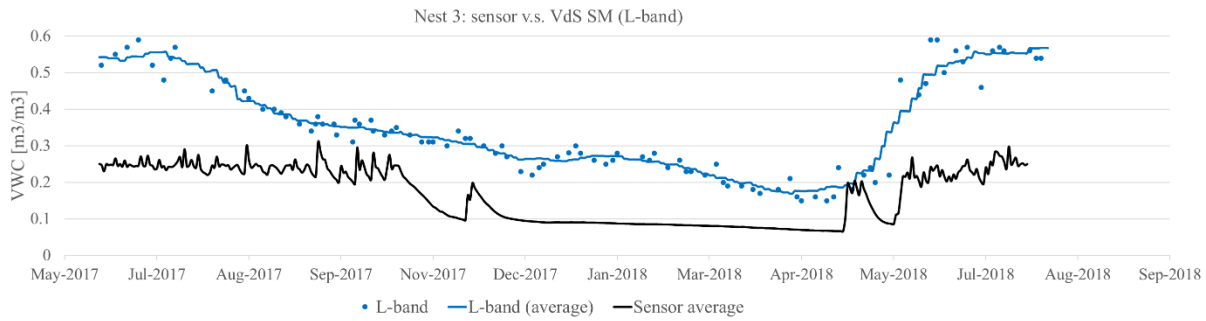
Nest 3: sensor v.s. VdS SM (L-band)
VWC [m3/m3]
0.6
0.5
0.4
0.3
0.2
0.1
0
May-2017
Jul-2017
Aug-2017
Sep-2017
Nov-2017
Dec-2017
Jan-2018
Mar-2018
Apr-2018
May-2018
Jul-2018
Aug-2018
Sep-2018
L-band
L-band (average)
Sensor average

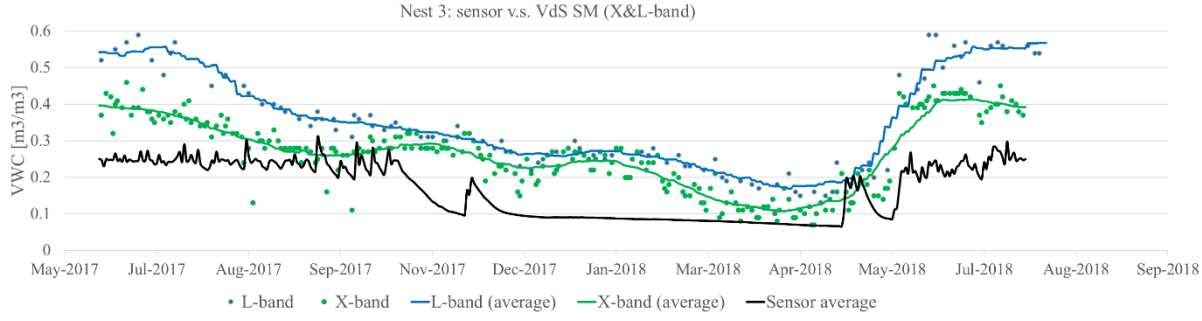
Nest 3: sensor v.s. VdS SM (X&L-band)
VWC [m3/m3]
0.6
0.5
0.4
0.3
0.2
0.1
0
May-2017
Jul-2017
Aug-2017
Sep-2017
Nov-2017
Dec-2017
Jan-2018
Mar-2018
Apr-2018
May-2018
Jul-2018
Aug-2018
Sep-2018
L-band
X-band
L-band (average)
X-band (average)
Sensor average

Nest 4: sensor v.s. VdS SM X & L-band

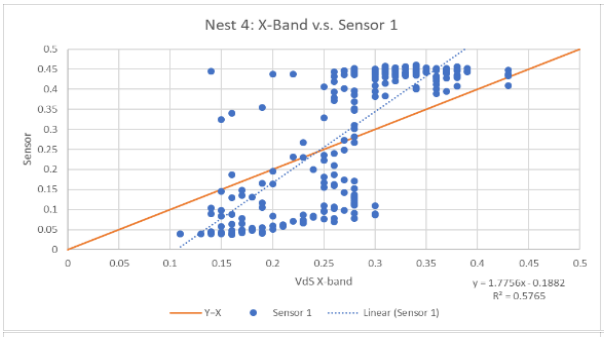

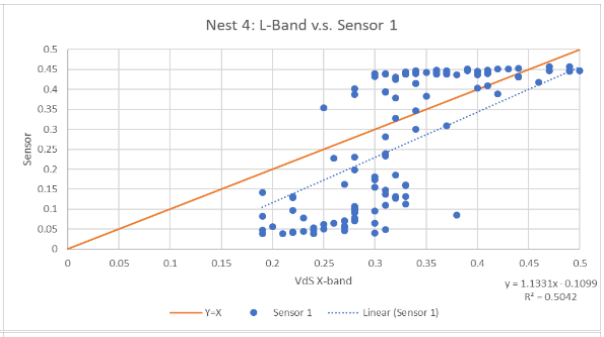

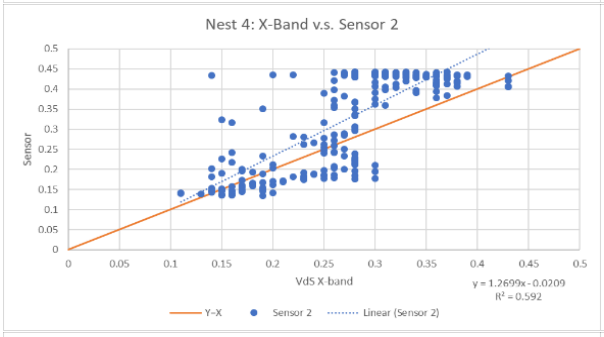

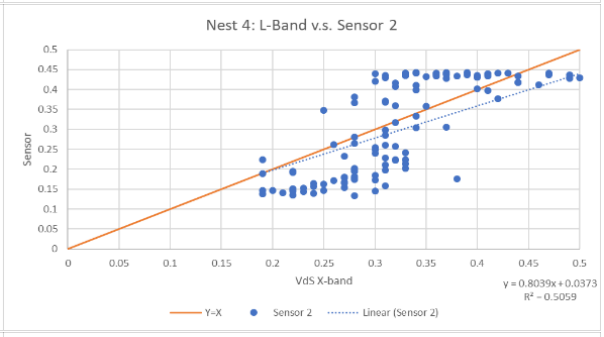

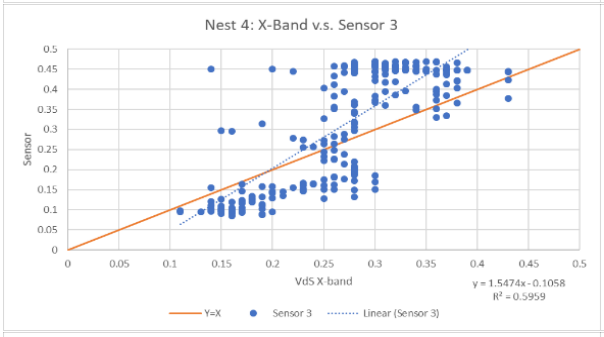

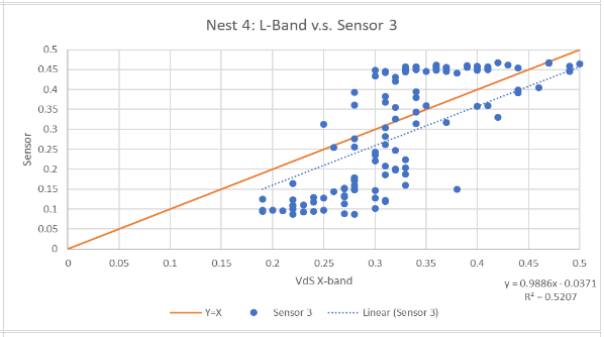

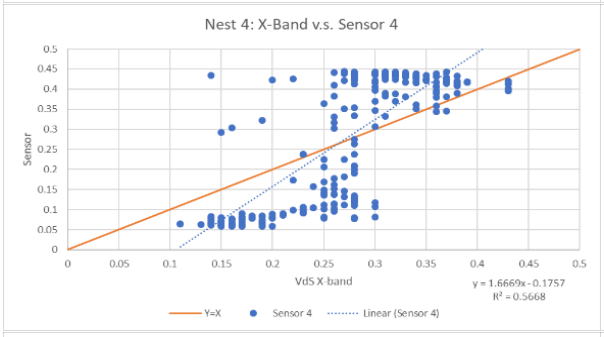

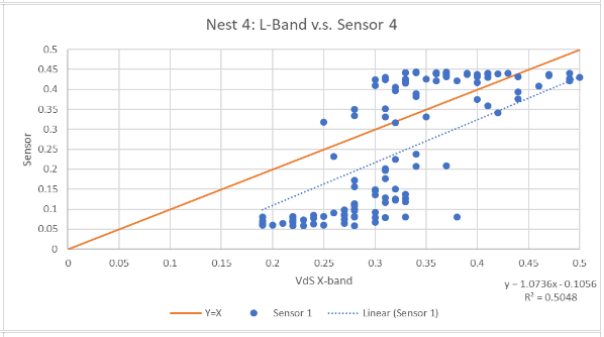

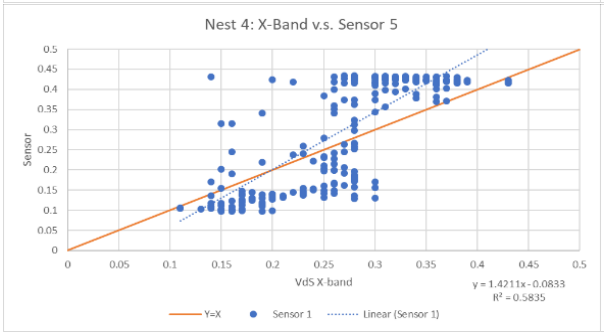

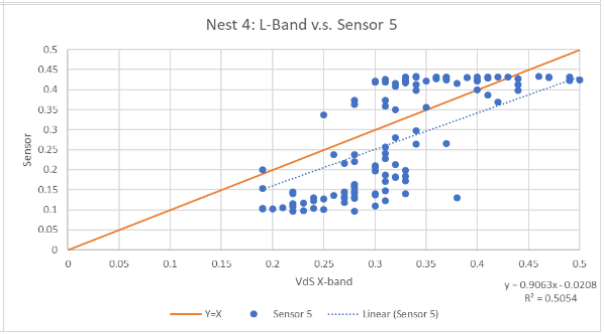

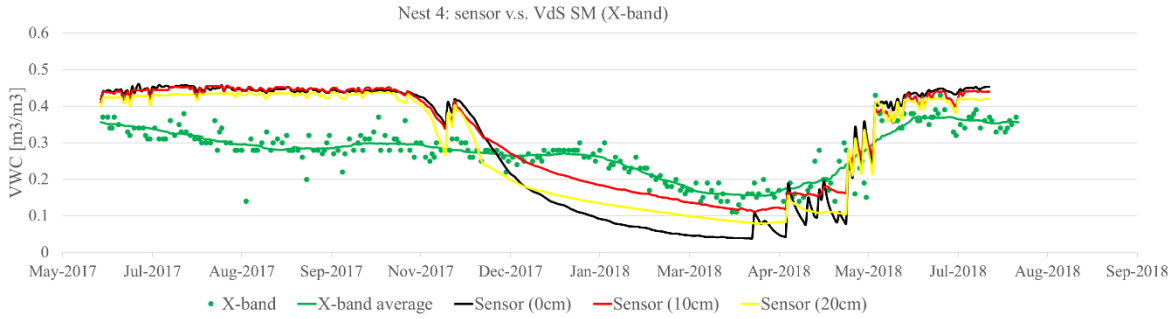
Nest 4: sensor v.s. VdS SM (X-band)
VWC [m3/m3]
0.6
0.5
0.4
0.3
0.2
0.1
0
May-2017
Jul-2017
Aug-2017
Sep-2017
Nov-2017
Dec-2017
Jan-2018
Mar-2018
Apr-2018
May-2018
Jul-2018
Aug-2018
Sep-2018
X-band
X-band average
Sensor (0cm)
Sensor (10cm)
Sensor (20cm)

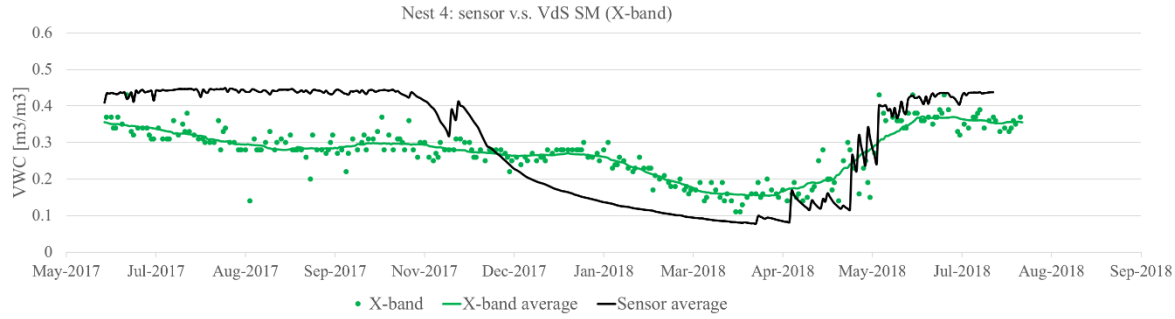
Nest 4: sensor v.s. VdS SM (X-band)
VWC [m3/m3]
0.6
0.5
0.4
0.3
0.2
0.1
0
May-2017
Jul-2017
Aug-2017
Sep-2017
Nov-2017
Dec-2017
Jan-2018
Mar-2018
Apr-2018
May-2018
Jul-2018
Aug-2018
Sep-2018
X-band
X-band average
Sensor average

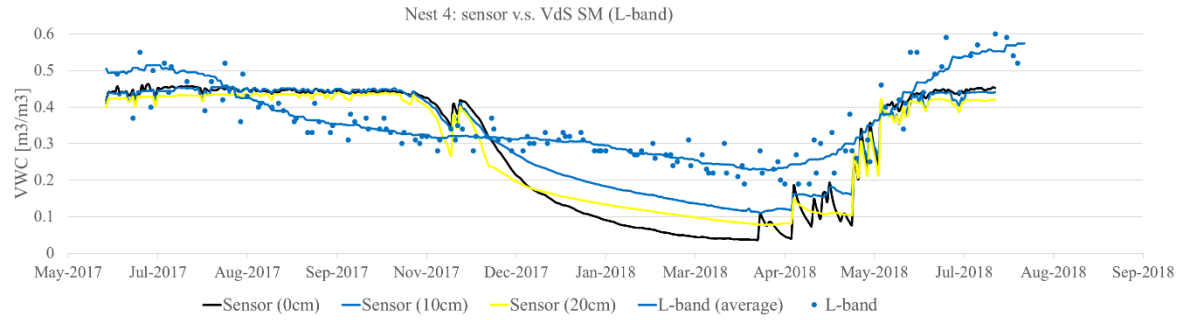
Nest 4: sensor v.s. VdS SM (L-band)
VWC [m3/m3]
0.6
0.5
0.4
0.3
0.2
0.1
0
May-2017
Jul-2017
Aug-2017
Sep-2017
Nov-2017
Dec-2017
Jan-2018
Mar-2018
Apr-2018
May-2018
Jul-2018
Aug-2018
Sep-2018
Sensor (0cm)
Sensor (10cm)
Sensor (20cm)
L-band (average)
L-band

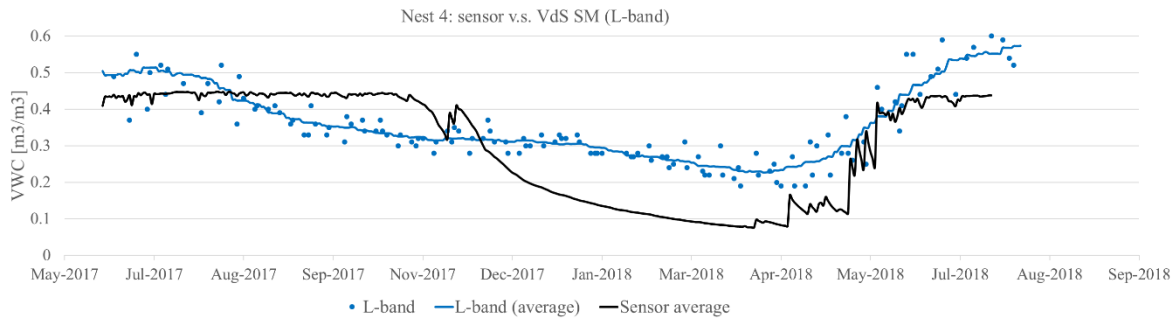
Nest 4: sensor v.s. VdS SM (L-band)
VWC [m3/m3]
0.6
0.5
0.4
0.3
0.2
0.1
0
May-2017
Jul-2017
Aug-2017
Sep-2017
Nov-2017
Dec-2017
Jan-2018
Mar-2018
Apr-2018
May-2018
Jul-2018
Aug-2018
Sep-2018
L-band
L-band (average)
Sensor average

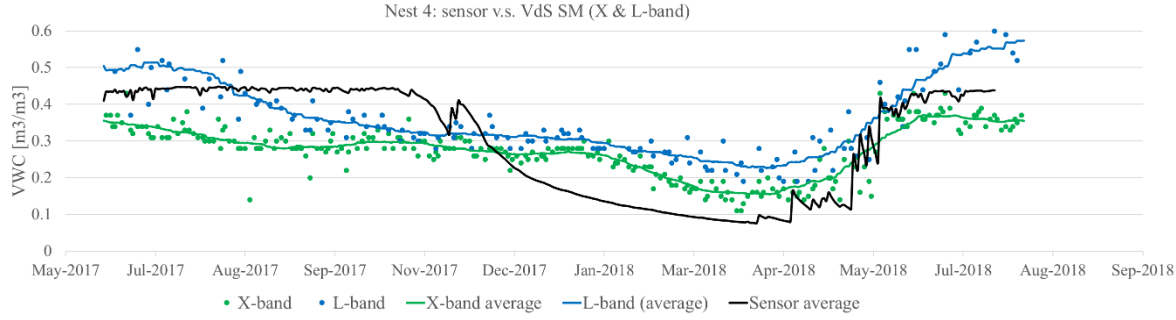
Nest 4: sensor v.s. VdS SM (X & L-band)
VWC [m3/m3]
0.6
0.5
0.4
0.3
0.2
0.1
0
May-2017
Jul-2017
Aug-2017
Sep-2017
Nov-2017
Dec-2017
Jan-2018
Mar-2018
Apr-2018
May-2018
Jul-2018
Aug-2018
Sep-2018
X-band
L-band
X-band average
L-band (average)
Sensor average

Nest 5: sensor v.s. VdS SM X & L-band

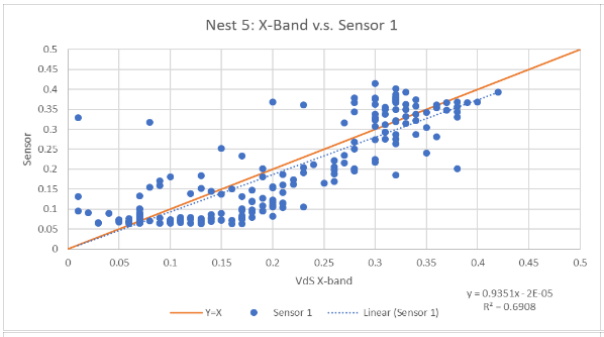

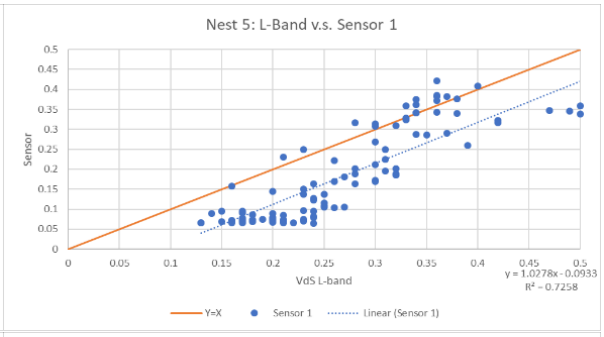

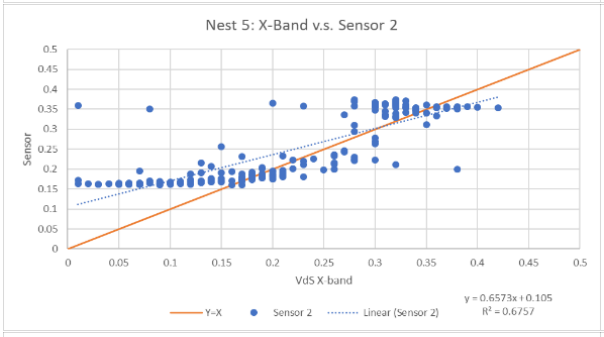

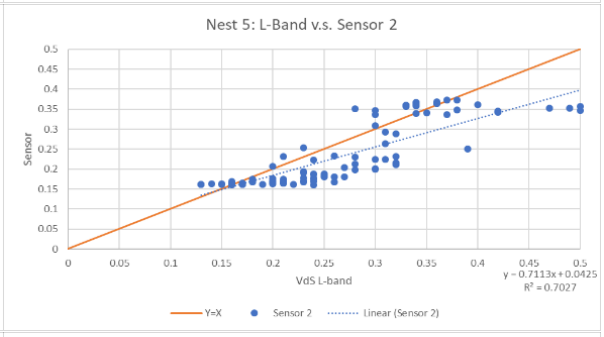

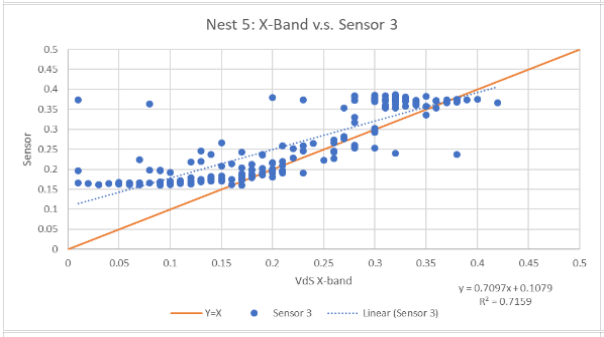

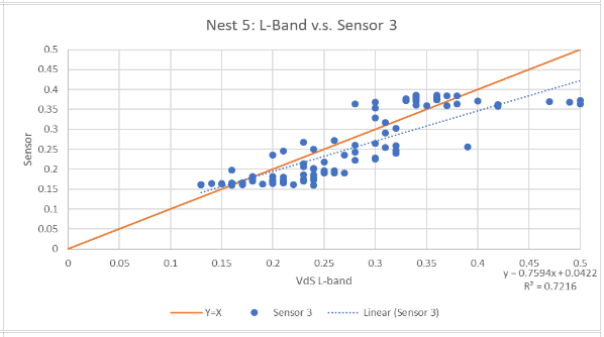

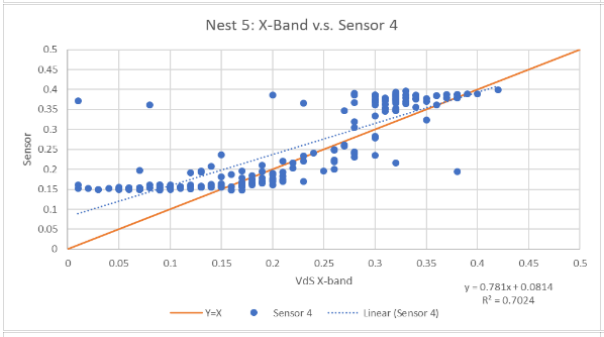

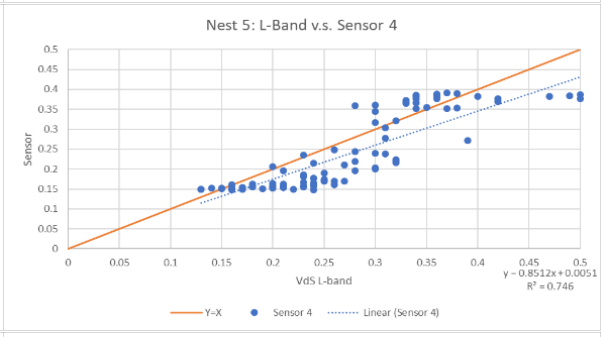

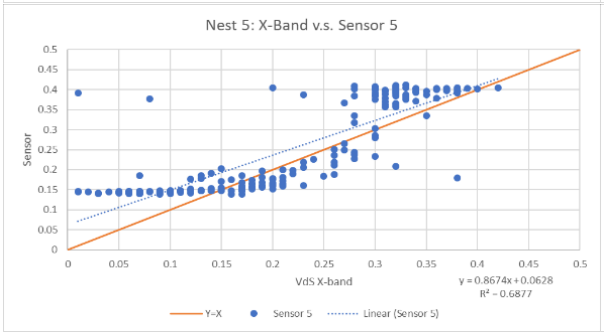

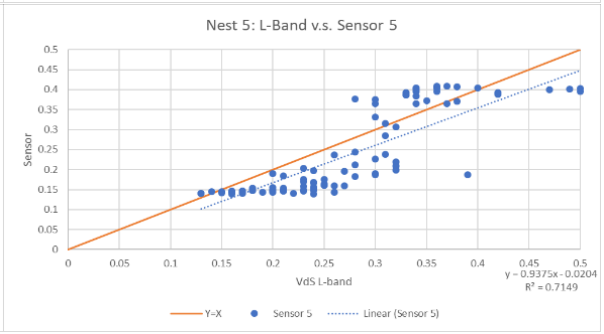

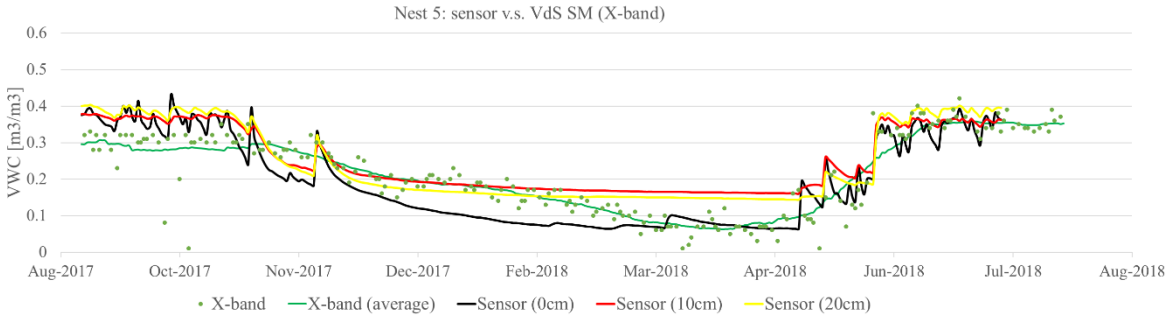
Nest 5: sensor v.s. VdS SM (X-band)
VWC [m3/m3]
0.6
0.5
0.4
0.3
0.2
0.1
0
Aug-2017
Oct-2017
Nov-2017
Dec-2017
Feb-2018
Mar-2018
Apr-2018
Jun-2018
Jul-2018
Aug-2018
X-band
X-band (average)
Sensor (0cm)
Sensor (10cm)
Sensor (20cm)

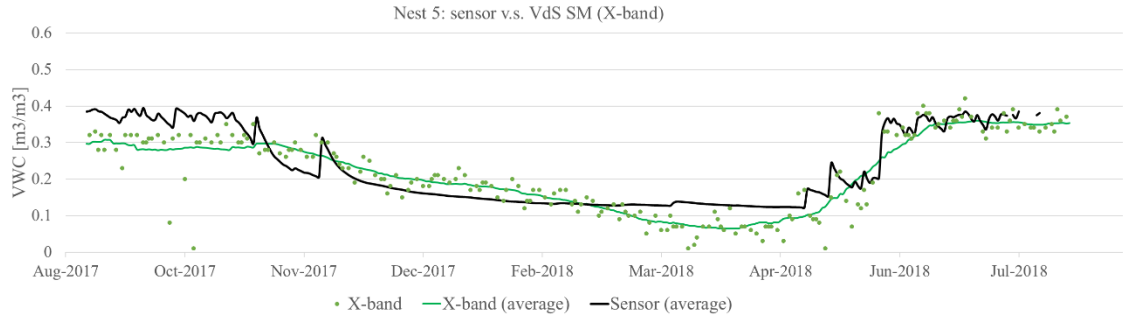
Nest 5: sensor v.s. VdS SM (X-band)
VWC [m3/m3]
0.6
0.5
0.4
0.3
0.2
0.1
0
Aug-2017
Oct-2017
Nov-2017
Dec-2017
Feb-2018
Mar-2018
Apr-2018
Jun-2018
Jul-2018
X-band
X-band (average)
Sensor (average)

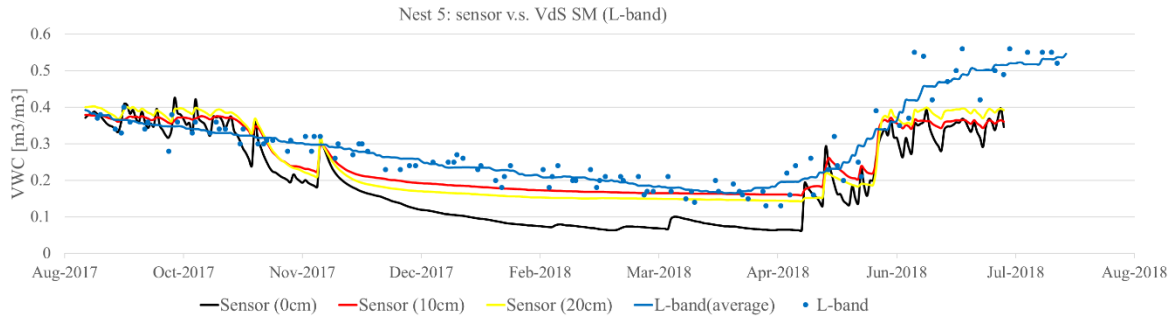
Nest 5: sensor v.s. VdS SM (L-band)
VWC [m3/m3]
0.6
0.5
0.4
0.3
0.2
0.1
0
Aug-2017
Oct-2017
Nov-2017
Dec-2017
Feb-2018
Mar-2018
Apr-2018
Jun-2018
Jul-2018
Aug-2018
Sensor (0cm)
Sensor (10cm)
Sensor (20cm)
L-band(average)
L-band

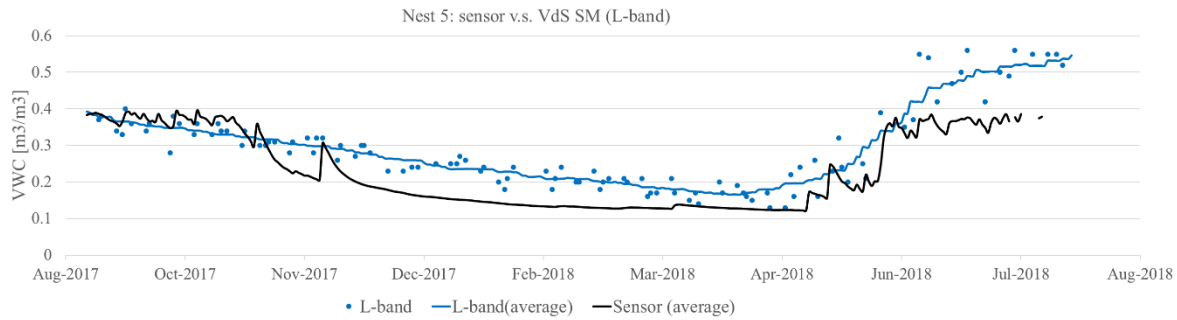
Nest 5: sensor v.s. VdS SM (L-band)
VWC [m3/m3]
0.6
0.5
0.4
0.3
0.2
0.1
0
Aug-2017
Oct-2017
Nov-2017
Dec-2017
Feb-2018
Mar-2018
Apr-2018
Jun-2018
Jul-2018
Aug-2018
L-band
L-band(average)
Sensor (average)

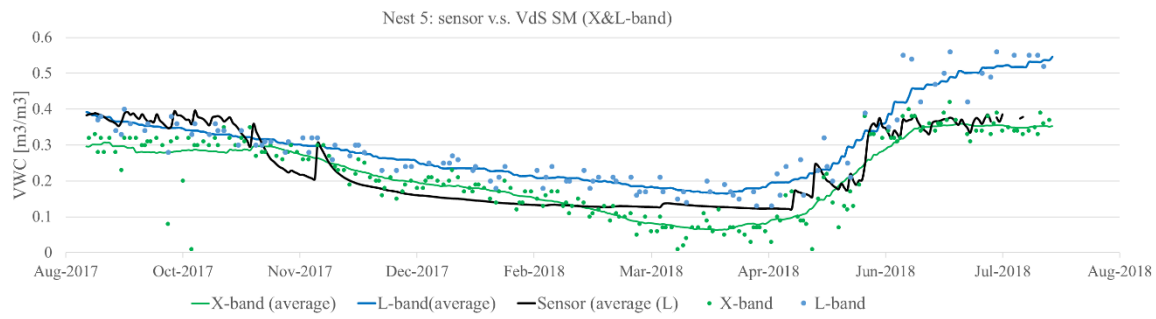
Nest 5: sensor v.s. VdS SM (X&L-band)
VWC [m3/m3]
0.6
0.5
0.4
0.3
0.2
0.1
0
Aug-2017
Oct-2017
Nov-2017
Dec-2017
Feb-2018
Mar-2018
Apr-2018
Jun-2018
Jul-2018
Aug-2018
X-band (average)
L-band(average)
Sensor (average (L)
X-band
L-band

9.6: In-situ soil moisture sensor data compared to volumetric soil moisture measurements and VanderSat X & L-band

Nest 1: Sensor v.s. Volumetric soil moisture measurements v.s. X & L-band

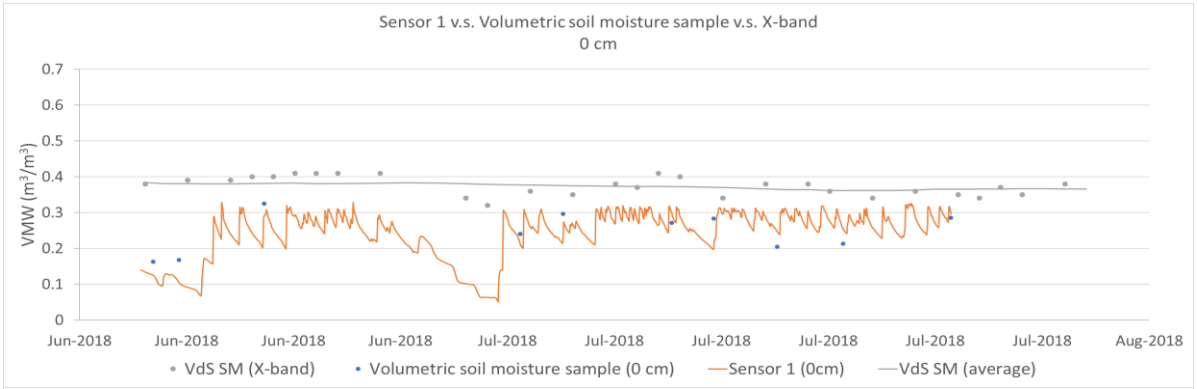

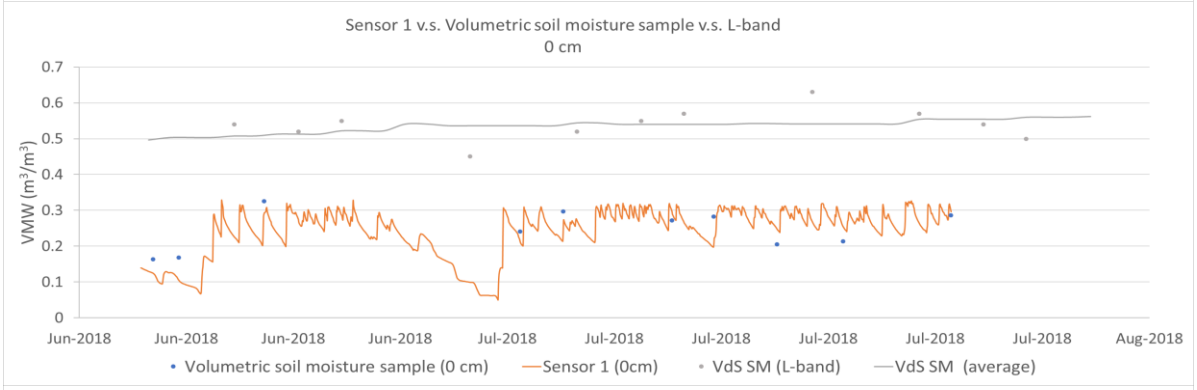

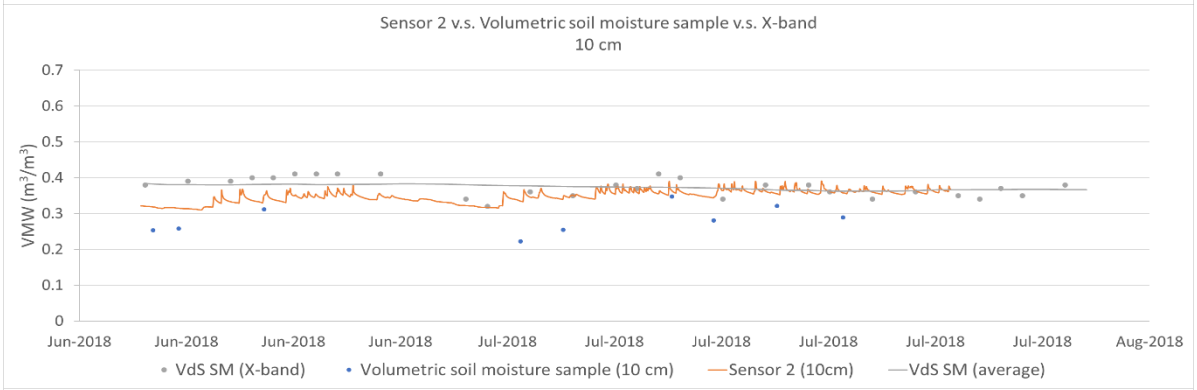

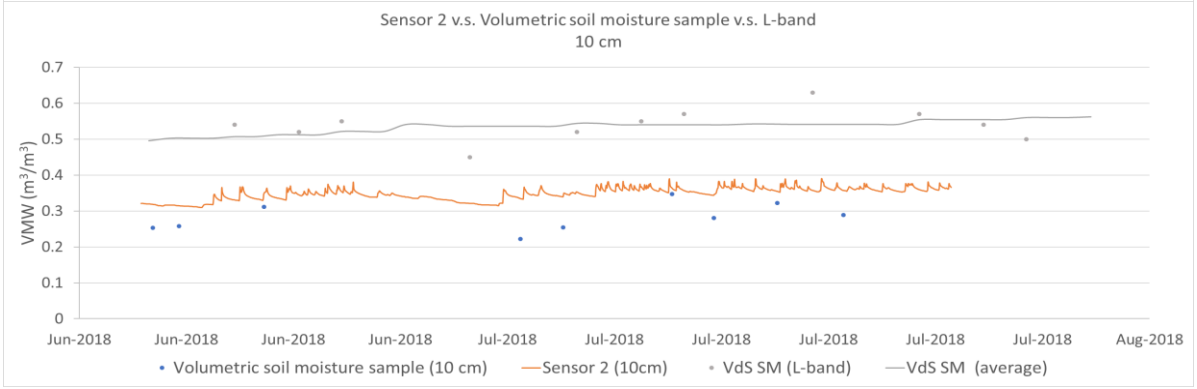

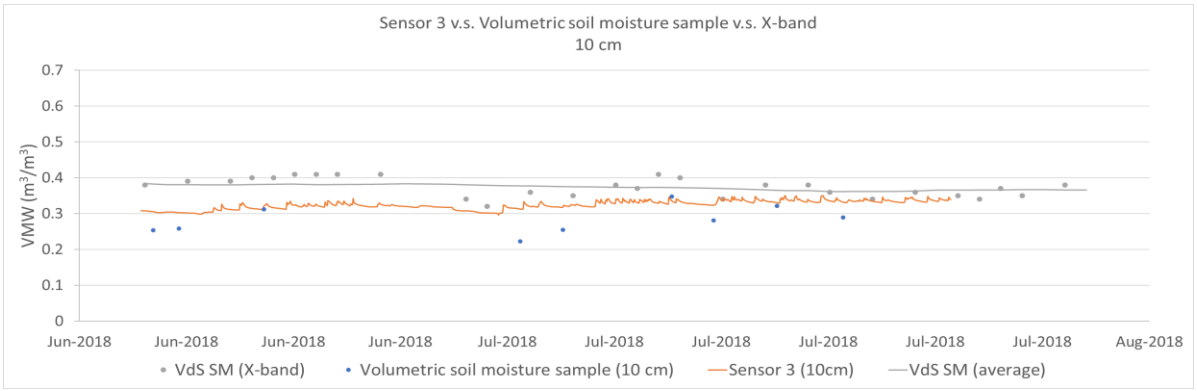
Sensor 3 v.s. Volumetric soil moisture sample v.s. X-band
10 cm
VMW (m³/m³)
0.7
0.6
0.5
0.4
0.3
0.2
0.1
0
Jun-2018
Jun-2018
Jun-2018
Jun-2018
Jul-2018
Jul-2018
Jul-2018
Jul-2018
Jul-2018
Jul-2018
Aug-2018
VdS SM (X-band)
Volumetric soil moisture sample (10 cm)
Sensor 3 (10cm)
VdS SM (average)

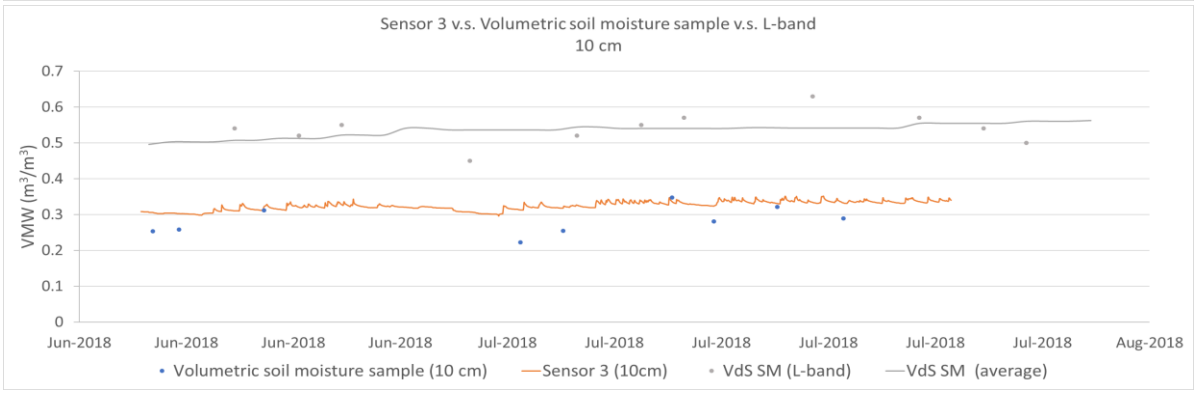
Sensor 3 v.s. Volumetric soil moisture sample v.s. L-band
10 cm
VMW (m³/m³)
0.7
0.6
0.5
0.4
0.3
0.2
0.1
0
Jun-2018
Jun-2018
Jun-2018
Jun-2018
Jul-2018
Jul-2018
Jul-2018
Jul-2018
Jul-2018
Jul-2018
Aug-2018
Volumetric soil moisture sample (10 cm)
Sensor 3 (10cm)
VdS SM (L-band)
VdS SM (average)

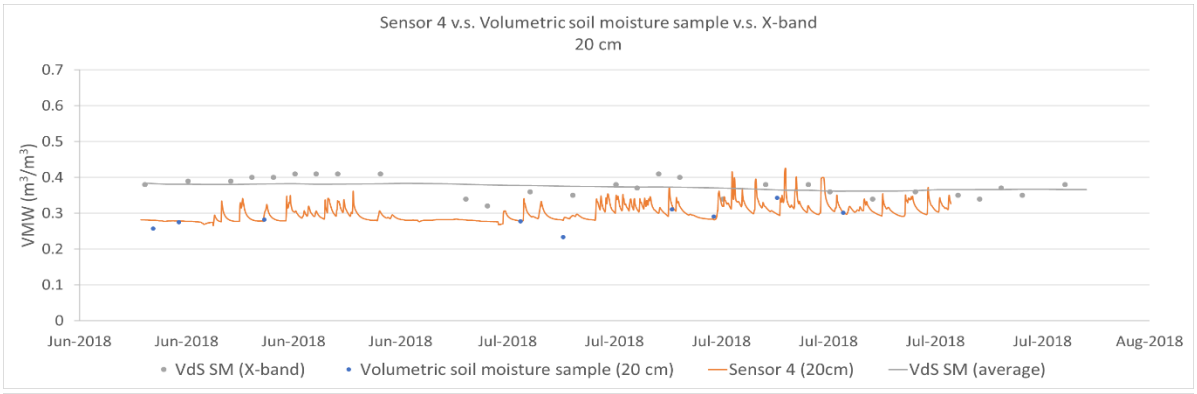
Sensor 4 v.s. Volumetric soil moisture sample v.s. X-band
20 cm
VMW (m³/m³)
0.7
0.6
0.5
0.4
0.3
0.2
0.1
0
Jun-2018
Jun-2018
Jun-2018
Jun-2018
Jul-2018
Jul-2018
Jul-2018
Jul-2018
Jul-2018
Jul-2018
Aug-2018
VdS SM (X-band)
Volumetric soil moisture sample (20 cm)
Sensor 4 (20cm)
VdS SM (average)

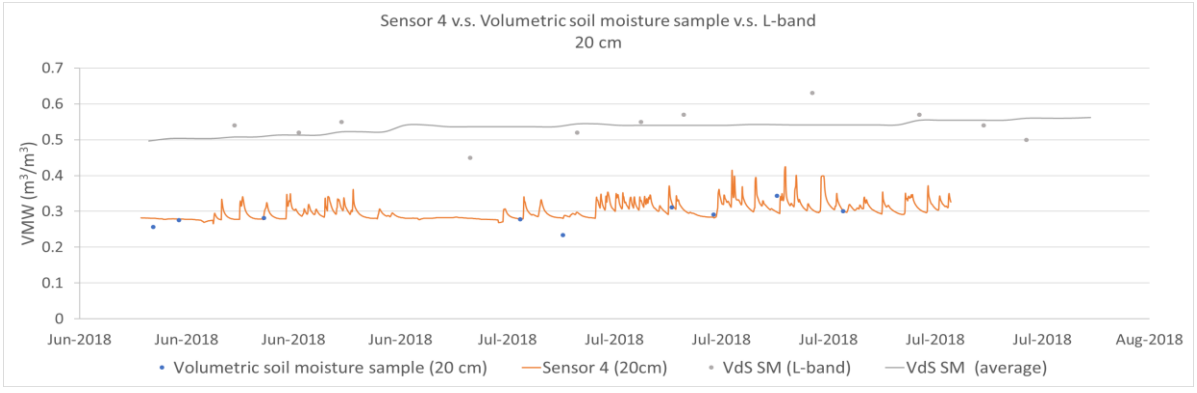
Sensor 4 v.s. Volumetric soil moisture sample v.s. L-band
20 cm
VMW (m³/m³)
0.7
0.6
0.5
0.4
0.3
0.2
0.1
0
Jun-2018
Jun-2018
Jun-2018
Jun-2018
Jul-2018
Jul-2018
Jul-2018
Jul-2018
Jul-2018
Jul-2018
Aug-2018
Volumetric soil moisture sample (20 cm)
Sensor 4 (20cm)
VdS SM (L-band)
VdS SM (average)

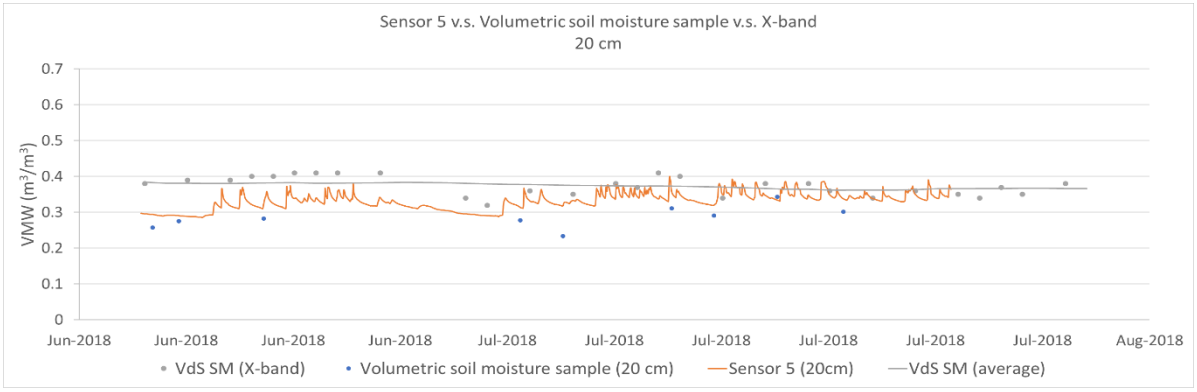

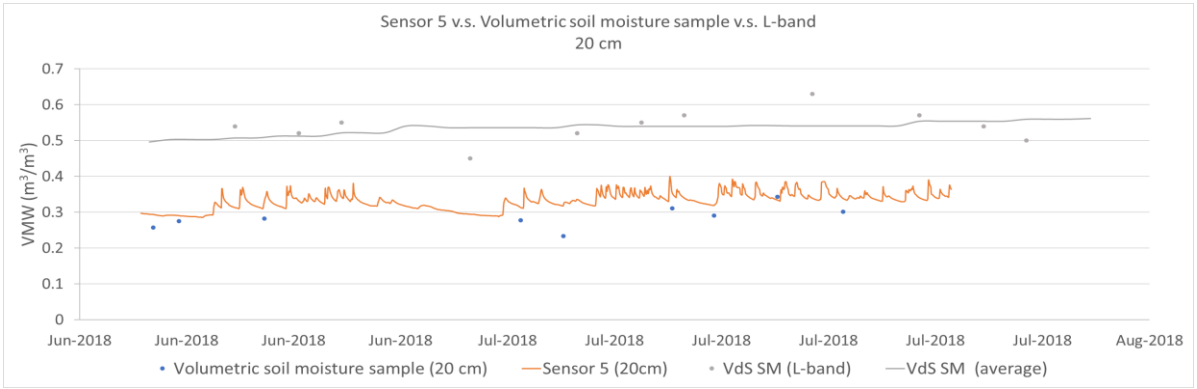

Nest 2: Sensor v.s. Volumetric soil moisture measurements v.s. X & L-band

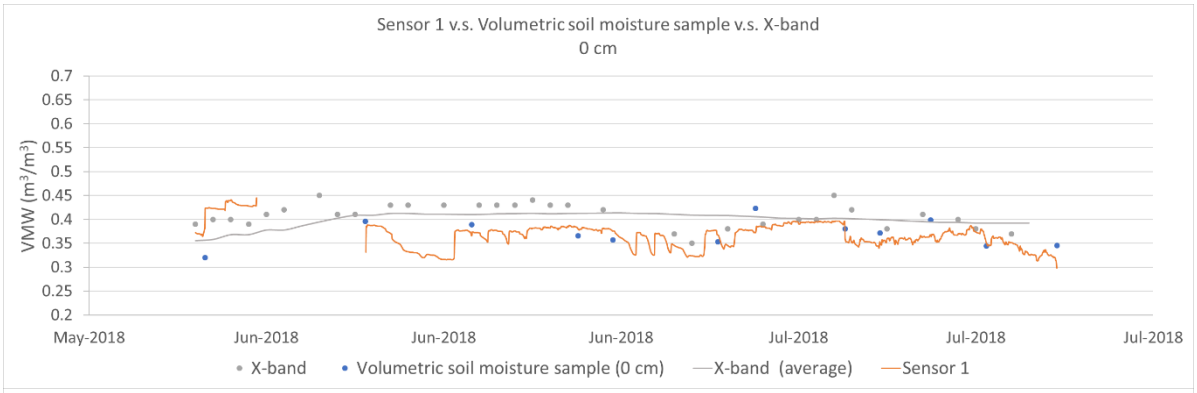

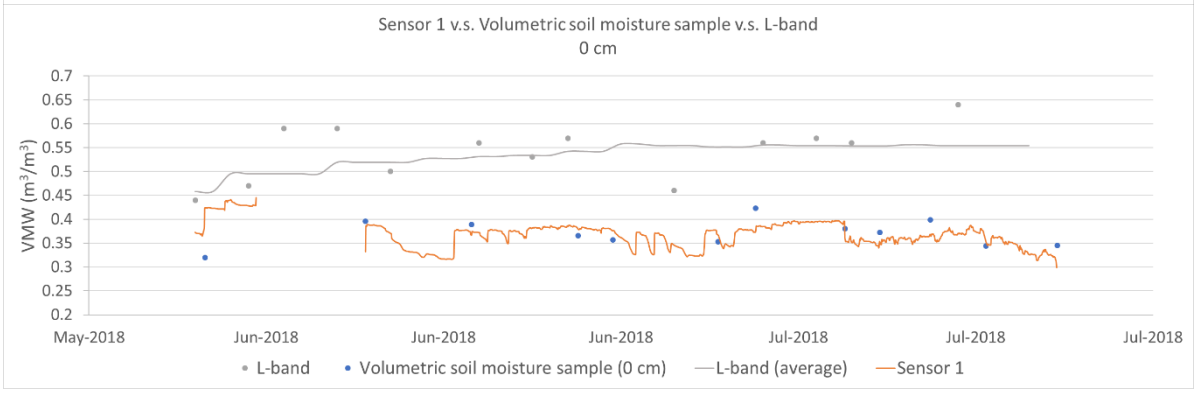

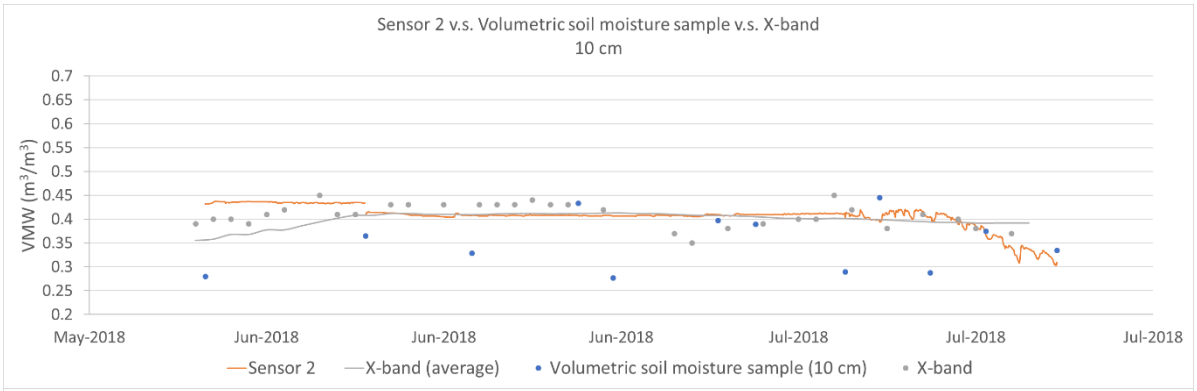
Sensor 2 v.s. Volumetric soil moisture sample v.s. X-band
10 cm
VMW (m³/m³)
0.7
0.65
0.6
0.55
0.5
0.45
0.4
0.35
0.3
0.25
0.2
May-2018
Jun-2018
Jun-2018
Jun-2018
Jul-2018
Jul-2018
Jul-2018
Sensor 2
X-band (average)
Volumetric soil moisture sample (10 cm)
X-band

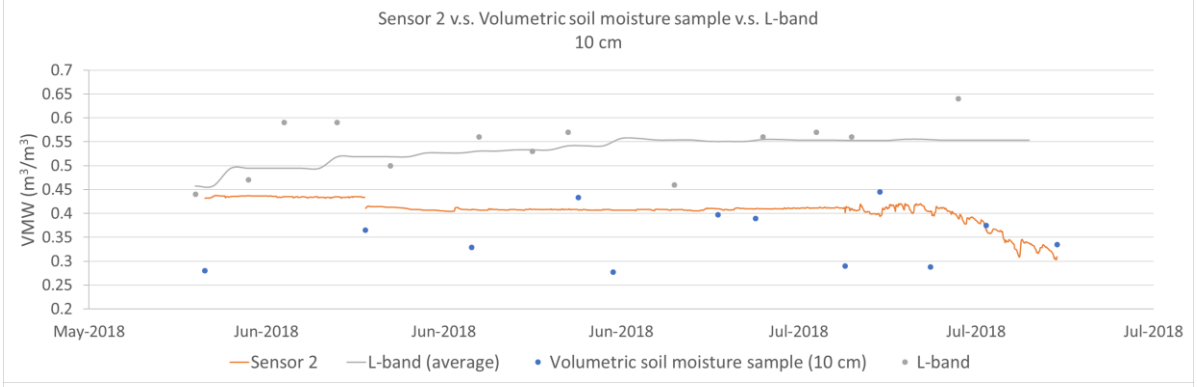
Sensor 2 v.s. Volumetric soil moisture sample v.s. L-band
10 cm
VMW (m³/m³)
0.7
0.65
0.6
0.55
0.5
0.45
0.4
0.35
0.3
0.25
0.2
May-2018
Jun-2018
Jun-2018
Jun-2018
Jul-2018
Jul-2018
Jul-2018
Sensor 2
L-band (average)
Volumetric soil moisture sample (10 cm)
L-band

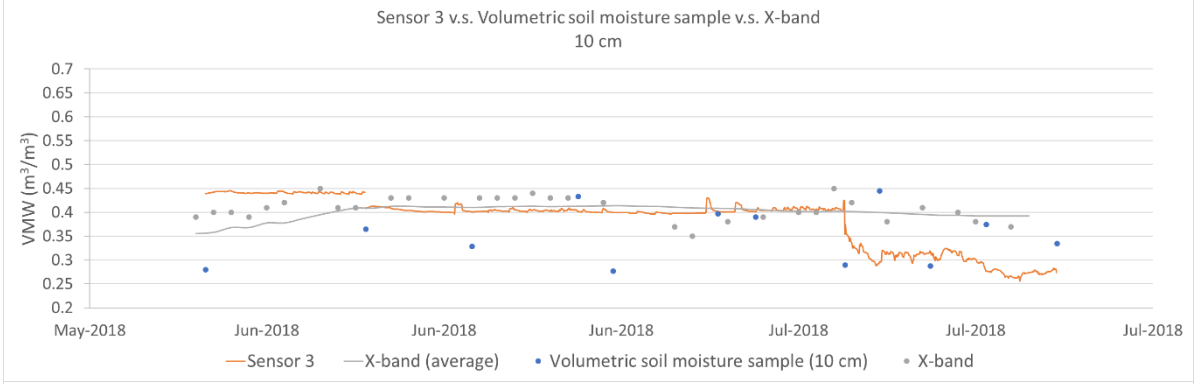
Sensor 3 v.s. Volumetric soil moisture sample v.s. X-band
10 cm
VMW (m³/m³)
0.7
0.65
0.6
0.55
0.5
0.45
0.4
0.35
0.3
0.25
0.2
May-2018
Jun-2018
Jun-2018
Jun-2018
Jul-2018
Jul-2018
Jul-2018
Sensor 3
X-band (average)
Volumetric soil moisture sample (10 cm)
X-band

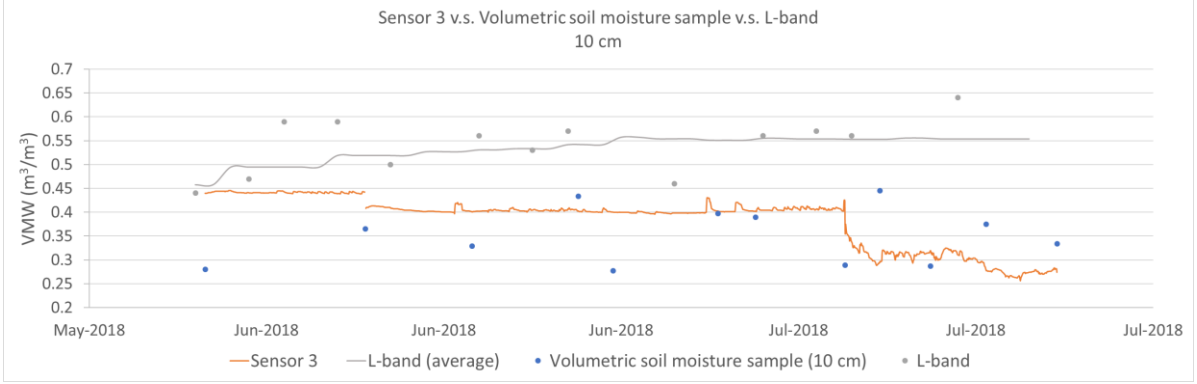
Sensor 3 v.s. Volumetric soil moisture sample v.s. L-band
10 cm
VMW (m³/m³)
0.7
0.65
0.6
0.55
0.5
0.45
0.4
0.35
0.3
0.25
0.2
May-2018
Jun-2018
Jun-2018
Jun-2018
Jul-2018
Jul-2018
Jul-2018
Sensor 3
L-band (average)
Volumetric soil moisture sample (10 cm)
L-band

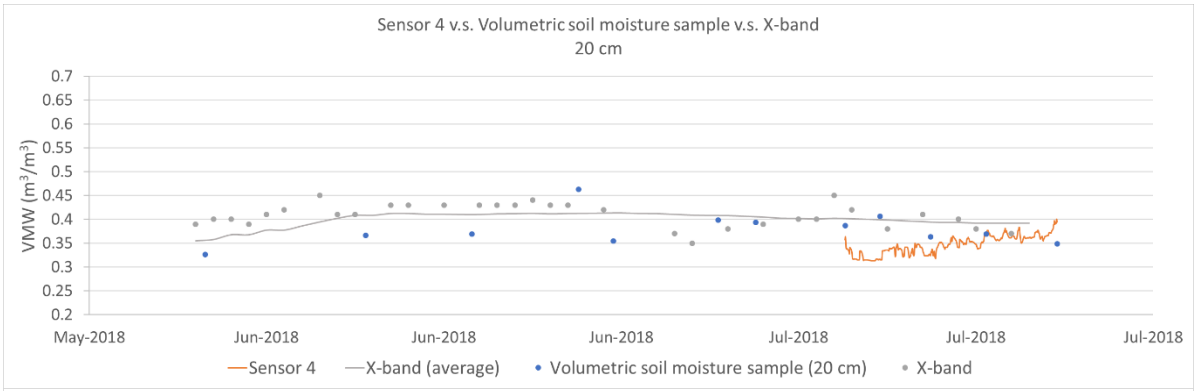
Sensor 4 v.s. Volumetric soil moisture sample v.s. X-band
20 cm
VMW (m³/m³)
0.7
0.65
0.6
0.55
0.5
0.45
0.4
0.35
0.3
0.25
0.2
May-2018
Jun-2018
Jun-2018
Jun-2018
Jul-2018
Jul-2018
Jul-2018
Sensor 4
X-band (average)
Volumetric soil moisture sample (20 cm)
X-band

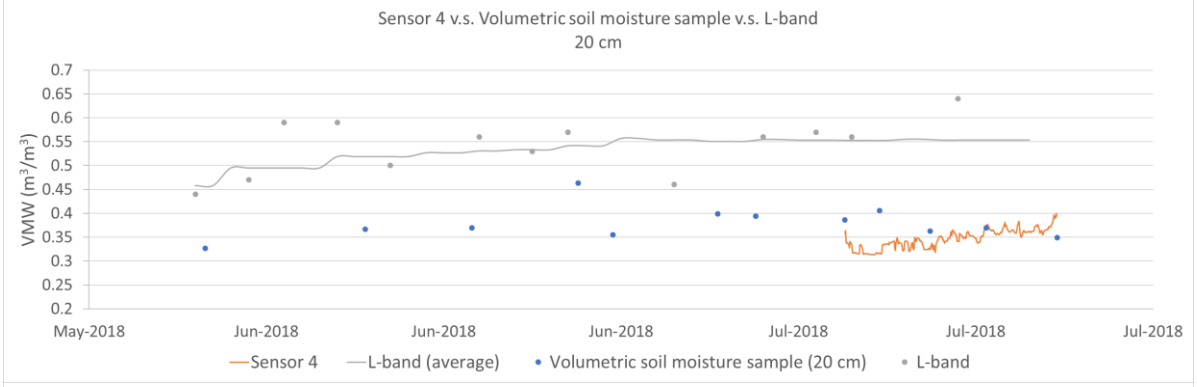
Sensor 4 v.s. Volumetric soil moisture sample v.s. L-band
20 cm
VMW (m³/m³)
0.7
0.65
0.6
0.55
0.5
0.45
0.4
0.35
0.3
0.25
0.2
May-2018
Jun-2018
Jun-2018
Jun-2018
Jul-2018
Jul-2018
Jul-2018
Sensor 4
L-band (average)
Volumetric soil moisture sample (20 cm)
L-band

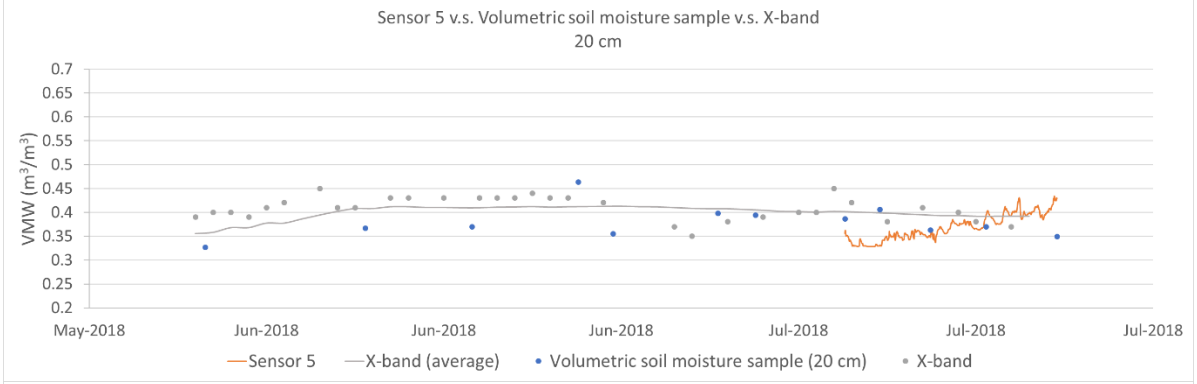
Sensor 5 v.s. Volumetric soil moisture sample v.s. X-band
20 cm
VMW (m³/m³)
0.7
0.65
0.6
0.55
0.5
0.45
0.4
0.35
0.3
0.25
0.2
May-2018
Jun-2018
Jun-2018
Jun-2018
Jul-2018
Jul-2018
Jul-2018
Sensor 5
X-band (average)
Volumetric soil moisture sample (20 cm)
X-band

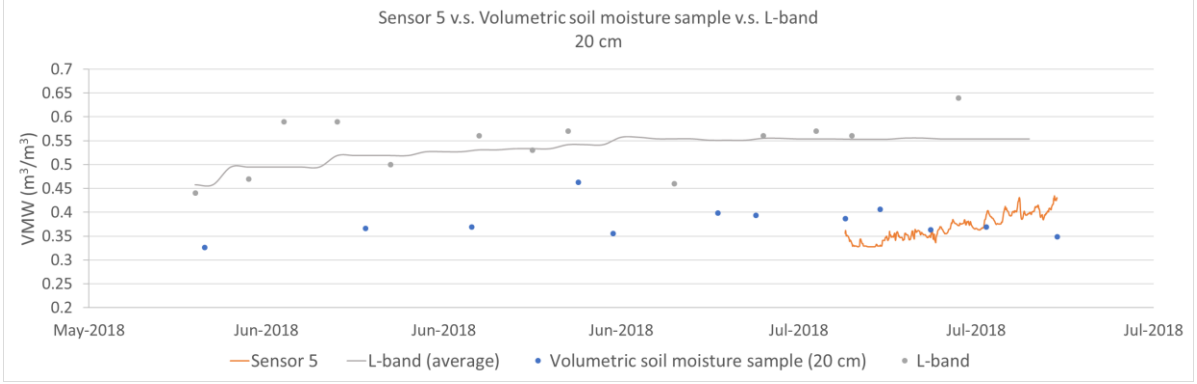
Sensor 5 v.s. Volumetric soil moisture sample v.s. L-band
20 cm
VMW (m³/m³)
0.7
0.65
0.6
0.55
0.5
0.45
0.4
0.35
0.3
0.25
0.2
May-2018
Jun-2018
Jun-2018
Jun-2018
Jul-2018
Jul-2018
Jul-2018
Sensor 5
L-band (average)
Volumetric soil moisture sample (20 cm)
L-band

Nest 3: Sensor v.s. Volumetric soil moisture measurements v.s. X & L-band

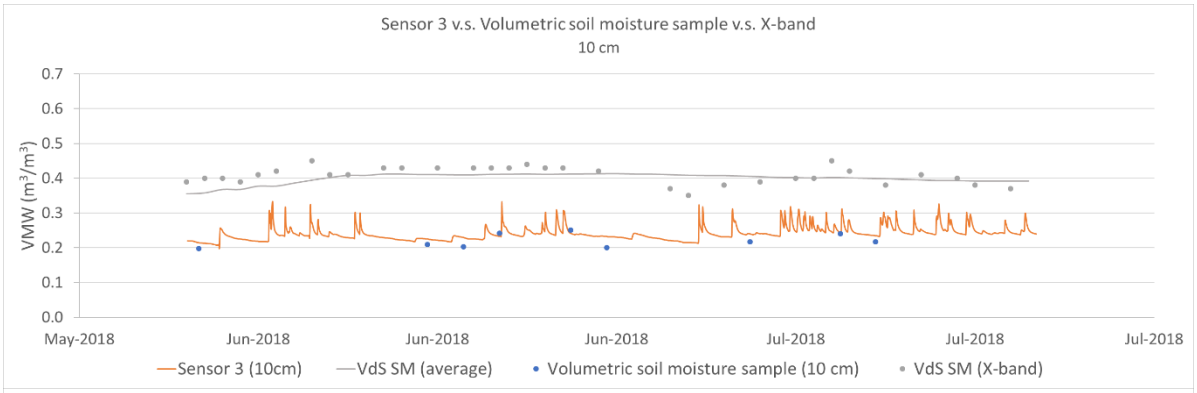
Sensor 3 v.s. Volumetric soil moisture sample v.s. X-band
10 cm
VMW (m³/m³)
0.7
0.6
0.5
0.4
0.3
0.2
0.1
0.0
May-2018
Jun-2018
Jun-2018
Jun-2018
Jul-2018
Jul-2018
Jul-2018
Sensor 3 (10cm)
VdS SM (average)
Volumetric soil moisture sample (10 cm)
VdS SM (X-band)

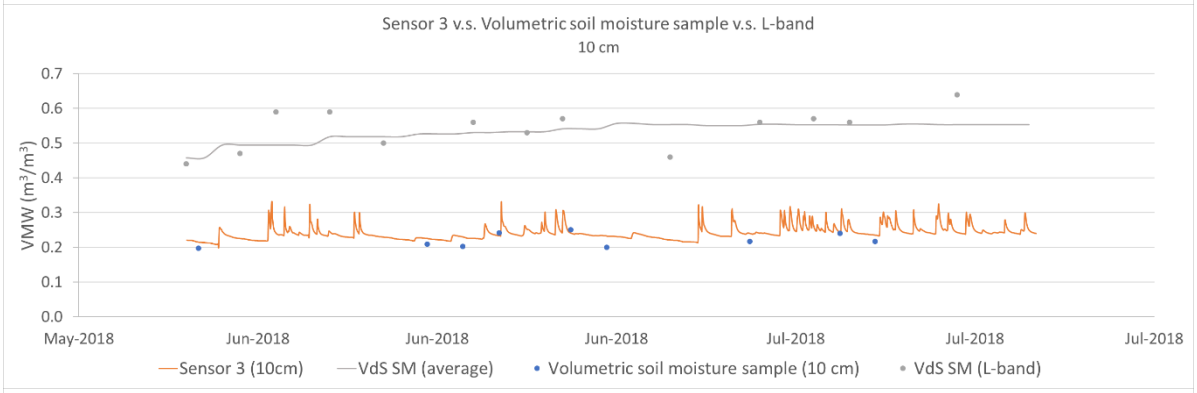
Sensor 3 v.s. Volumetric soil moisture sample v.s. L-band
10 cm
VMW (m³/m³)
0.7
0.6
0.5
0.4
0.3
0.2
0.1
0.0
May-2018
Jun-2018
Jun-2018
Jun-2018
Jul-2018
Jul-2018
Jul-2018
Sensor 3 (10cm)
VdS SM (average)
Volumetric soil moisture sample (10 cm)
VdS SM (L-band)

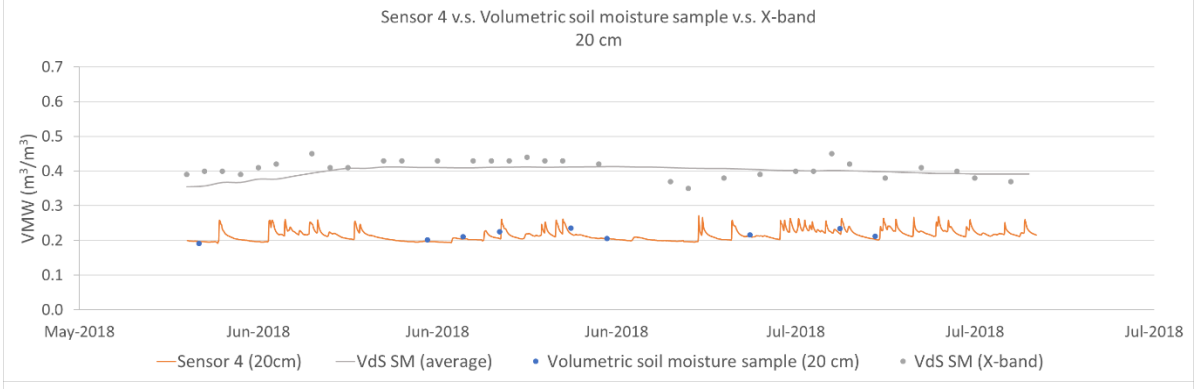
Sensor 4 v.s. Volumetric soil moisture sample v.s. X-band
20 cm
VMW (m³/m³)
0.7
0.6
0.5
0.4
0.3
0.2
0.1
0.0
May-2018
Jun-2018
Jun-2018
Jun-2018
Jul-2018
Jul-2018
Jul-2018
Sensor 4 (20cm)
VdS SM (average)
Volumetric soil moisture sample (20 cm)
VdS SM (X-band)

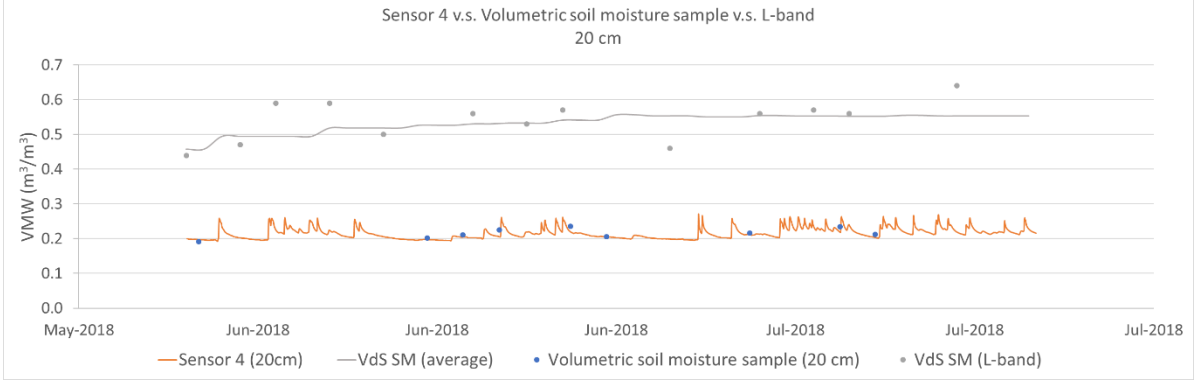
Sensor 4 v.s. Volumetric soil moisture sample v.s. L-band
20 cm
VMW (m³/m³)
0.7
0.6
0.5
0.4
0.3
0.2
0.1
0.0
May-2018
Jun-2018
Jun-2018
Jun-2018
Jul-2018
Jul-2018
Jul-2018
Sensor 4 (20cm)
VdS SM (average)
Volumetric soil moisture sample (20 cm)
VdS SM (L-band)

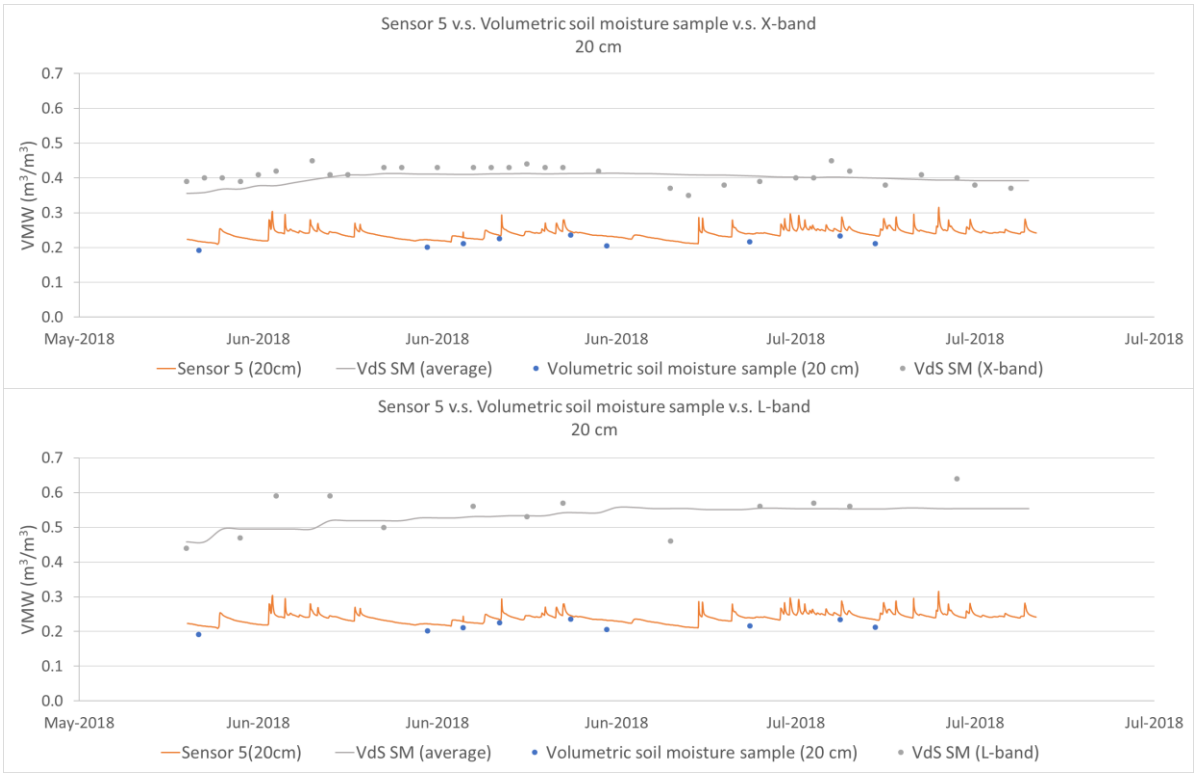

Nest 4: Sensor v.s. Volumetric soil moisture measurements v.s. X & L-band

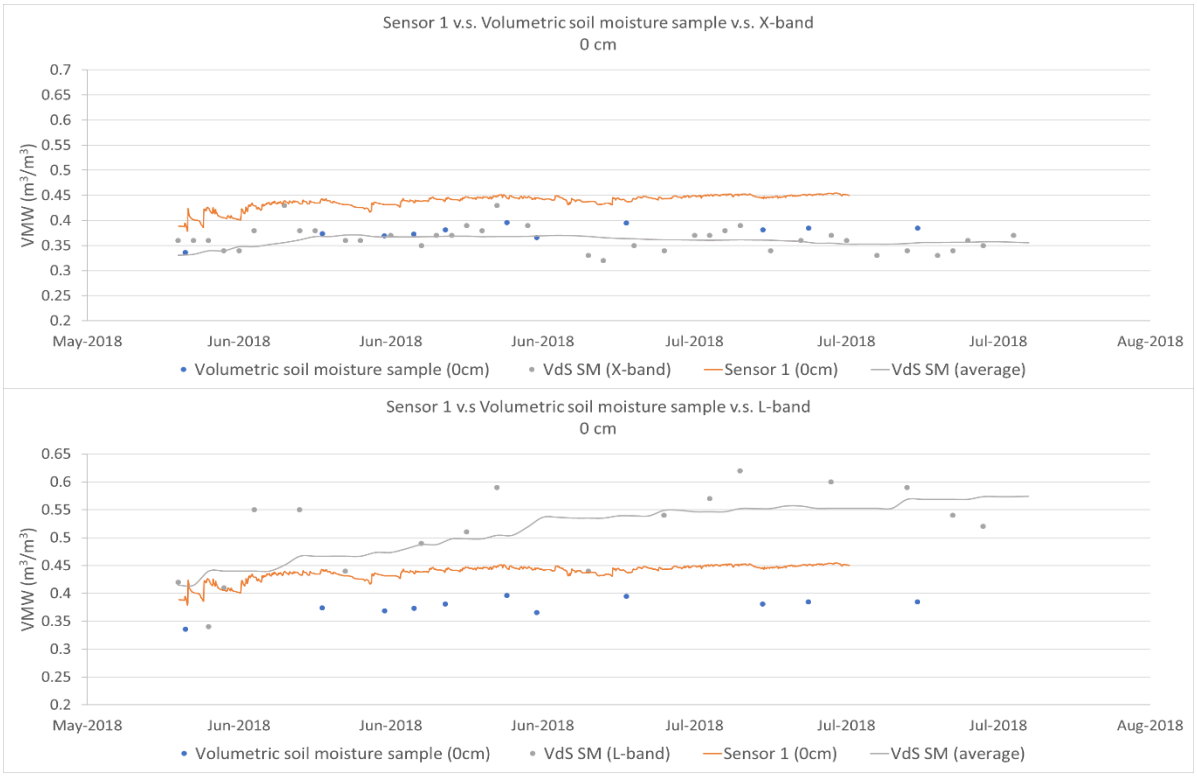

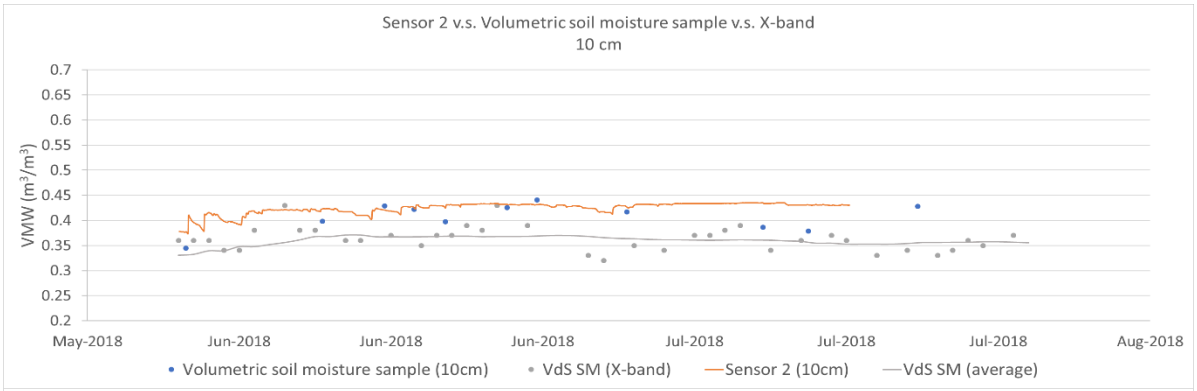
Sensor 2 v.s. Volumetric soil moisture sample v.s. X-band
10 cm
VMW (m³/m³)
0.7
0.65
0.6
0.55
0.5
0.45
0.4
0.35
0.3
0.25
0.2
May-2018
Jun-2018
Jun-2018
Jun-2018
Jul-2018
Jul-2018
Jul-2018
Aug-2018
Volumetric soil moisture sample (10cm)
VdS SM (X-band)
Sensor 2 (10cm)
VdS SM (average)

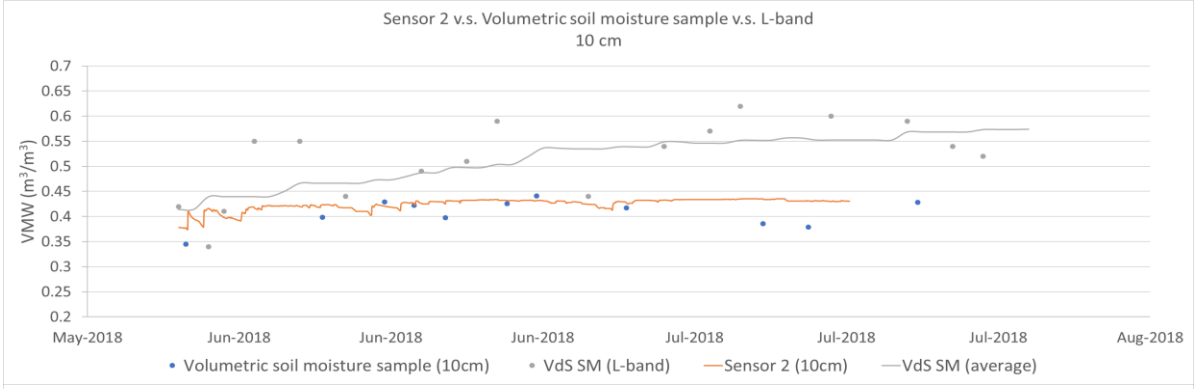
Sensor 2 v.s. Volumetric soil moisture sample v.s. L-band
10 cm
VMW (m³/m³)
0.7
0.65
0.6
0.55
0.5
0.45
0.4
0.35
0.3
0.25
0.2
May-2018
Jun-2018
Jun-2018
Jun-2018
Jul-2018
Jul-2018
Jul-2018
Aug-2018
Volumetric soil moisture sample (10cm)
VdS SM (L-band)
Sensor 2 (10cm)
VdS SM (average)

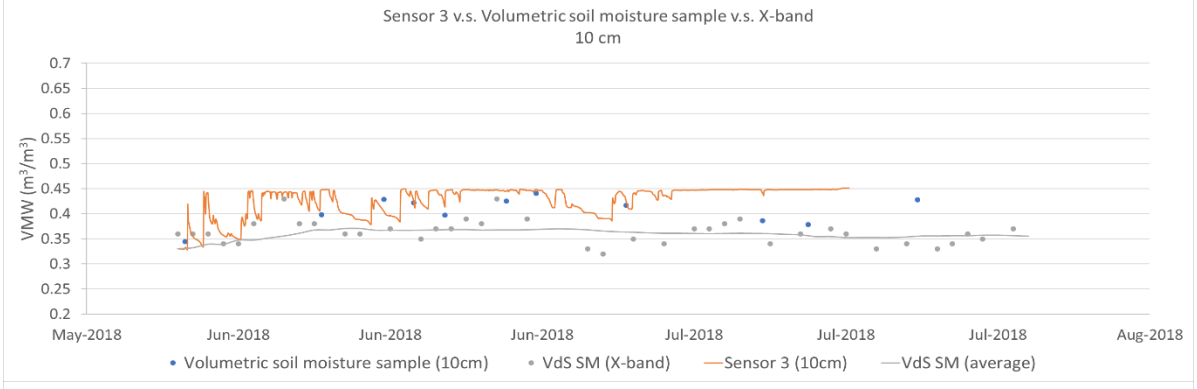
Sensor 3 v.s. Volumetric soil moisture sample v.s. X-band
10 cm
VMW (m³/m³)
0.7
0.65
0.6
0.55
0.5
0.45
0.4
0.35
0.3
0.25
0.2
May-2018
Jun-2018
Jun-2018
Jun-2018
Jul-2018
Jul-2018
Jul-2018
Aug-2018
Volumetric soil moisture sample (10cm)
VdS SM (X-band)
Sensor 3 (10cm)
VdS SM (average)

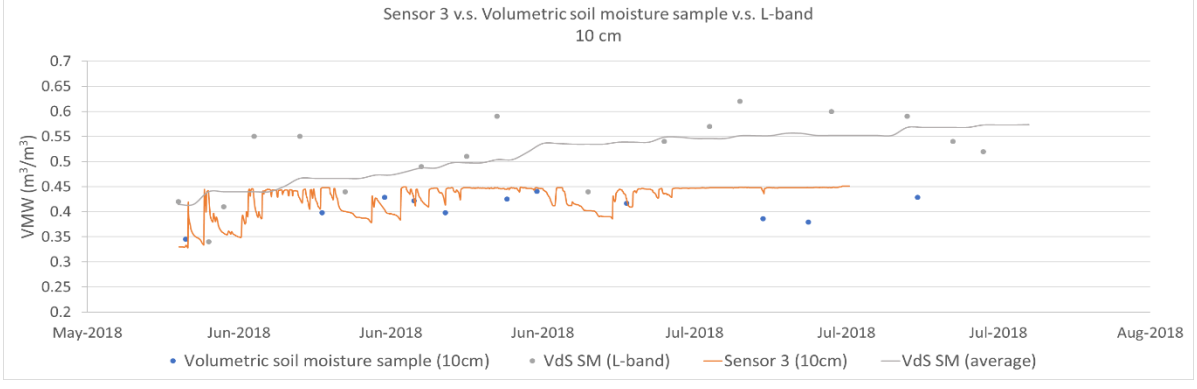
Sensor 3 v.s. Volumetric soil moisture sample v.s. L-band
10 cm
VMW (m³/m³)
0.7
0.65
0.6
0.55
0.5
0.45
0.4
0.35
0.3
0.25
0.2
May-2018
Jun-2018
Jun-2018
Jun-2018
Jul-2018
Jul-2018
Jul-2018
Aug-2018
Volumetric soil moisture sample (10cm)
VdS SM (L-band)
Sensor 3 (10cm)
VdS SM (average)

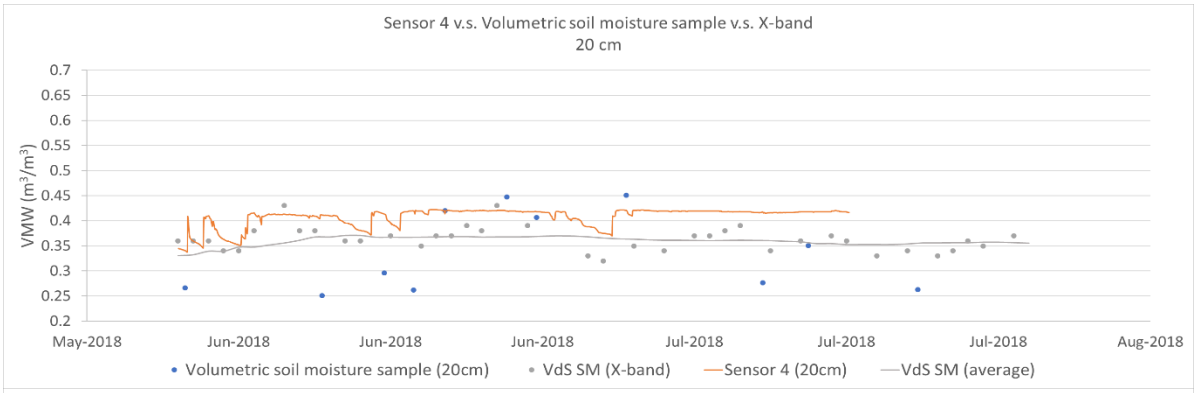
Sensor 4 v.s. Volumetric soil moisture sample v.s. X-band
20 cm
VMW (m³/m³)
0.7
0.65
0.6
0.55
0.5
0.45
0.4
0.35
0.3
0.25
0.2
May-2018
Jun-2018
Jun-2018
Jun-2018
Jul-2018
Jul-2018
Jul-2018
Aug-2018
Volumetric soil moisture sample (20cm)
VdS SM (X-band)
Sensor 4 (20cm)
VdS SM (average)

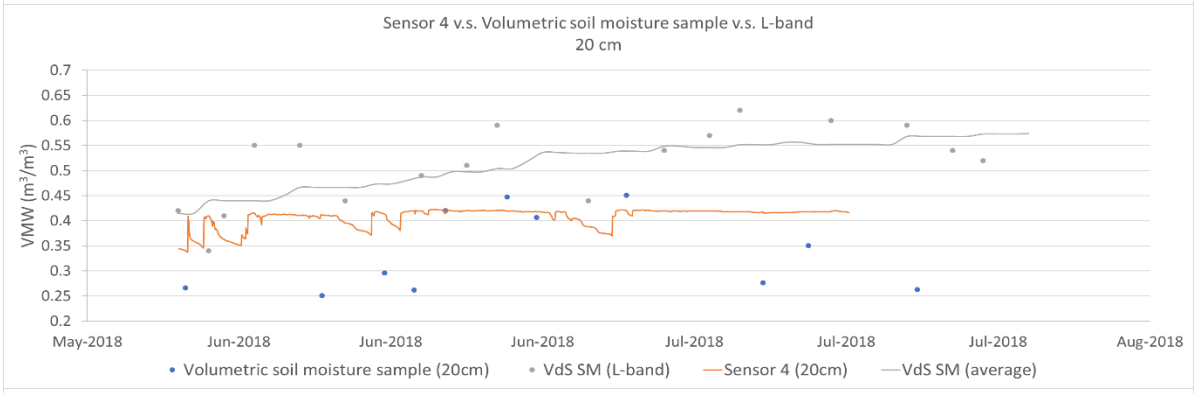
Sensor 4 v.s. Volumetric soil moisture sample v.s. L-band
20 cm
VMW (m³/m³)
0.7
0.65
0.6
0.55
0.5
0.45
0.4
0.35
0.3
0.25
0.2
May-2018
Jun-2018
Jun-2018
Jun-2018
Jul-2018
Jul-2018
Jul-2018
Aug-2018
Volumetric soil moisture sample (20cm)
VdS SM (L-band)
Sensor 4 (20cm)
VdS SM (average)

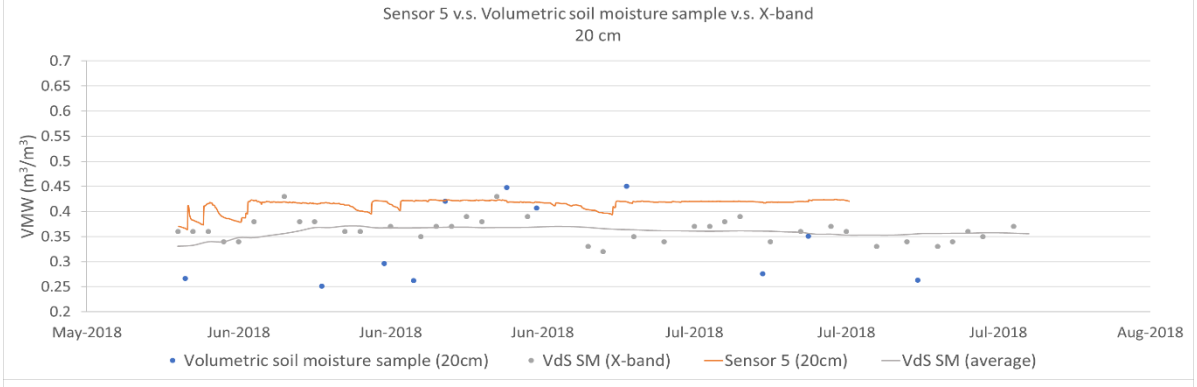
Sensor 5 v.s. Volumetric soil moisture sample v.s. X-band
20 cm
VMW (m³/m³)
0.7
0.65
0.6
0.55
0.5
0.45
0.4
0.35
0.3
0.25
0.2
May-2018
Jun-2018
Jun-2018
Jun-2018
Jul-2018
Jul-2018
Jul-2018
Aug-2018
Volumetric soil moisture sample (20cm)
VdS SM (X-band)
Sensor 5 (20cm)
VdS SM (average)

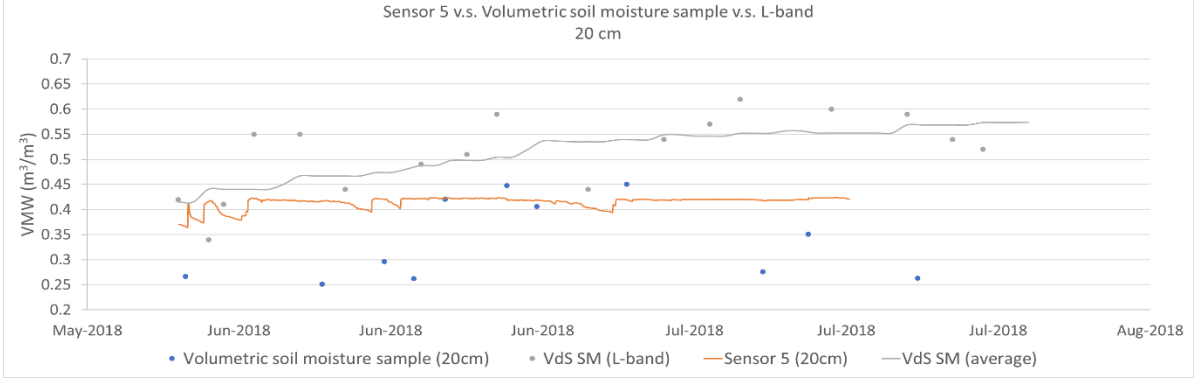
Sensor 5 v.s. Volumetric soil moisture sample v.s. L-band
20 cm
VMW (m³/m³)
0.7
0.65
0.6
0.55
0.5
0.45
0.4
0.35
0.3
0.25
0.2
May-2018
Jun-2018
Jun-2018
Jun-2018
Jul-2018
Jul-2018
Jul-2018
Aug-2018
Volumetric soil moisture sample (20cm)
VdS SM (L-band)
Sensor 5 (20cm)
VdS SM (average)

Nest 5: Sensor v.s. Volumetric soil moisture measurements v.s. X & L-band

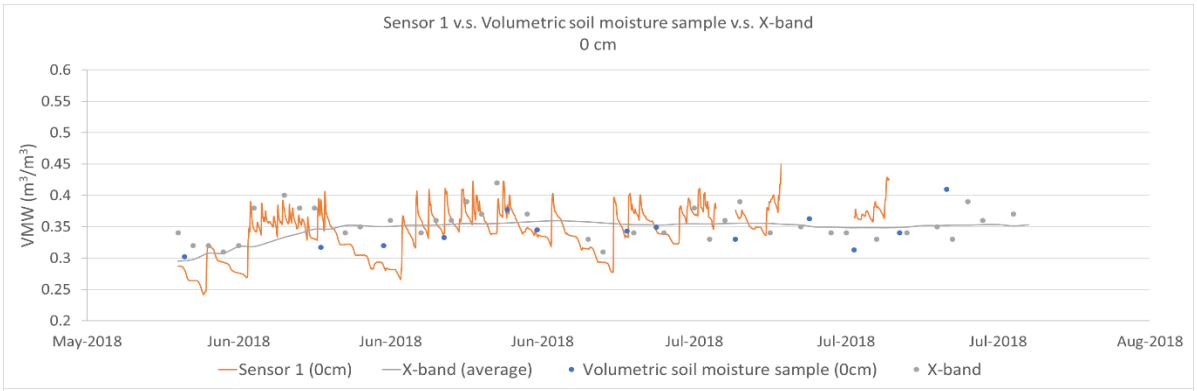

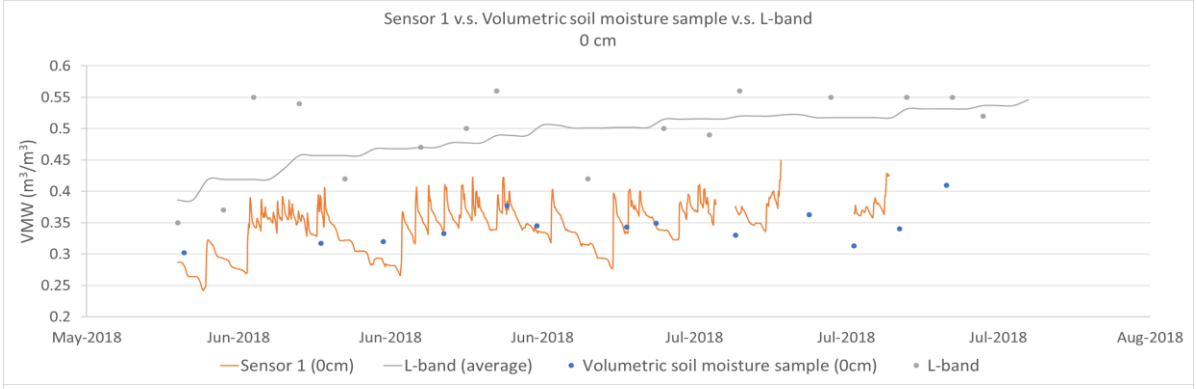

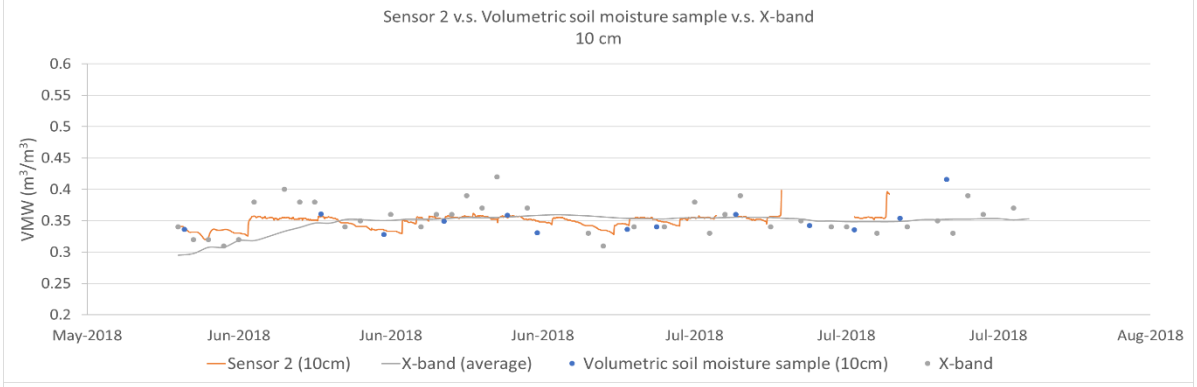

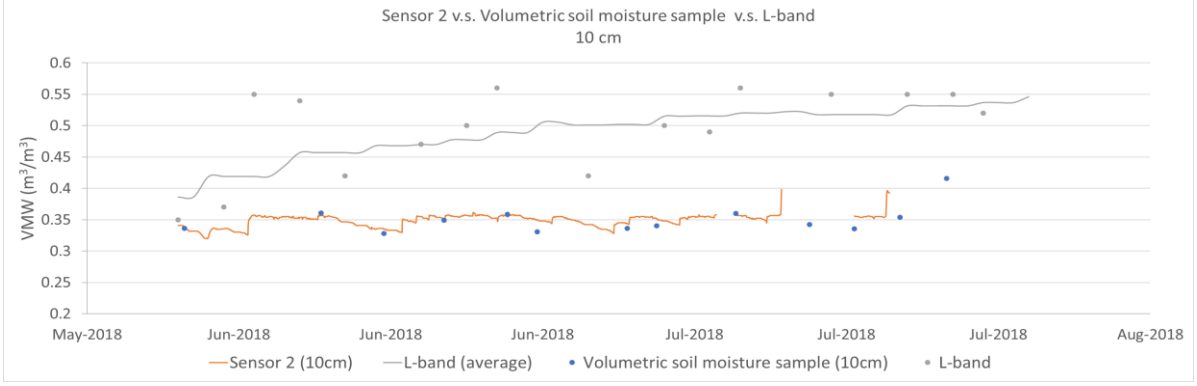

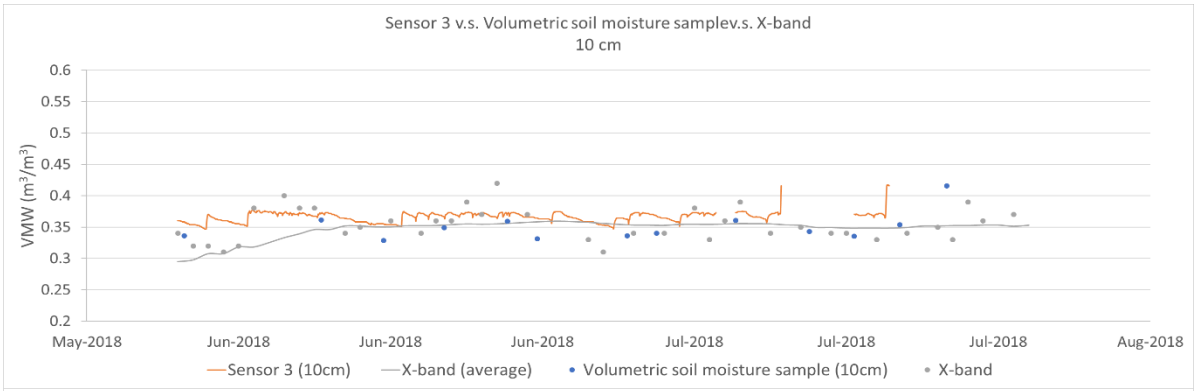
Sensor 3 v.s. Volumetric soil moisture samplev.s. X-band
10 cm
VMW (m³/m³)
0.6
0.55
0.5
0.45
0.4
0.35
0.3
0.25
0.2
May-2018
Jun-2018
Jun-2018
Jun-2018
Jul-2018
Jul-2018
Jul-2018
Aug-2018
Sensor 3 (10cm)
X-band (average)
Volumetric soil moisture sample (10cm)
X-band

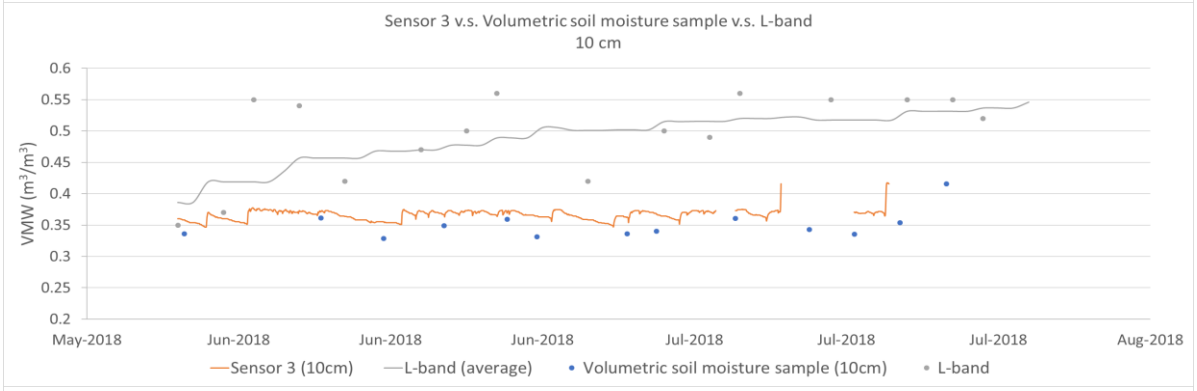
Sensor 3 v.s. Volumetric soil moisture sample v.s. L-band
10 cm
VMW (m³/m³)
0.6
0.55
0.5
0.45
0.4
0.35
0.3
0.25
0.2
May-2018
Jun-2018
Jun-2018
Jun-2018
Jul-2018
Jul-2018
Jul-2018
Aug-2018
Sensor 3 (10cm)
L-band (average)
Volumetric soil moisture sample (10cm)
L-band

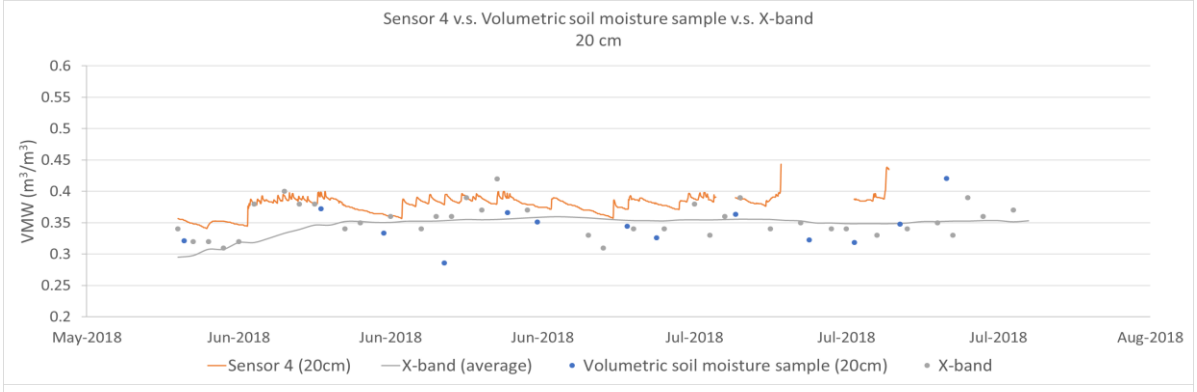
Sensor 4 v.s. Volumetric soil moisture sample v.s. X-band
20 cm
VMW (m³/m³)
0.6
0.55
0.5
0.45
0.4
0.35
0.3
0.25
0.2
May-2018
Jun-2018
Jun-2018
Jun-2018
Jul-2018
Jul-2018
Jul-2018
Aug-2018
Sensor 4 (20cm)
X-band (average)
Volumetric soil moisture sample (20cm)
X-band

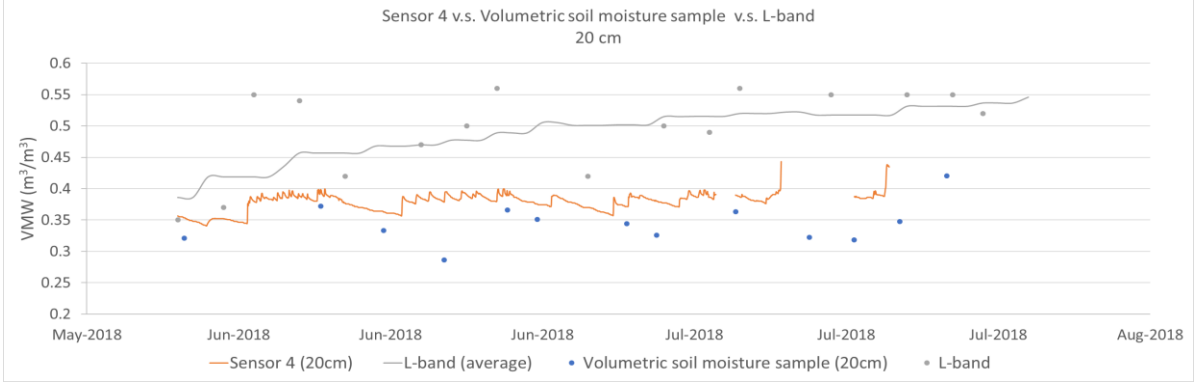
Sensor 4 v.s. Volumetric soil moisture sample v.s. L-band
20 cm
VMW (m³/m³)
0.6
0.55
0.5
0.45
0.4
0.35
0.3
0.25
0.2
May-2018
Jun-2018
Jun-2018
Jun-2018
Jul-2018
Jul-2018
Jul-2018
Aug-2018
Sensor 4 (20cm)
L-band (average)
Volumetric soil moisture sample (20cm)
L-band


Sensor 5 v.s. Volumetric soil moisture sample v.s. X-band
20 cm
VMW (m³/m³)
0.6
0.55
0.5
0.45
0.4
0.35
0.3
0.25
0.2
May-2018
Jun-2018
Jun-2018
Jun-2018
Jul-2018
Jul-2018
Jul-2018
Aug-2018
Sensor 5 (20cm)
X-band (average)
Volumetric soil moisture sample (20cm)
X-band

Sensor 5 v.s. Volumetric soil moisture sample v.s. L-band
20 cm
VMW (m³/m³)
0.6
0.55
0.5
0.45
0.4
0.35
0.3
0.25
0.2
May-2018
Jun-2018
Jun-2018
Jun-2018
Jul-2018
Jul-2018
Jul-2018
Aug-2018
Sensor 5 (20cm)
L-band (average)
Volumetric soil moisture sample (20cm)
L-band

9.7: In-situ soil moisture sensor data compared to VanderSat X & L-band and VOD

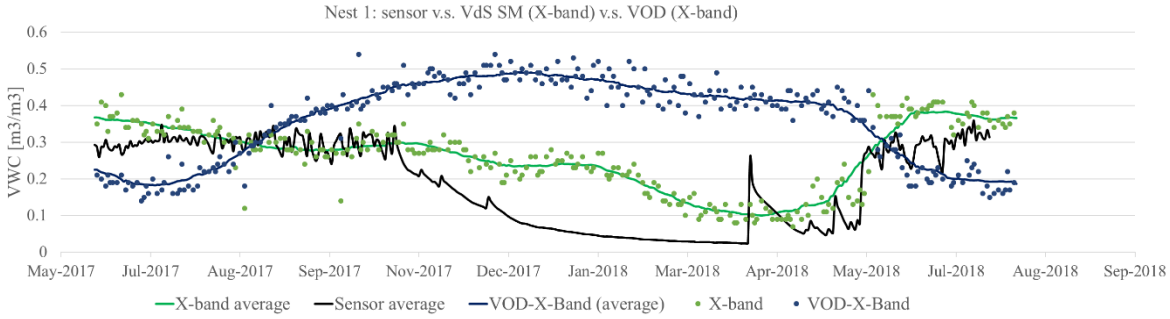

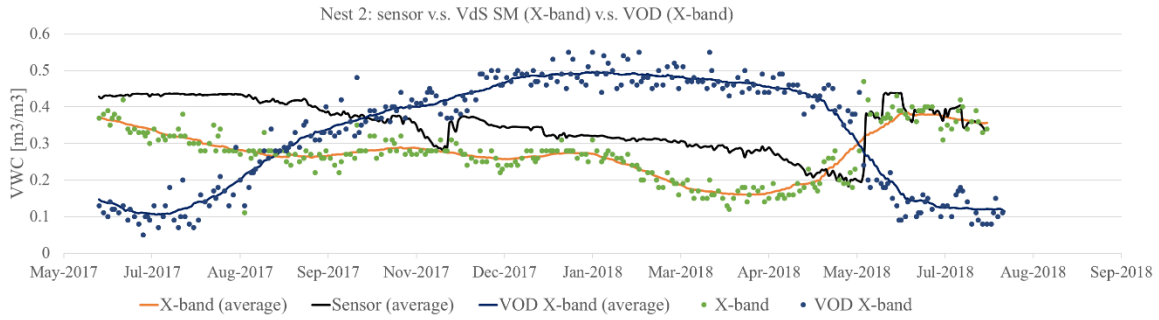

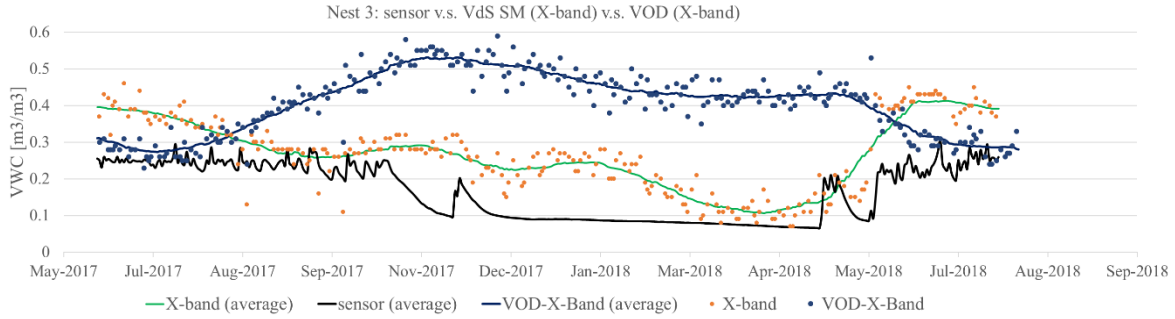

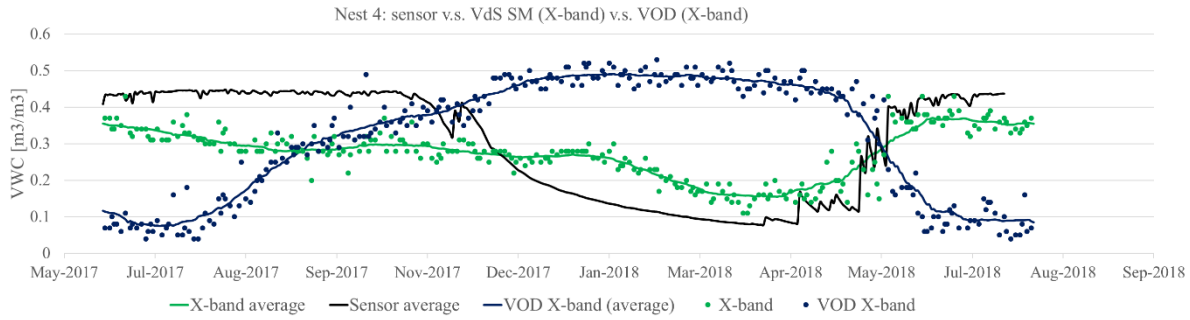

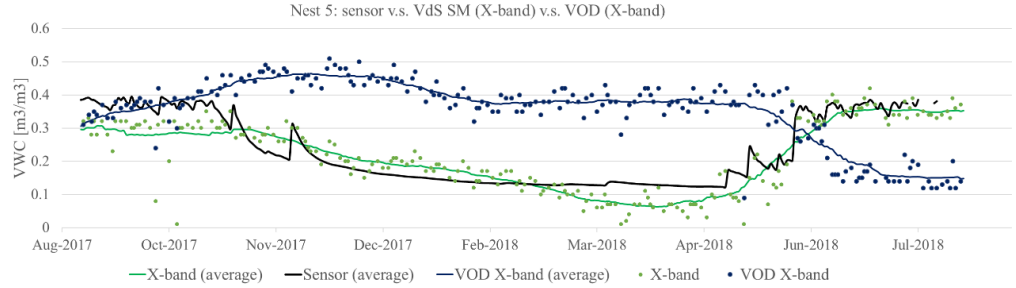

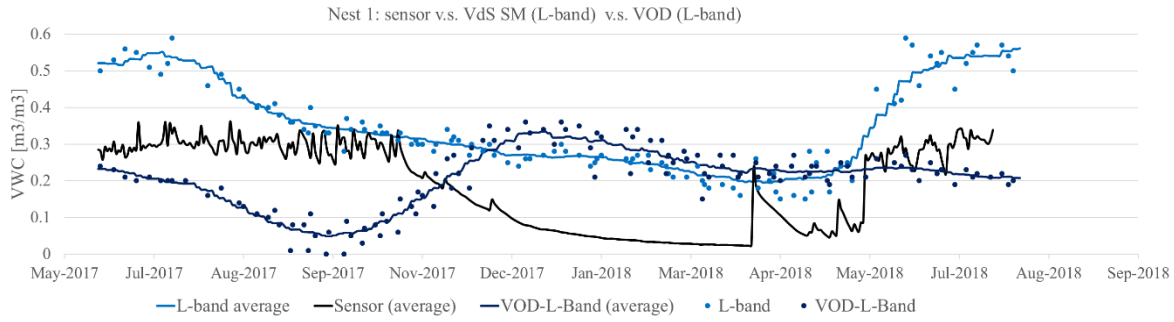
Nest 1: sensor v.s. VdS SM (L-band) v.s. VOD (L-band)
VWC [m3/m3]
0.6
0.5
0.4
0.3
0.2
0.1
0
May-2017 Jul-2017 Aug-2017 Sep-2017 Nov-2017 Dec-2017 Jan-2018 Mar-2018 Apr-2018 May-2018 Jul-2018 Aug-2018 Sep-2018
L-band average
Sensor (average)
VOD-L-Band (average)
L-band
VOD-L-Band

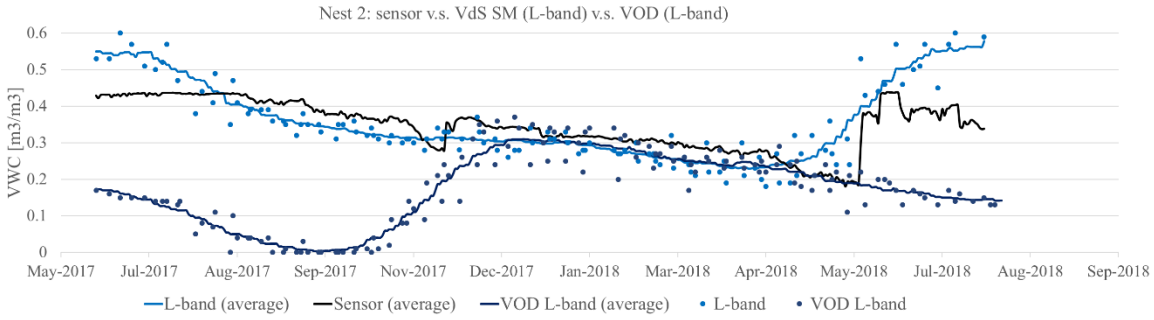
Nest 2: sensor v.s. VdS SM (L-band) v.s. VOD (L-band)
VWC [m3/m3]
0.6
0.5
0.4
0.3
0.2
0.1
0
May-2017 Jul-2017 Aug-2017 Sep-2017 Nov-2017 Dec-2017 Jan-2018 Mar-2018 Apr-2018 May-2018 Jul-2018 Aug-2018 Sep-2018
L-band (average)
Sensor (average)
VOD L-band (average)
L-band
VOD L-band

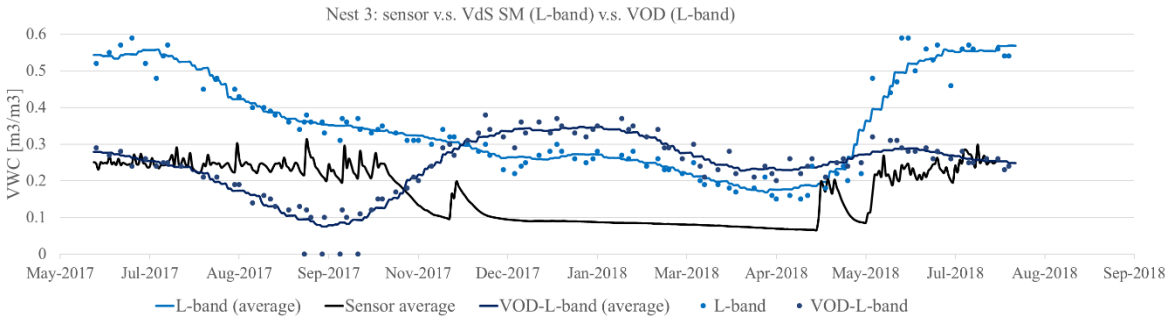
Nest 3: sensor v.s. VdS SM (L-band) v.s. VOD (L-band)
VWC [m3/m3]
0.6
0.5
0.4
0.3
0.2
0.1
0
May-2017 Jul-2017 Aug-2017 Sep-2017 Nov-2017 Dec-2017 Jan-2018 Mar-2018 Apr-2018 May-2018 Jul-2018 Aug-2018 Sep-2018
L-band (average)
Sensor average
VOD-L-band (average)
L-band
VOD-L-band

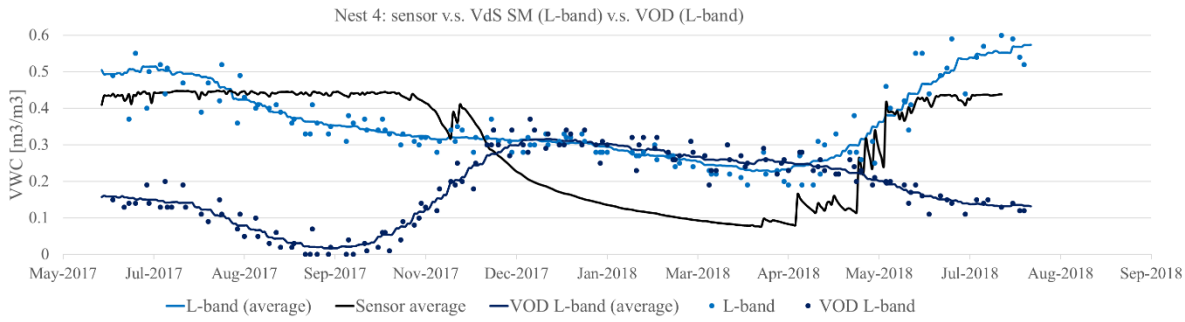
Nest 4: sensor v.s. VdS SM (L-band) v.s. VOD (L-band)
VWC [m3/m3]
0.6
0.5
0.4
0.3
0.2
0.1
0
May-2017 Jul-2017 Aug-2017 Sep-2017 Nov-2017 Dec-2017 Jan-2018 Mar-2018 Apr-2018 May-2018 Jul-2018 Aug-2018 Sep-2018
L-band (average)
Sensor average
VOD L-band (average)
L-band
VOD L-band

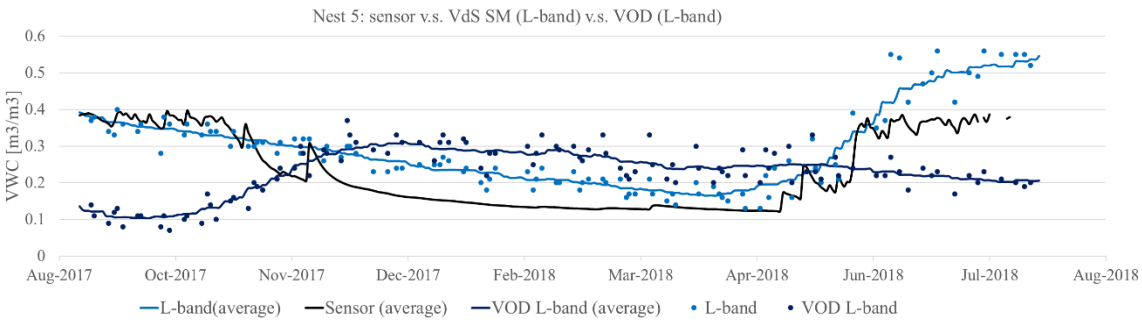
Nest 5: sensor v.s. VdS SM (L-band) v.s. VOD (L-band)
VWC [m3/m3]
0.6
0.5
0.4
0.3
0.2
0.1
0
Aug-2017 Oct-2017 Nov-2017 Dec-2017 Feb-2018 Mar-2018 Apr-2018 Jun-2018 Jul-2018 Aug-2018
L-band(average)
Sensor (average)
VOD L-band (average)
L-band
VOD L-band

9.8 NDVI timeseries of each sensor nest

Nest 1

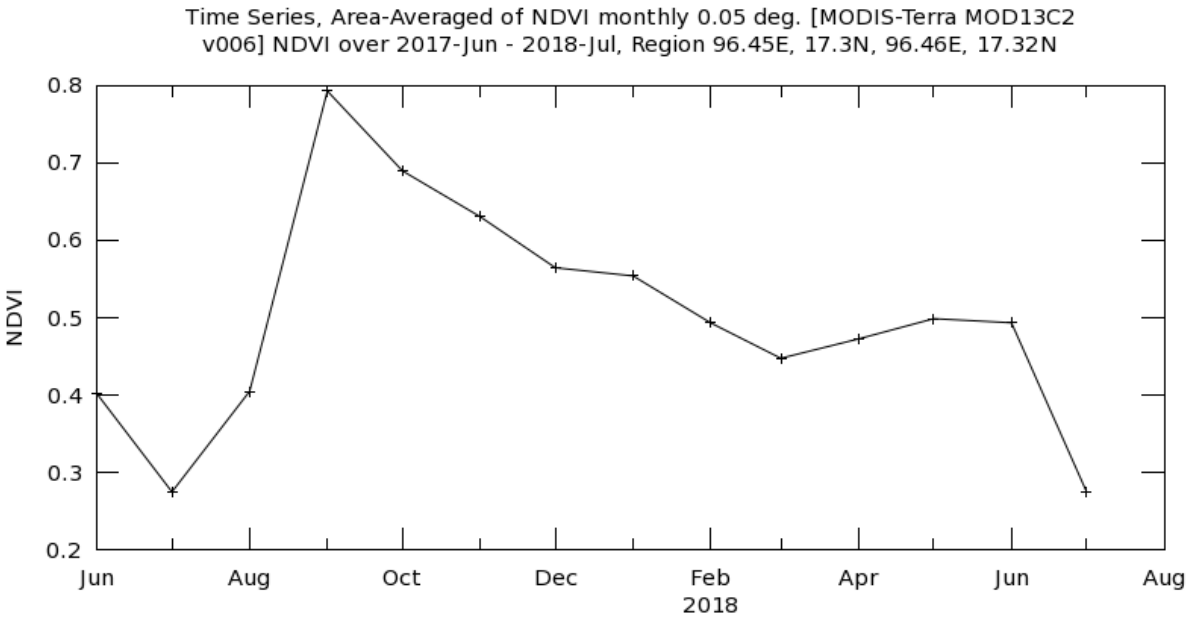

Nest 2

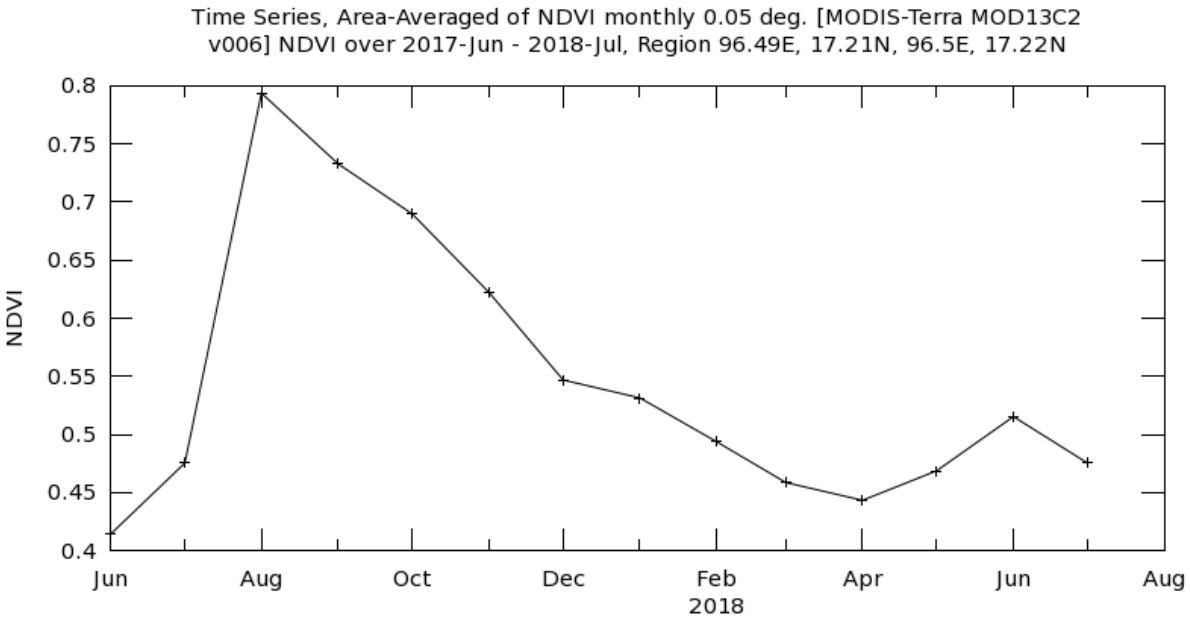

Nest 3

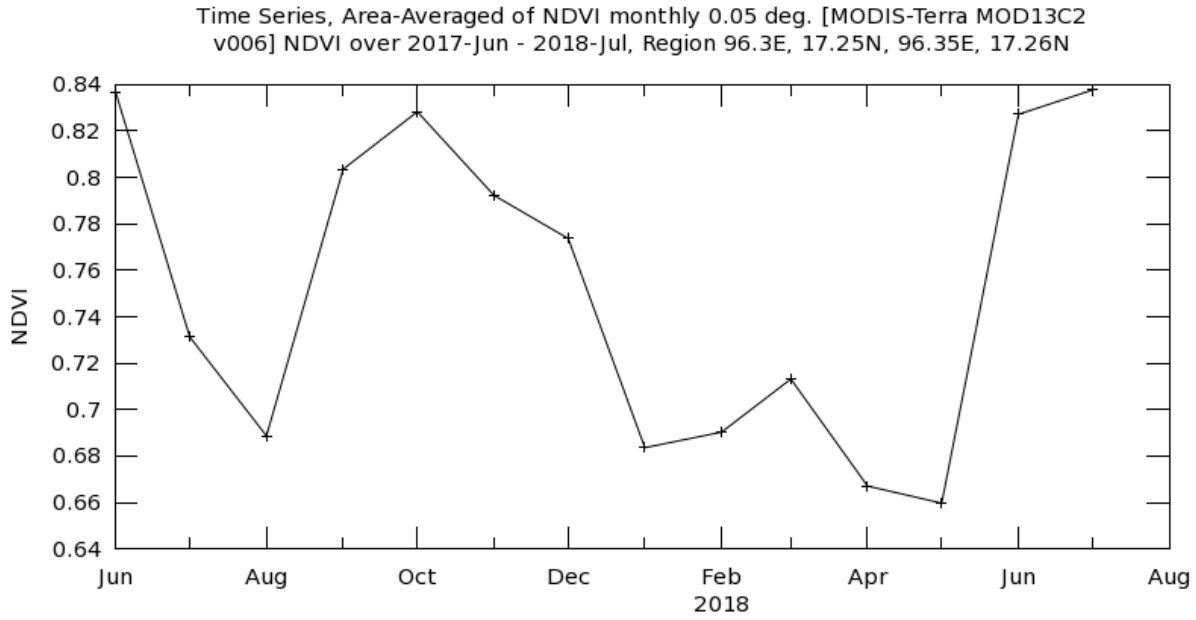
Time Series, Area-Averaged of NDVI monthly 0.05 deg. [MODIS-Terra MOD13C2 v006] NDVI over 2017-Jun - 2018-Jul, Region 96.3E, 17.25N, 96.35E, 17.26N
NDVI
0.84
0.82
0.8
0.78
0.76
0.74
0.72
0.7
0.68
0.66
0.64
Jun
Aug
Oct
Dec
Feb
2018
Apr
Jun
Aug

Nest 4

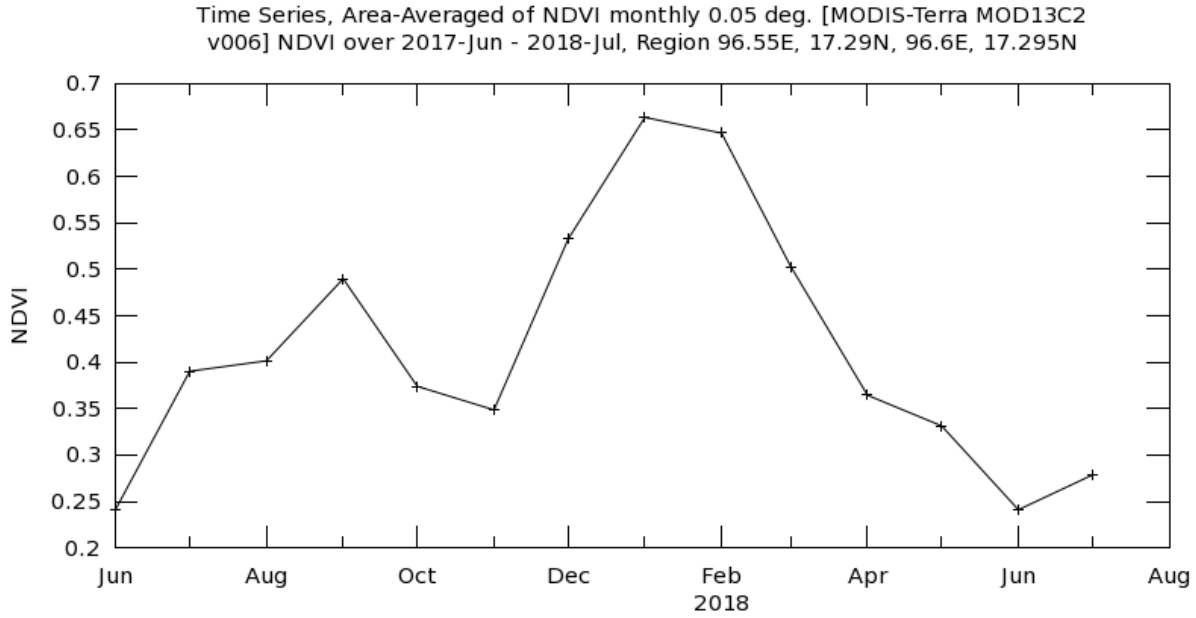
Time Series, Area-Averaged of NDVI monthly 0.05 deg. [MODIS-Terra MOD13C2 v006] NDVI over 2017-Jun - 2018-Jul, Region 96.55E, 17.29N, 96.6E, 17.295N
NDVI
0.7
0.65
0.6
0.55
0.5
0.45
0.4
0.35
0.3
0.25
0.2
Jun
Aug
Oct
Dec
Feb
2018
Apr
Jun
Aug

Nest 5

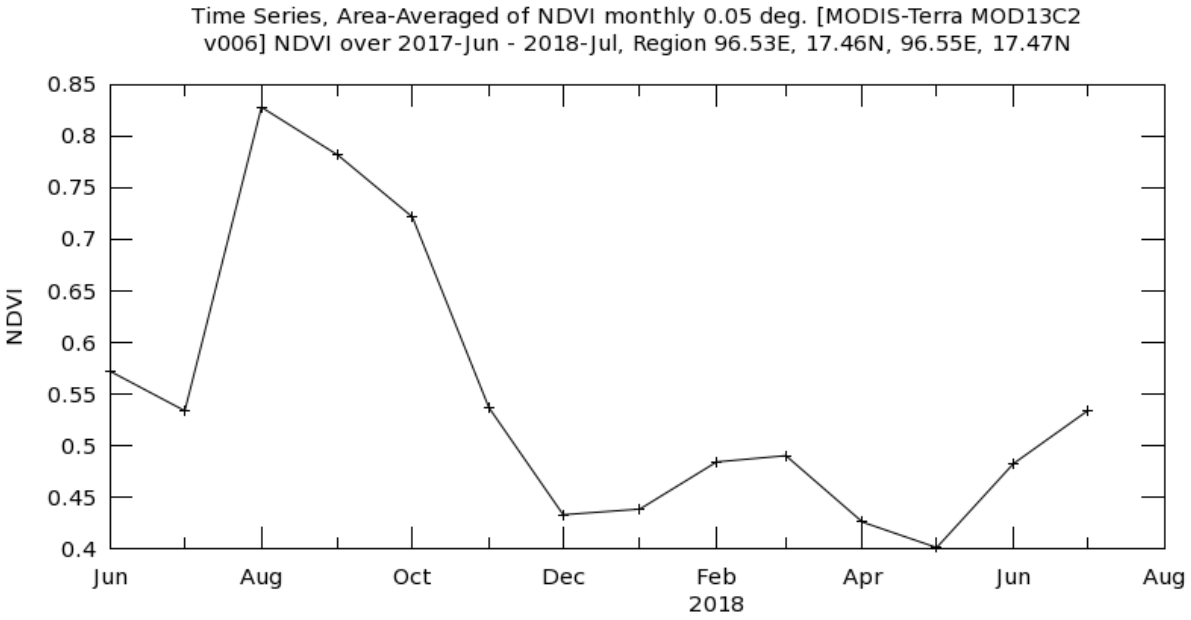
Time Series, Area-Averaged of NDVI monthly 0.05 deg. [MODIS-Terra MOD13C2 v006] NDVI over 2017-Jun - 2018-Jul, Region 96.53E, 17.46N, 96.55E, 17.47N
NDVI
0.85
0.8
0.75
0.7
0.65
0.6
0.55
0.5
0.45
0.4
Jun
Aug
Oct
Dec
Feb
2018
Apr
Jun
Aug